Supplementary Information for:

Fate of organic contaminants in electrochemical nitrogen recovery from urine

Anna Kogler[1], William A. Tarpeh[1,2*]

[1] Department of Civil and Environmental Engineering, Stanford University, Stanford, CA, 94305, USA

[2] Department of Chemical Engineering, Stanford University, Stanford, CA, 94305, USA

*Corresponding author, Email: wtarpeh@stanford.edu. Address: 443 Via Ortega, Room 387, Stanford CA, 94305. Telephone: 650-497-1324

Pages: 74

Figures: 27

Tables: 31

1 Materials and Methods

1.1 Urine Characterization

Total ammonia nitrogen (TAN) was measured via a phenol-based colorimetric method by segmented flow analysis with a SEAL Analytical AA500 AutoAnalyzer (Mequon, WI). Anion concentrations (i.e., fluoride, chloride, nitrite, bromide, nitrate, phosphate, and sulfate) were measured via anion chromatography (4.5 mM carbonate/0.8 mM bicarbonate eluent at 1.0 mL/min, AS23-4µm column at 30 °C, suppressed) and cation concentrations (i.e., lithium, sodium, ammonium, potassium, magnesium, calcium) were measured via cation chromatography (4 mM tartaric acid and 2 mM oxalic acid eluent at 1.0 mL/min, IonPac SCS1 column at 30°C, unsuppressed) on a Thermo Fisher Scientific Dionex ICS-6000 system (Waltham, MA). Samples were acidified with 2 M sulfuric acid prior to TAN and cation analysis to prevent ammonia volatilization and allow accurate quantification of TAN. pH of raw samples was measured with a pH/conductivity meter (FiveEasy F20, Mettler Toledo, Columbus, OH). Pharmaceutical and DBP concentrations in urine were measured as described below (Sections S1.4 and S1.5).

Table S1-1. Average composition of influent urine across all experiments. Note that for atenolol, concentrations were lower for BPED experiments (2.18 ±0.54 µg/L) than ED and ECS experiments (19.3 ±2.4 µg/L), suggesting that atenolol may have degraded or precipitated during storage. Diclofenac concentrations tended to be more variable within analytical and experimental replicates across all processes.

	Urine
TAN (mg/L)	3,280 ± 360
Cations (mg/L)	
Na^+	1,090 ± 42
K^+	1,150 ± 190
Mg^{2+}	0.418 ± 1.2
Ca^{2+}	-
Anions (mg/L)	
SO_4^{2-}	548 ± 63
Cl^-	1,860 ± 70
PO_4^{3-}	462 ± 14
Other	
pH	9.32 ± 0.08
COD (mg/L)	3,180 ± 69
Pharmaceuticals (µg/L)	
Atenolol	15.0 ± 7.9
Trimethoprim	20.1 ± 3.5
Metoprolol	26.1 ± 5.1
Bezafibrate	13.4 ± 1.2
Propranolol	30.7 ± 3.6
Carbamazepine	18.6 ± 3.2
Diclofenac	28.9 ± 19.6

1.2 Chemicals

Sodium chloride and sodium sulfate used to prepare background electrolyte solutions were obtained from Acros Organics (ACS reagent, 99+%, Belgium) and Millipore Sigma (ACS Tracepur, ≥ 99.0%, Burlington, MA), respectively. Sulfuric acid used to prepare product recovery solutions was purchased from Sigma-Aldrich (ACS reagent, 95.0 – 98.0%, St. Louis, MO). A Milli-Q® IQ 7000 Ultrapure Lab Water System from EMD Millipore (Burlington, MA) was used to obtain 18.2MΩ-cm water used throughout all experiments.

Primary standards and deuterated internal standards of the pharmaceuticals used in this work were purchased from several suppliers including Sigma-Aldrich (St. Louis, MO), Santa Cruz Biotechnology (Dallas, TX), Toronto Research Chemicals (Toronto, Ontario), Alfa Aesar (Haverhill, MA), CDN Isotopes (Pointe-Claire, Canada), and ApexBio Technology LLC (Houston, TX). Optima LC-MS grade methanol, acetone, acetonitrile, water, and ammonium formate were obtained from Fisher Scientific (Waltham, MA). Ascorbic acid for quenching chlorine in samples prior to pharmaceutical and disinfection byproduct analysis[104] was obtained from Sigma-Aldrich (St. Louis, MO).

Reagents for segmented flow analysis of total ammonia nitrogen included: sodium citrate dihydrate (99.0−101.0 %, Avantor Performance Materials), sodium nitroferricyanide dihydrate (ACS grade, Acros Organics, Belgium), sodium hydroxide (ACS reagent, 97.0%, Ricca Chemical), phenol (ACS reagent, 99.0%, Sigma-Aldrich), and sodium hypochlorite (reagent grade, 10−15% available chlorine, Sigma-Aldrich). Ammonium sulfate for preparation of segmented flow analysis standards was obtained from Sigma-Aldrich (ACS reagent, ≥ 99.0%, St. Louis, MO). Reagents for anion chromatography (4.5 mM carbonate/0.8 mM bicarbonate eluent) were obtained from Thermo Fisher Scientific (Waltham, MA). Reagents for cation chromatography (oxalic acid and tartaric acid) were purchased from Sigma-Aldrich (St. Louis, MO). Standards for anion and cation chromatography were obtained from Thermo Fisher Scientific (Waltham, MA).

Reagents for disinfection byproduct analysis included: GC-grade methyl tert-butyl ether (puriss. p.a., ≥ 99.5%, Sigma Aldrich, St. Louis, MO), Optima HPLC/GC grade methylene chloride (Fisher Scientific, Waltham, MA), methanol (LC/MS grade, ≥ 99.9%, Fisher Chemical, Pittsburgh, PA), and sodium bicarbonate (Certified ACS, 99.7–100.3%, Fisher Chemical, Pittsburgh, PA). Standards for disinfection byproducts included: 1,2-dibromopropane (certified reference material, AccuStandard, New Haven, CT), EPA 552.2 haloacetic acids mix (certified reference material, Sigma Aldrich, St. Louis, MO), trihalomethanes mix (certified reference material, AccuStandard, New Haven, CT), M551.1B disinfectant by-products mix (certified reference material, AccuStandard, New Haven, CT), trichloroacetamide (HPLC grade, 98+%, Thermo Scientific Chemicals, Waltham, MA), and dichloroacetamide (98+%, Thermo Scientific Chemicals, Waltham, MA). Iodinated DBP standards, which were ultimately not quantified, were obtained from CanSyn Chemical Corporation (Toronto, Ontario).

1.3 Operation of Electrochemical Nitrogen Recovery Processes

ECS experiments were performed in a three-chambered, parallel-plate reactor similar to previous reports,[19,105] in which three square acrylic frames (internal dimensions: 8 x 8 x 1.9 cm^3) were compressed between two larger square acrylic plates (10 x 10 x 1.9 cm^3) to create three chambers (122 mL each, Figure 1A). Chambers 1 and 2 contained an anode and cathode, respectively, and were separated by a Selemion CMVN cation exchange membrane (AGC Engineering Co., Ltd., Japan). Chambers 2 and 3 were separated by a microporous polyethylene membrane (Aquastill, Netherlands). The anode was a Ti mesh coated with Ta_2O_5 / IrO_2 mixed metal oxide (Magneto Special Anodes, Netherlands), and the cathode was a 304L stainless steel mesh (0.425 mm hole, 190 μm wire diameter, 42% open area; Yikai Industrial Scientific). Both electrodes had a 64 cm^2 geometric surface area and were positioned immediately adjacent to the cation exchange membrane. Urine was introduced into Chamber 1, 0.1 M NaCl solution was used as a background electrolyte in Chamber 2, and 1 M H_2SO_4 was used to recover TAN in Chamber 3. Reactor components were separated by Buna-N gaskets (USA Sealing, Buffalo, NY) and held together by compression with stainless steel rods to prevent leaks.

ED experiments were performed in a three-chambered, parallel-plate reactor in which three square acrylic frames were compressed between two larger square acrylic plates (10 x 10 x 1.9 cm^3) to create three chambers (Figure 1B). The outer chambers were the same size as those used for ECS (internal dimensions: 8 x 8 x 1.9 cm^3, volume: 122 mL), while the middle chamber was thinner (internal dimensions: 8 x 8 x 0.95 cm^3, volume: 61 mL). We selected a three-chambered reactor as a minimum reactor representative of ED reactor configurations without stacked chambers, which have been studied for urine treatment.[106–110] We used a thinner middle chamber, which contained urine, to reduce the contribution of solution resistance to overall electrochemical cell resistance and allow the reactor to operate longer within potentiostat limits. This reactor is comparable to three-chambered ECS by facilitating cation removal via migration across a cation exchange membrane although the ED reactor has the added ability to remove anions via migration across an anion exchange membrane. Chambers 2 and 3 were separated by a Selemion CMVN cation exchange membrane (AGC Engineering Co., Ltd., Japan). Chambers 1 and 3, the outermost chambers, contained an anode and cathode, respectively. The anode was a Ti mesh coated with Ta_2O_5 / IrO_2 mixed metal oxide (Magneto Special Anodes, Netherlands), and the cathode was a 304L stainless steel mesh (0.425 mm hole, 190 μm wire diameter, 42% open area; Yikai Industrial Scientific); both electrodes had a 64 cm^2 geometric surface area. Chambers 1 and 2 were separated by an anion exchange membrane (AMI-7001S, Membranes International Inc., Ringwood, NJ). An electrode rinse solution of 0.1 M Na_2SO_4 was recirculated in Chamber 1 (anode chamber); background electrolyte of 0.1 M NaCl was recirculated in Chamber 3 (concentrate/cathode chamber) when the experiment began. Urine was introduced and recirculated within Chamber 2 (diluate chamber). Reactor components were separated by Buna-N gaskets (USA Sealing, Buffalo, NY) and held together by compression with stainless steel rods to prevent leaks.

BPED experiments were performed in a four-chambered, parallel-plate reactor in which four square acrylic frames (internal dimensions: 8 x 8 x 1.9 cm^3) were compressed between two larger square acrylic plates (10 x 10 x 1.9 cm^3) to create four chambers (122 mL each, Figure 1C).

Chambers 1 and 2 were separated by a bipolar membrane (FumaTech Fumasep FBM, Fuel Cell Store, Bryan, TX). Chambers 2 and 3 were separated by a Selemion CMVN cation exchange membrane (AGC Engineering Co., Ltd., Japan), and Chambers 3 and 4 were separated by an anion exchange membrane (AMI-7001S, Membranes International Inc., Ringwood, NJ). Chambers 1 and 4, the outermost chambers, contained an anode and cathode, respectively. The anode was a Ti mesh coated with Ta_2O_5 / IrO_2 mixed metal oxide (Magneto Special Anodes, Netherlands), and the cathode was a 304L stainless steel mesh (0.425 mm hole, 190 µm wire diameter, 42% open area; Yikai Industrial Scientific); both electrodes had a 64 cm^2 geometric surface area. An electrode rinse solution of 0.1 M Na_2SO_4 was recirculated within Chamber 1 (anode chamber); background electrolyte of 0.1 M NaCl was recirculated in Chambers 3 and 4 (concentrate and cathode chambers, respectively) when the experiment began. Urine was introduced into Chamber 2 (diluate chamber). Reactor components were separated by Buna-N gaskets (USA Sealing, Buffalo, NY) and held together by compression with stainless steel rods to prevent leaks. This BPED configuration was chosen over other BPED variations[111,112] because it has been studied for urine treatment[113,114] and is most similar to conventional electrodialysis, which facilitates more direct comparison of the two processes (e.g., evaluating the impact of more rapid acidification of influent urine).

Samples were collected and stored as described in Table S1-2.

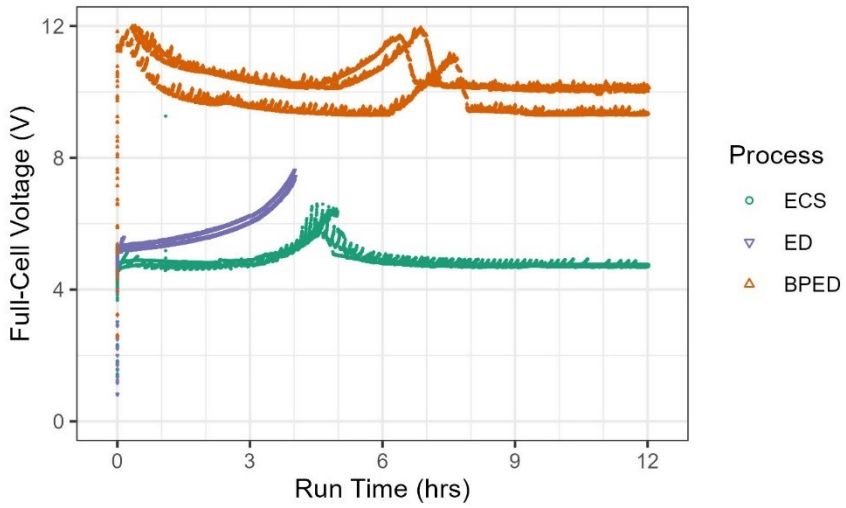

Figure S1-1. Full-cell voltage observed during ECS, ED, and BPED experiments. For ED, full-cell voltage increased rapidly as Chamber 2 became depleted of both anions and cations, causing high resistance.

Table S1-2. Sample collection and storage protocol

Analyte	Sampling Times (hrs)	Reactor Chambers	Sample Volume	Sample Preservation	Sample Storage
TAN, pH	ECS/BPED: 0, 0.25, 0.5, 1, 2, 3, 6, 9, 12 ED: 0, 0.25, 0.5, 1, 2, 3, 4	All	2 mL	Acidification to pH 2 using 2 M H_2SO_4 (after measuring pH)	20-25°C
Anions	ECS/BPED: 0, 12 ED: 0, 4	All	2 mL	-	20-25°C
X-DBPs	ECS/BPED: 0, 3, 9, 12 ED: 0, 3, 4	All at initial & final Influent and anode also at intermediate	3 x 10 mL	33 mg/L ascorbic acid; acidify to pH ~3.7 using concentrated H_2SO_4	4°C
HAAs	ECS/BPED: 0, 3, 9, 12 ED: 0, 3, 4	All at initial & final Influent and anode also at intermediate	3 x 10 mL	33 mg/L ascorbic acid; acidify to pH ≤ 0.5 with concentrated H_2SO_4	4°C
Pharmaceuticals	0, 12	All	3 x 50 mL	33 mg/L ascorbic acid	4°C

1.4 Pharmaceutical Analysis

1.4.1 Sample Preparation

50 mL of samples spiked with 200 µg/L of internal standards (emtricitabine-^{13}C,$^{15}N_2$, atenolol-d_7, sulfamethoxazole-d_4, N4 acetyl-sulfamethoxazole-d_4, trimethoprim-d_3, metoprolol-d_7, naproxen-d_3, bezafibrate-d_4, propranolol-d_7, carbamazepine-d_{10}, diclofenac-d_4, iopromide-d_3) were processed by solid phase extraction (SPE) using Waters Oasis HLB cartridges (3 cc / 60 mg, 30-um diameter sorbent) (Milford, MA). Cartridges were conditioned with 2 mL methanol, followed by 2 mL water prior to sample loading. After sample loading, the cartridges were dried under vacuum for about one hour. Pharmaceuticals were then eluted by gravity with 2 mL methanol/acetone (1:1 mixture, v/v), and the samples were concentrated further to 0.5 mL under nitrogen gas. Extracts were stored at -20°C until analysis via liquid chromatography-mass spectrometry (LC-MS) for target analysis and liquid chromatography-high resolution mass spectrometry (LC-HRMS) for non-target analysis.

1.4.2 Target Analysis

Samples were analyzed on an Agilent 1260 HPLC with an Agilent 6460 Triple Quadrupole MS using an Agilent Poroshell 120 EC-C18 2.7 µm, 3.0 x 50 mm column (Agilent, Santa Clara, CA). Compounds (Table S1-3) were separated with a 16-minute gradient method (Table S1-4) using 5 mM aqueous ammonium formate (mobile phase A) and acetonitrile (mobile phase B) at a flowrate of 0.6 mL/min. 10 µL of sample were injected during each run. Compounds were detected using positive electrospray ionization mode with a gas temperature of 300°C, gas flowrate of 7 L/min, a nebulizer pressure of 45 psi, a sheath gas temperature of 250°C, a sheath gas flowrate of 9 L/min,

a capillary voltage of 3500 V, and a nozzle voltage of 500 V. Compounds were quantified using multiple-reaction monitoring (MRM) with compound-specific MR parameters and retention times shown in Table S1-5.

Table S1-3. Target pharmaceuticals, their properties, and internal standards. Pharmaceuticals that were spiked into urine but are not listed in this table (i.e., emtricitabine, sulfamethoxazole, N4 acetyl-sulfamethoxazole, naproxen, iopromide) were not quantified as target pharmaceuticals due to issues with internal standard detection and/or poor calibration curves. pKa's were found in previous literature[19] unless otherwise indicated. MW= molecular weight; IS= internal standard.

Abbrev.	**Compound**	**Structure**	**Function**	**MW (g/mol)**	**pKa**	**IS**
ATE	Atenolol	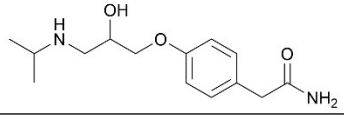	Beta-blocker	266.34	9.6	ATE-d7
TMP	Trimethoprim	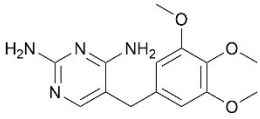	Antibiotic	290.32	7.4	TMP-d3
MET	Metoprolol	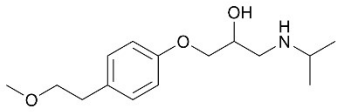	Beta-blocker	267.37	9.5	MET-d7
BZF	Bezafibrate	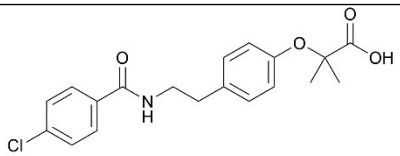	Lipid regulator	361.8	3.83[115]	BZF-d4
PRO	Propranolol	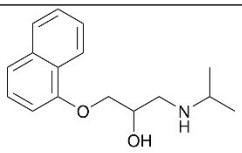	Beta-blocker	259.34	9.1	PRO-d7
CBZ	Carbamazepine	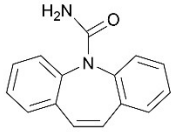	Antiepileptic	236.27	~1, 13.9[116]	CBZ-d10
DIC	Diclofenac	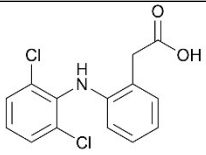	Pain reliever	296.1	3.99-4.3[117]	DIC-d4

Table S1-4. Mobile phase gradient for LC-MS method for target pharmaceutical analysis where mobile phase A is 5 mM aqueous ammonium formate and mobile phase B is acetonitrile.

Time (min)	A (%)	B (%)
0	98	2
2	98	2
10	0	100
11	0	100
13	98	2
16	98	2

Table S1-5. Mass spectrometry parameters for target pharmaceutical analysis.

Compound	Retention Time (min)	Precursor Ion m/z	Product Ion m/z	Quantifying or Qualifying	Fragmentor Voltage (V)	Collision Energy (V)	Dwell (s)
ATE	5.18	267	145	Qualifying	130	24	100
ATE	5.18	267	190	Quantifying	130	16	100
ATE-d7	5.15	274	145	Quantifying	130	24	100
TMP	5.85	291	123	Qualifying	140	20	7
TMP	5.85	291	261	Quantifying	140	17	7
TMP-d3	5.82	294	123	Qualifying	140	20	7
TMP-d3	5.82	294	264	Quantifying	140	17	7
MET	6.25	268	159	Quantifying	130	17	7
MET	6.25	268	116	Qualifying	130	14	7
MET-d7	6.25	275	159	Quantifying	130	17	7
MET-d7	6.25	275	123	Qualifying	130	14	7
BZF	8.27	362	139	Quantifying	138	21	7
BZF	8.27	362	316	Qualifying	138	5	7
BZF-d4	8.25	366	143	Quantifying	138	21	7
BZF-d4	8.25	366	320	Qualifying	138	5	7
PRO	6.97	260	116	Quantifying	98	13	7
PRO	6.96	260	183	Qualifying	98	12	7
PRO-d7	6.95	267	190	Qualifying	98	12	7
PRO-d7	6.95	267	116	Quantifying	98	13	7
CBZ	7.51	237	179	Qualifying	120	35	7
CBZ	7.51	237	194	Quantifying	120	15	7
CBZ-d10	7.48	247	204	Quantifying	120	20	7
CBZ-d10	7.48	247	189	Qualifying	120	35	7
DIC	9.12	296	250	Qualifying	118	5	7
DIC	9.11	296	214	Quantifying	118	29	7
DIC-d4	9.10	300	254	Qualifying	118	5	7
DIC-d4	9.10	300	218	Quantifying	118	29	7

1.4.3 Suspect Screening

Samples were analyzed on a Thermo Scientific Orbitrap Exploris 240 mass spectrometer (Thermo Scientific, Waltham, MA) using an Agilent Poroshell 120 EC-C18 2.7 µm, 3.0 x 50 mm column (Agilent, Santa Clara, CA) for ECS and a Kinetex Core-Shell C18 2.6 µm, 2.1 x 150 mm column (Phenomenex, Torrance, CA) for ED and BPED. Compounds were separated with a 22-minute gradient method (Table S1-6) using 0.1% aqueous formic acid (mobile phase A) and methanol (mobile phase B) at a flowrate of 0.2 mL/min. 10 µL of sample were injected during each run. Compounds were detected using positive and negative electrospray ionization mode with collision gas pressure of 1 mTorr, spray voltages of 3500 V (positive) and 2500 V (negative), ion transfer tube temperature of 320°C, vaporizer temperature of 275°C, and expected peak width of 6 seconds. For the MasterScan, MS data were collected with an Orbitrap resolution of 120000, an m/z scan range of 100 to 1000 and a radio frequency lens of 70% in positive and negative modes. All-ion fragmentation data were collected using an HCD (high-energy collisional dissociation) collision energy of 30%, Orbitrap resolution of 60000, m/z scan range of 50 to 1000, m/z isolation range of 100 to 1000, and a radio frequency lens of 70% in both positive and negative modes. Data were collected in both positive and negative mode, but only data in positive mode were used for analysis to keep the quantity of data manageable and because all target compounds were detected in positive mode so we could not validate the suspect screening workflow in negative mode.

Table S1-6. Mobile phase gradient for LC-HRMS method for non-target analysis where mobile phase A is 0.1% aqueous formic acid and mobile phase B is methanol.

Time (min)	**A (%)**	**B (%)**
0	98	2
2	98	2
10	0	100
14	0	100
15	98	2
22	98	2

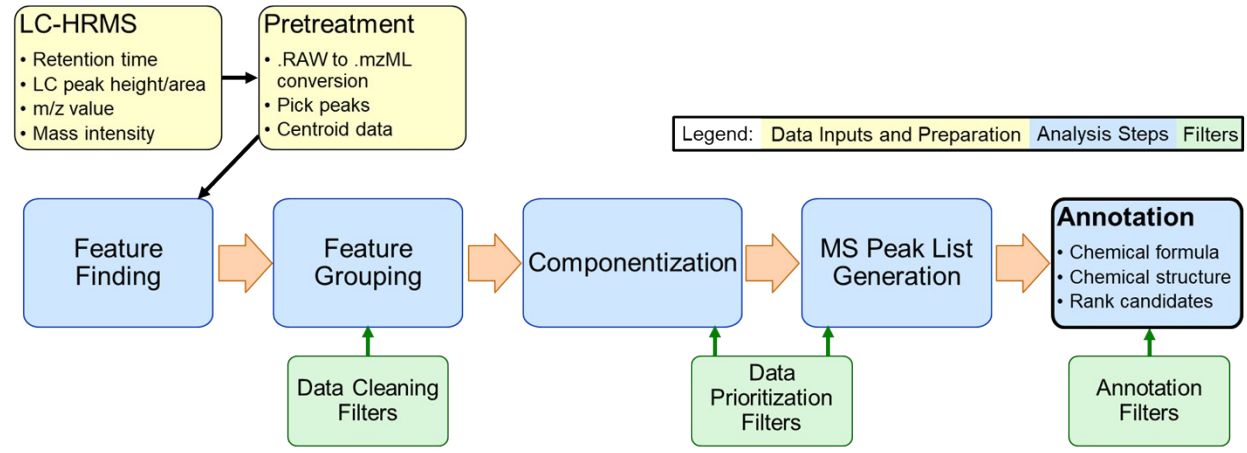

Figure S1-2. Illustration of suspect screening analysis workflow.

Table S1-7. Parameters for data pretreatment using Proteowizard MSconvert.

Parameter	**Value**
Output format	mzML
Binary coding precision	64-bit
Polarity	positive
Peak picking: algorithm	CWT (continuous wavelet transform)
Peak picking: MS levels	1
Peak picking: minimum signal-to-noise ratio	0.1
Peak picking: minimum peak spacing	0.1

Table S1-8. Parameters for feature finding in patRoon. These parameter values were determined by using patRoon's built-in feature finding optimization function with positive-mode data collected for spiked DI standards (0.5 µg/L) that were analyzed with samples for ECS and BPED. Feature finding parameters were separately optimized using the entire dataset for standards and samples analyzed for ED experiments to improve detection of target compounds during suspect screening.

Parameter	**Value for ECS & BPED**	**Value for ED**
Algorithm	openms	openms
Noise intensity threshold (noiseThrInt)	5400	13000
Minimum signal-to-noise ratio of mass trace (chromSNR)	10.9	5.32
Retention time range in which to look for coeluting/isotopic mass traces (localRTRange)	23	30.5
m/z range in which to look for coeluting/isotopic mass traces (localMZRange)	19.8	12.6
Retention time window that is used to find the closest data point to the retention time to obtain the intensity of a feature (intSearchRTWindow, seconds)	9.2	1
Expected chromatographic peak width (chromFWHM, seconds)	5	1
Allowed mass deviation from trace detection (mzPPM, ppm)	10	24
Minimum chromatographic peak width (minFWHM, seconds)	1	1
Maximum chromatographic peak width (maxFWHM, seconds)	20	15.248

Table S1-9. Parameters for feature grouping and feature group filtering in patRoon. Parameter values for feature grouping were determined by using patRoon's built-in feature grouping optimization function with positive-mode data collected for spiked DI standards (0.5 µg/L) that were analyzed with ECS and BPED samples. Feature grouping parameters were separately optimized using the entire dataset for standards and samples analyzed for ED experiments to improve detection of target compounds during suspect screening. Parameters for feature group filtering were set so that no target compounds were eliminated during filtering, which was checked using patRoon's suspect screening function.

Parameter	**Value for ECS & BPED**	**Value for ED**
Feature Grouping		
Algorithm	openms	openms
Enable retention time alignment (rtalign)	TRUE	TRUE
Maximum retention time difference for feature pairing during retention alignment (maxAlignRT, seconds)	15	15
Maximum m/z difference for feature pairing during retention alignment (maxAlignMZ, Da)	0.002	0.002
Maximum retention time difference for feature pairing during feature grouping (maxGroupRT, seconds)	12	6
Maximum m/z difference for feature pairing during feature grouping (maxGroupMZ, Da)	0.0065	0.002
Feature Group Filtering[118]		
Retention time shift of samples based on time-position of peak apex (ElutionShiftScore)	0.8 – 1	0.8 – 1
Retention time alignment of samples by comparing the time at the center index of the time vector (RetentionTimeCorrelationScore)	0.9 – 1	0.9 – 1
Shape quality based on normalized variance between a point and its immediate neighbor on either side (ZigZagScore)	0.9 – 1	0.9 – 1
Measurement of first unexpected change in direction of intensity to detect splitting and integration of multiple peaks (ModalityScore)	> 0.3	> 0.3
Measurement of correlation between left and right halves of peaks (SymmetryScore)	> 0.4	> 0.4
Shape quality based on comparing peak area to area of triangle formed by apex and boundaries (TPASRScore)	> 0.25	> 0.25
Completeness of integration based on boundary-over-apex intensity ratio (ApexBoundaryRatioScore)	> 0.55	> 0.55
Separation of peaks by measuring peak-width at half-max vs. peak-width at base (FWHM2BaseScore)	> 0.15	> 0.15
Shape quality based on number of changes in direction over length of intensity vector (JaggednessScore)	> 0.3	> 0.3
Similarity of peak to Gaussian-fitted curve (GaussianSimilarityScore)	> 0.6	> 0.6

Table S1-10. Parameters for componentization and generating MS peak lists in patRoon.

Parameter	**Value**
Componentization	
Algorithm	openms
Ionization	positive
Potential adducts (probability)	$[M+H]^+$ (0.34), $[M+Na]^+$ (0.33), $[M+NH4]^+$ (0.33)
Preferential adduct	$[M+H]^+$
Generating MS Peak Lists	
Algorithm	mzr
Maximum m/z window used to cluster mass peaks when averaging (clusterMzWindow)	0.005
Maximum time window around feature RT to collect spectra for averaging (maxMSRtWindow, seconds)	5
Maximum precursor m/z search window to find MS/MS spectra (precursorMzWindow)	NULL
Number of most intense mass peaks to retain (topMost)	NULL
Intensity below which mass peaks will be removed before/after averaging (minIntensityPre, minIntensityPost)	500
Function used to calculate avg m/z values (avgFun)	mean
Method for producing averaged MS spectra (method)	hclust (hierarchical clustering)
Remove peak lists without precursor peaks (pruneMissingPrecursorMS)	TRUE
Retain MS/MS precursor mass peak even if not among topMost peaks for MS/MS (retainPrecursorMSMS)	TRUE
Absolute minimum MS mass peak intensity (absMSIntThr)	500
Relative minimum MS/MS mass peak intensity (relMSMSIntThr)	0.02
Number of most intense MS/MS peaks to retain (topMSMSPeaks)	10

Table S1-11. Parameters for annotation with formulas and compounds in patRoon.

Parameter	Value
Formula Annotation	
Algorithm	genform
Maximum relative m/z deviation for formula to be considered (relMzDev, ppm)	5
Maximum m/z window used to re-align peaks (absAlignMzDev)	0.005
Elements to consider (elements)	CHNOSCl
Minimum relative amount that candidate formula for feature group should be found among all annotated features (featThresholdAnn)	0.75
Only consider organic formulas (oc)	TRUE
Data (MS, MSMS, or both) used for formula generation (MSMode)	Both
Formulas calculated for individual features and pooled for feature groups (calculateFeatures)	FALSE
Compound Annotation	
Algorithm	metfrag
Method	CL
Database	pubchemlite
Relative mass deviation for database search (dbRelMzDev, ppm)	5
Relative mass deviation for fragment matching (fragRelMzDev, ppm)	5
Absolute mass deviation for fragment matching (fragAbsMzDev, Da)	0.002
Number of candidates after which search stops and no results will be returned for feature group (maxCandidatesToStop)	2500
Scoring types and weights	default
Compound Filtering	
Minimum number of annotated MS/MS peaks for candidate (minExplainedPeaks)	1

1.4.4 Metrics for Pharmaceutical Fate

Table S1-12. Existing water reuse guidelines for pharmaceuticals.

Abbrev.	**Compound**	**California Recycled Water Policy Reporting Limit**[119]		**Australian Recycled Drinking Water Guideline (µg/L)**[120]
		Surface Application (µg/L)[a]	Subsurface Application (µg/L)[b]	
-	Gemfibrozil	0.01	-	600
-	Iohexol	0.05	-	720
ATE	Atenolol	-	-	-
TMP	Trimethoprim	-	-	70
MET	Metoprolol	-	-	25
BZF	Bezafibrate	-	-	300
PRO	Propranolol	-	-	40
CBZ	Carbamazepine	-	-	100
DIC	Diclofenac	-	-	1.8

[a] Groundwater recharge via surface application
[b] Reservoir water augmentation and groundwater recharge via subsurface application

Table S1-13. Samples for calculation of pharmaceutical fold changes.

Subscript	ECS	ED	BPED
influent	Chamber 1, initial	Chamber 2 (Diluate), initial	Chamber 2 (Diluate), initial
product	Chamber 3, final	Chamber 3 (Concentrate), final	Chamber 3 (Concentrate), final
effluent	Chamber 1, final	Chamber 2 (Diluate), final	Chamber 2 (Diluate), final

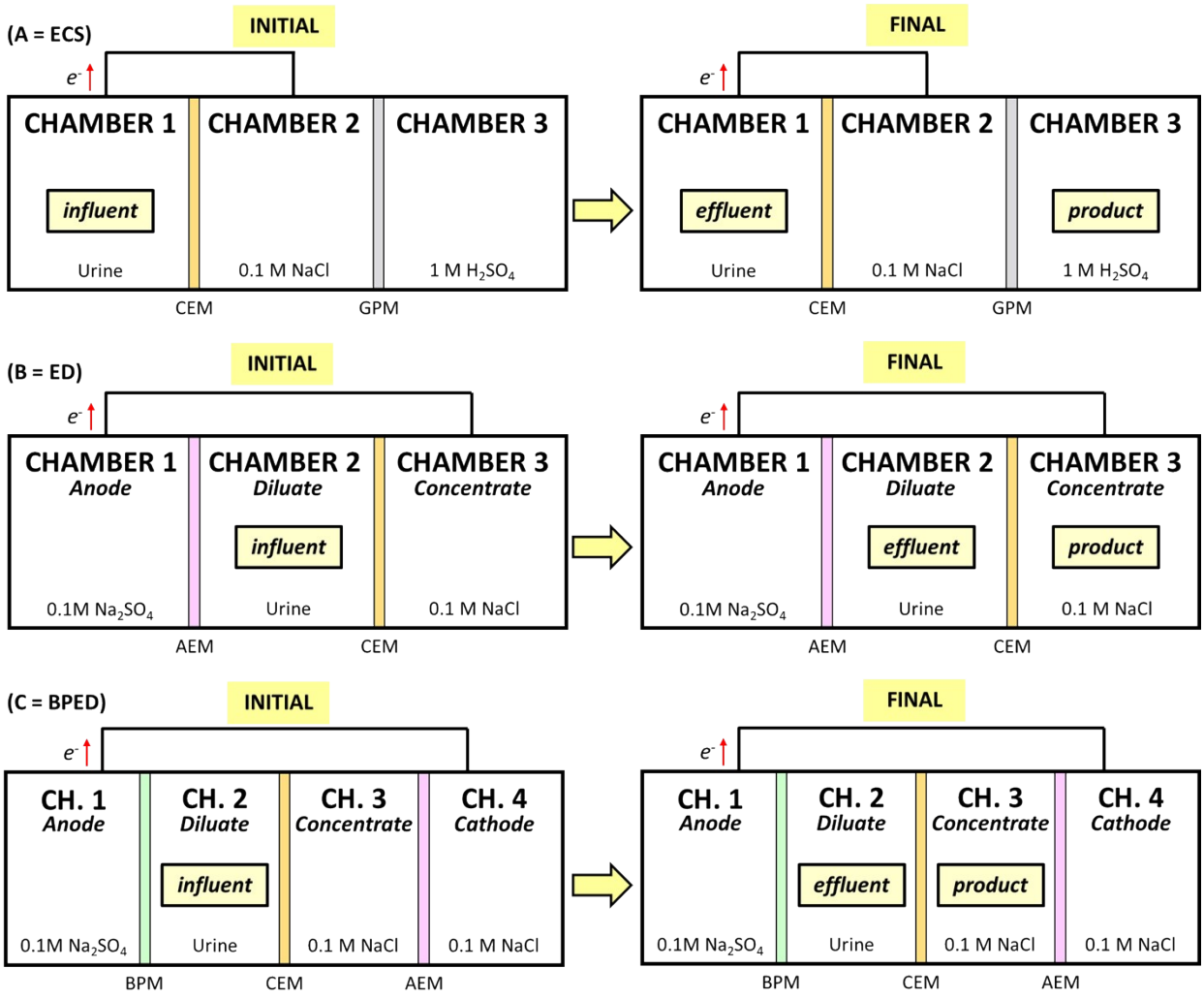

Figure S1-3. Samples for calculating fold changes of pharmaceuticals and features detected during suspect screening for ECS (A), ED (B), and BPED (C). Sample names are indicated in bold italic font in yellow boxes. Names of chamber solutions for ED and BPED are indicated in bold italic font. Solution composition and reactor components are indicated in regular font at the bottom of diagrams (CEM = cation exchange membrane, GPM = gas permeable membrane, AEM = anion exchange membrane, BPM = bipolar membrane).

1.5 Disinfection Byproduct Analysis

THMs included chloroform ($CHCl_3$, TCM), bromodichloromethane (BDCM), dibromochloromethane (DBCM), and bromoform ($CHBr_3$, TBM), which are regulated in drinking water as total THMs.[121] HAAs included dichloroacetic acid (DCAA), chloroacetic acid (CAA), trichloroacetic acid (TCAA), bromoacetic acid (BAA), and dibromoacetic acid (DBAA), which are regulated in drinking water as HAA5,[121] as well as bromochloroacetic acid (BCAA). Additional HAAs, including chlorodibromoacetic acid (CDBAA), bromodichloroacetic acid (BDCAA), and tribromoacetic acid (TBAA), were measured but not detected; concentrations were not reported due to poor calibration curves. HANs included bromochloroacetonitrile (BCAN), dibromoacetonitrile (DBAN), dichloroacetonitrile (DCAN), and trichloroacetonitrile (TCAN). HALs included trichloroacetaldehyde (chloral hydrate; TCAL). HKs included 1,1-dichloropropanone (1,1-DCP) and 1,1,1-trichloropropanone (1,1,1-TCP). Only one HNM, trichloronitromethane or chloropicrin (TCNM), was included as in previous DBP studies.[96,122,123] HAMs included dichloroacetamide (DCAM) and trichloroacetamide (TCAM).

THMs, HANs, HALs, HKs, HNMs, and HAMs were extracted by modified USEPA Method 551.1, while HAAs were extracted by modified USEPA Method 552.3.[96,122–127] For THMs, HANs, HALs, HKs, HNMs, and HAMs, 10 mL aliquots supplemented with 3 g of sodium sulfate were extracted into 2 mL of methyl tert-butyl ether (MTBE) containing 300 μg/L 1,2-dibromopropane as an internal standard. Extracts were concentrated to ~0.5 mL under nitrogen. For HAAs, 10 mL aliquots acidified to pH < 0.5 with sulfuric acid and supplemented with 3 g of sodium sulfate were extracted into 2 mL of MTBE containing 300 μg/L 1,2-dibromopropane as an internal standard. Recovered MTBE extracts were mixed with 0.8 mL of acidic methanol (with 10% concentrated H2SO4, v/v) and incubated at 50°C in a water bath for 2 hours. The mixture was extracted with 2.5 mL of 150 g/L Na_2SO_4 solution, neutralized by 1 mL of saturated $NaHCO_3$ solution, and further concentrated to a final volume of ~0.5 mL under a gentle nitrogen stream. All DBPs were analyzed by GC-MS using an Agilent 7890A GC with a DB-1701 fused silica capillary column coupled with an Agilent 240 Ion Trap mass spectrometer (Agilent, Santa Clara, CA) using electron ionization mode for THMs, HANs, HALs, HKs, HNM, and HAAs and chemical ionization mode with methanol as the reagent gas for HAMs. These DBPs were quantified using standard curves in water and urine (0.5 – 100 μg/L).

Table S1-14. Summary of disinfection byproducts quantified in this study with limits of detection (LODs). Calibration curves were fit for the normalized peak area (analyte peak area divided by internal standard peak area for sample with analyte peak area divided by internal standard peak area for blank subtracted) vs. the expected concentration of the standard. LODs were determined as 3.3 times the standard error in the estimated normalized peak area divided by the slope of the calibration curve. Limits of quantification (LOQs, not shown here) were determined as 10 times the standard error in the estimated normalized peak area divided by the slope of the calibration curve. LODs were determined for each set of samples and the averages and standard deviations across all sets are summarized in this table. Asterisks indicate species that were not detected (i.e., no GC-MS peaks) in any samples and not quantified due to poor calibration curves in urine likely due to matrix effects; for these species, GC-MS peaks were only detected at the top two to three concentrations of the standard range, which we considered insufficient for creating reliable calibration curves.

Species	**Abbreviation**	**Detection Limit in Water (µg/L)**	**Detection Limit in Urine (µg/L)**
Trihalomethanes (THMs)			
Chloroform ($CHCl_3$)	TCM	5.5 ± 6.7	4.3 ± 4.6
Bromodichloromethane	BDCM	1.6 ± 1.2	0.6 ± 0.6
Dibromochloromethane	DBCM	0.7 ± 0.6	0.5 ± 0.4
Bromoform ($CHBr_3$)	TBM	1.0 ± 0.9	0.3 ± 0.2
Total trihalomethanes	THM4 = TCM + BDCM + DBCM + TBM		
Haloacetic acids (HAAs)			
Chloroacetic acid	CAA	4.3 ± 2.9	2.4 ± 0.7
Dichloroacetic acid	DCAA	2.2 ± 1.2	9.5 ± 2.3
Trichloroacetic acid	TCAA	2.1 ± 1.1	5.5 ± 2.2
Bromoacetic acid	BAA	1.7 ± 0.6	1.8 ± 1.5
Dibromoacetic acid	DBAA	1.5 ± 0.2	10.9 ± 27
Total haloacetic acids	HAA5 = CAA + DCAA + TCAA + BAA + DBAA		
Bromochloroacetic acid	BCAA	1.1 ± 0.27	18.2 ± 13.7
Chlorodibromoacetic acid	CDBAA*	-	-
Bromodichloroacetic acid	BDCAA*	-	-
Tribromoacetic acid	TBAA*	-	-
Haloacetonitriles (HANs)			
Bromochloroacetonitrile	BCAN	1.1 ± 0.89	5.3 ± 5.7
Dibromoacetonitrile	DBAN	1.9 ± 1.7	5.2 ± 3.0
Dichloroacetonitrile	DCAN	0.7 ± 0.5	4.2 ± 4.6
Trichloroacetonitrile	TCAN	0.6 ± 0.3	38 ± 40
Haloacetaldehydes (HALs)			
Trichloroacetaldehyde or chloral hydrate	TCAL	3.3 ± 3.0	21.0 ± 14
Haloketones (HKs)			
1,1-dichloropropanone	1,1-DCP	0.84 ± 0.84	1.5 ± 0.90
1,1,1-trichloropropanone	1,1,1-TCP	3.8 ± 4.0	21.6 ± 26
Halonitromethanes (HNMs)			
Trichloronitromethane or chloropicrin	TCNM	1.1 ± 0.90	24.9 ± 28
Haloacetamides (HAMs)			
Dichloroacetamide	DCAM	0.83 ± 0.41	1.0 ± 0.30
Trichloroacetamide	TCAM	1.6 ± 3.5	0.88 ± 0.88

2 Results & Discussion

2.1 Nitrogen Removal and Recovery Performance

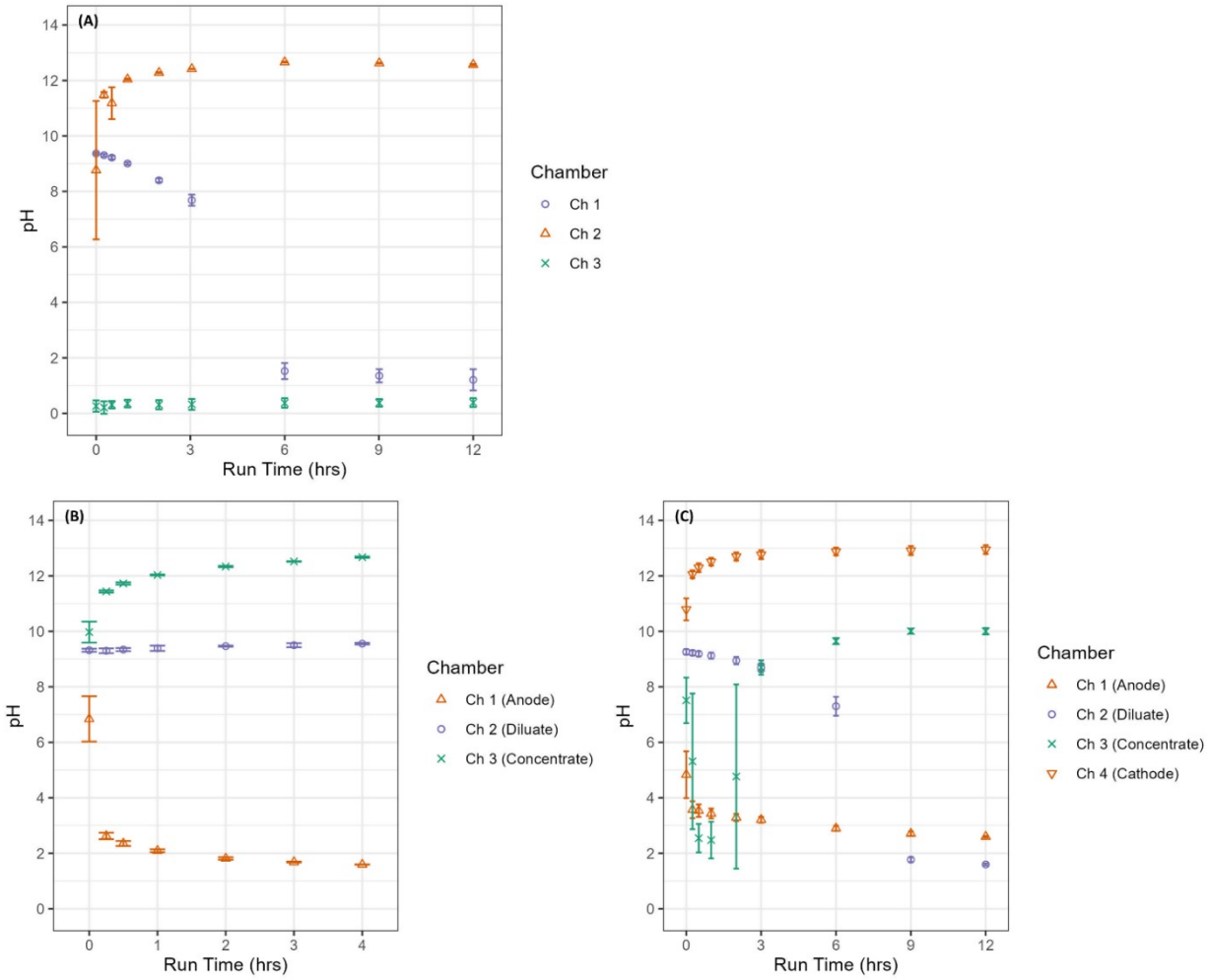

Figure S2-1. pH values observed for ECS (A), ED (B), and BPED (C).

Table S2-1. Average composition of final treated urine across all experiments for each process with influent urine composition included for comparison (also in Table S1-1). For pharmaceuticals, values in parenthesis indicate the number of samples that were non-detect for the compound. For ECS, atenolol was only quantified in 2 of 6 samples because the internal standard was not detected in the other samples.

	Influent Urine	**ECS Effluent**	**ED Effluent**	**BPED Effluent**
TAN (mg/L)	3,280 ± 360	70.4 ± 10	1,110 ± 38	272 ± 21
Cations (mg/L)				
Na^+	1,090 ± 42	293 ± 22	481 ± 19	298 ± 9.3
K^+	1,150 ± 190	73.5 ± 8.5	219 ± 9.2	75.1 ± 0.85
Mg^{2+}	0.418 ± 1.2	-	-	-
Ca^{2+}	-	-	-	-
Anions (mg/L)				
SO_4^{2-}	548 ± 63	603 ± 25	226 ± 21	545 ± 9.8
Cl^-	1,860 ± 70	1990 ± 37	180 ± 3.9	2030 ± 41
PO_4^{3-}	462 ± 14	500 ± 3.0	295 ± 14	452 ± 5.0
Other				
pH	9.32 ± 0.08	1.21 ± 0.38	9.56 ± 0.03	1.60 ± 0.04
COD (mg/L)	3,180 ± 69	2,790 ± 52	2,130 ± 19	2,230 ± 830
Pharmaceuticals (µg/L)				
Atenolol	15.0 ± 7.9	10.9 ± 0.80	17.9 ± 0.52	0.26 (all ND)
Trimethoprim	20.1 ± 3.5	0.57 ± 0.64 (5 of 6 ND)	21.5 ± 1.9	11.7 ± 1.4
Metoprolol	26.1 ± 5.1	13.5 ± 1.8	16.8 ± 1.4	7.28 ± 0.51
Bezafibrate	13.4 ± 1.2	8.89 ± 1.5	10.9 ± 0.50	5.06 ± 5.4
Propranolol	30.7 ± 3.6	1.03 ± 0.62 (2 of 6 ND)	16.7 ± 4.4	4.13 ± 0.38
Carbamazepine	18.6 ± 3.2	7.21 ± 5.6 (2 of 6 ND)	18.3 ± 0.17	15.5 ± 0.56
Diclofenac	28.9 ± 19.6	0.54 (all ND)	22.1 ± 5.2	0.79 (all ND)

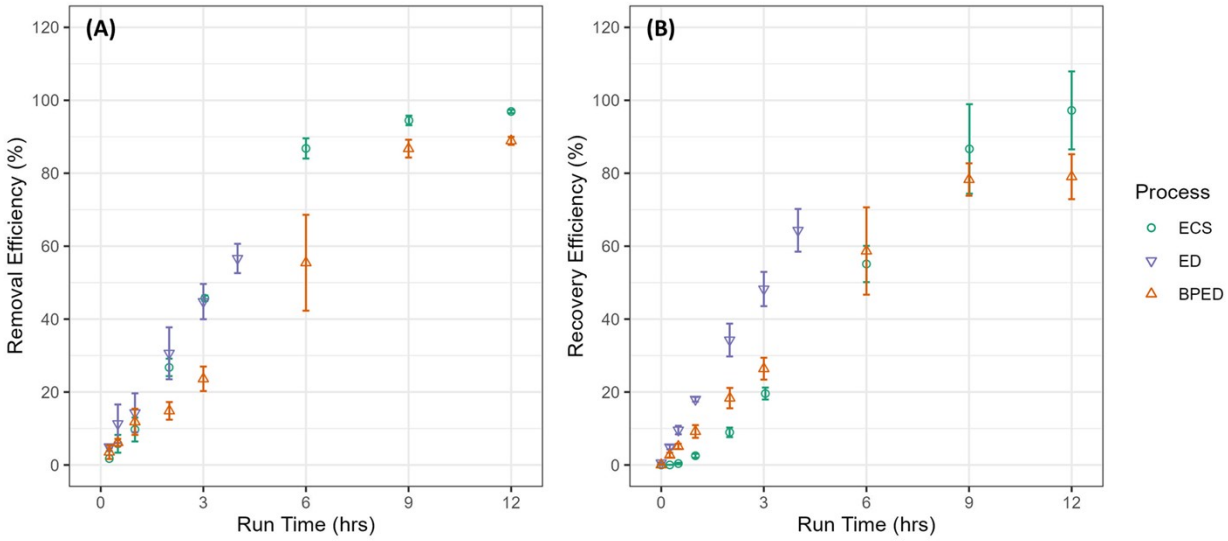

Figure S2-2. TAN removal (A) and recovery efficiencies (B) over time for ECS, ED, and BPED.

Table S2-2. p-values for comparison between final TAN fold changes and removal/recovery efficiencies across processes using two-sided t-tests. Statistically significant differences (p-values < 0.05) are highlighted in yellow.

Fold Change Type / Efficiency	ECS vs. ED	ECS vs. BPED	ED vs. BPED
Removal	0.0030	0.0023	0.0031
Enrichment / Recovery	0.0172	0.0785	0.0401

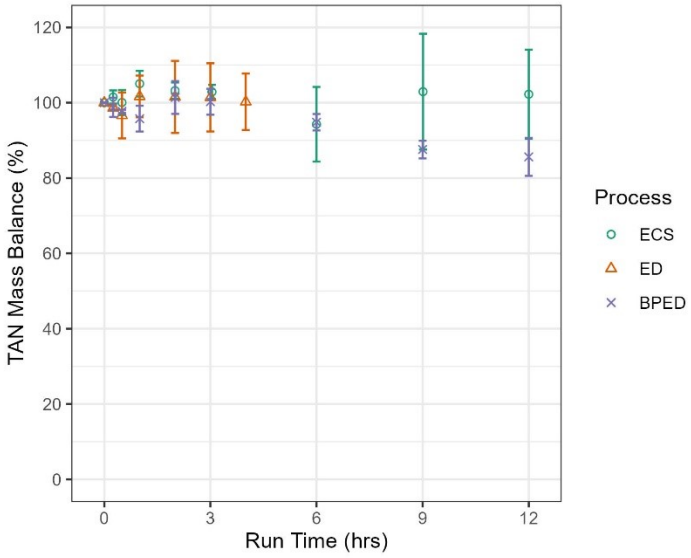

Figure S2-3. Total ammonia nitrogen (TAN) mass balances for ECS, ED, and BPED.

2.2 Fate of Organic Contaminants

Table S2-3. Summary of suspect screening workflow and validation with target analysis.

		ECS	**ED**	**BPED**
Features	Total found	474318	425845	544468
Feature groups	Raw	171296	193429	185542
	After filtering	12562	17735	16235
Formula	Total candidates	262019	398402	357275
	Correctly ranked 1st	5/7	4/7 (ATE not identified)	5/7
	Correctly ranked 2nd	1/7	2/7 (ATE not identified)	1/7
	Correctly ranked 3rd	1/7	-	1/7
Compounds	Total candidates	129001 (raw) / 108537 (filtered)	162146 (raw) / 144623 (filtered)	157636 (raw) / 138590 (filtered)
	Correctly ranked 1st	7/7	6/7 (ATE not identified)	7/7

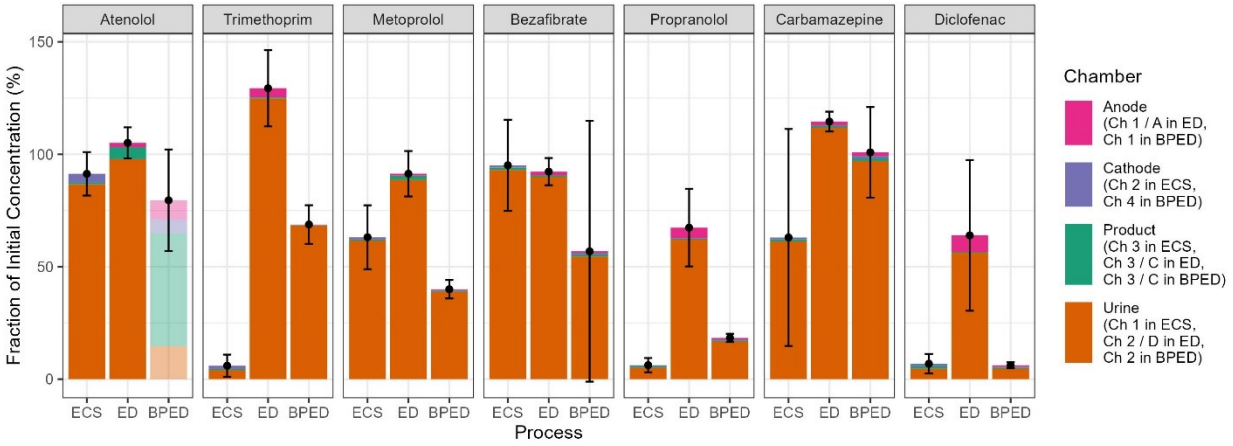

Figure S2-4. Mass balance on target pharmaceuticals for ECS, ED, and BPED. For compounds totaling to less than 100% of the initial concentration, the balance is assumed to be transformed or lost from solution (e.g., sorbed by membrane, volatilized). The mass balance for atenolol during BPED treatment is shown with lighter colors because the internal standard atenolol-d7 was not detected in multiple samples from each replicate experiment, making quantification of atenolol concentration uncertain.

Table S2-4. Target pharmaceuticals, their fates (enrichment and removal ratios, ER and RR), and their properties. pKa's were found in previous literature[19] unless otherwise indicated. MW = molecular weight.

Compound	ER			RR			Structure	MW (g/mol)	pK_a	K_H (atm-m^3/mol)	log K_{ow}
	ECS	ED	BPED	ECS	ED	BPED					
Atenolol (ATE)	0.007 ± 0.0005	0.086 ± 0.011	0.72 ± 0.21	1.0 ± 0.076	1.6 ± 0.15	0.21 ± 0.008	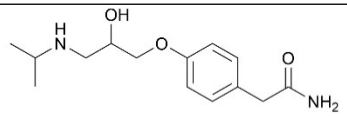	266.34	9.6	$1.378x10^{-18}$ (128)	0.16
Trimethoprim (TMP)	0.006 ± 0.001	0.009 ± 0.0005	0.002 ± 0.00006	0.040 ± 0.03	2.0 ± 0.23	0.87 ± 0.11	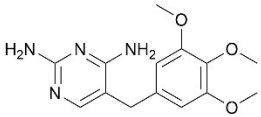	290.32	7.4	$2.4x10^{-14}$	0.91
Metoprolol (MET)	0.006 ± 0.0007	0.032 ± 0.03	0.005 ± 0.004	0.66 ± 0.07	1.4 ± 0.14	0.49 ± 0.04	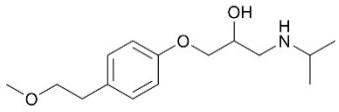	267.37	9.5	$2.1x10^{-11}$	1.88
Bezafibrate (BZF)	0.012 ± 0.002	0.012 ± 0.001	0.011 ± 0.001	1.0 ± 0.05	1.5 ± 0.13	0.69± 0.74	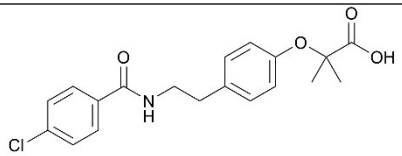	361.8	3.83[115]	$2.24x10^{-11}$ (129)	3.62[129]
Propranolol (PRO)	0.006 ± 0.0009	0.008 ± 0.001	0.006 ± 0.0002	0.059 ± 0.04	1.0 ± 0.38	0.22 ± 0.02	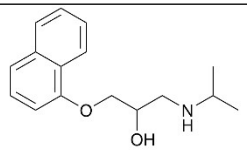	259.34	9.1	$7.98x10^{-13}$ (130)	3.48[130]
Carbamazepine (CBZ)	0.010 ± 0.002	0.014 ± 0.001	0.015 ± 0.0006	0.61 ± 0.5	1.8 ± 0.13	1.3 ± 0.07	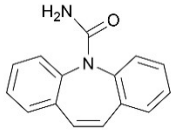	236.27	~1, 13.9[116]	$1.1x10^{-10}$	2.45
Diclofenac (DIC)	0.012 ± 0.002	0.006 ± 0.002	0.006 ± 0.0002	0.052 ± 0.01	0.91 ± 0.09	0.060 ± 0.002	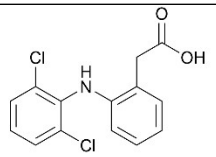	296.1	3.99-4.3[117]	$4.73x10^{-12}$ (131)	4.51

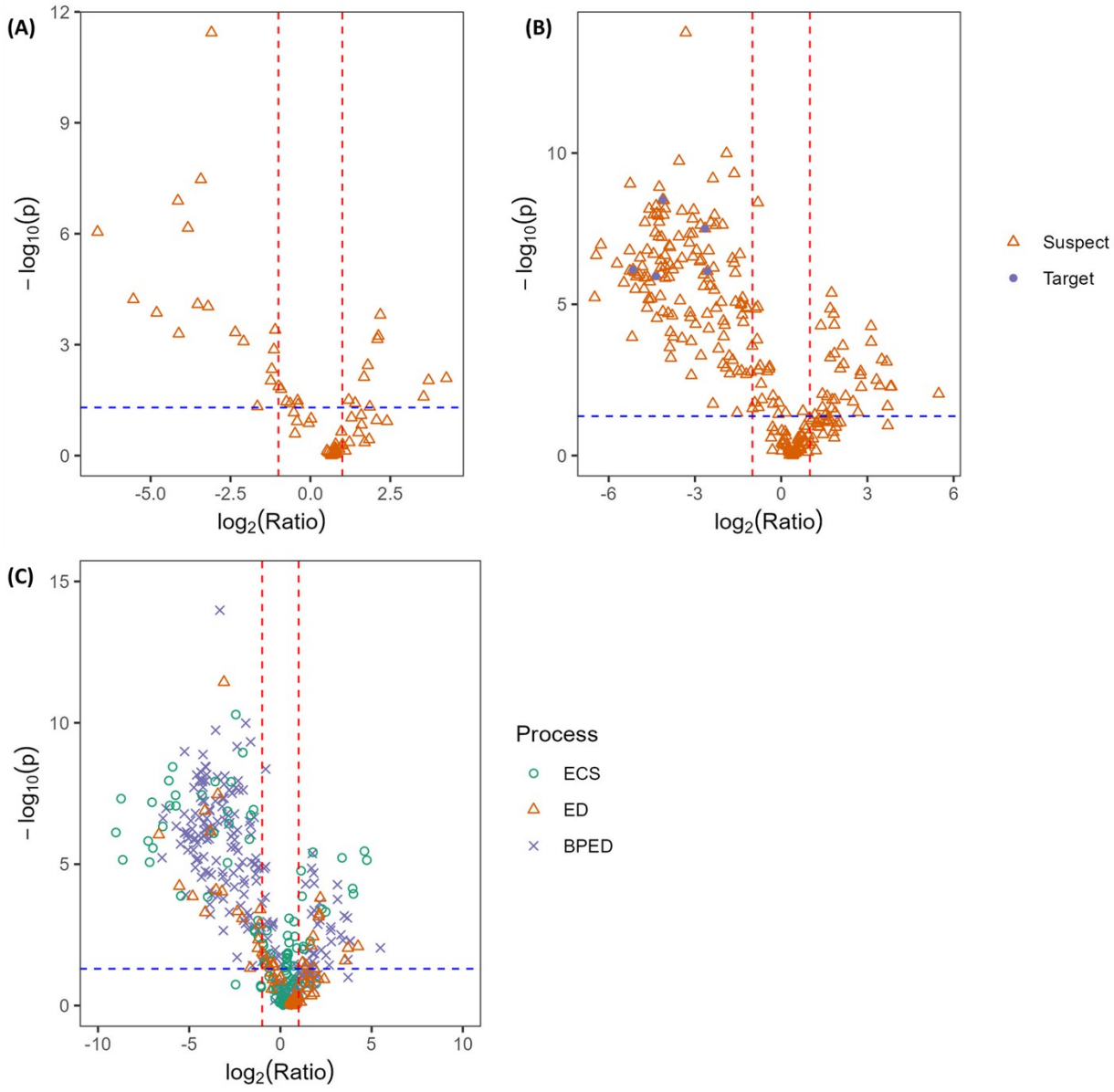

Figure S2-5. Volcano plots for enrichment ratio for ED (A) and BPED (B) as calculated for each of the target pharmaceuticals and all features detected during suspect screening. Volcano plots for enrichment ratio overlaid for all processes (C) based on all features detected during suspect screening.

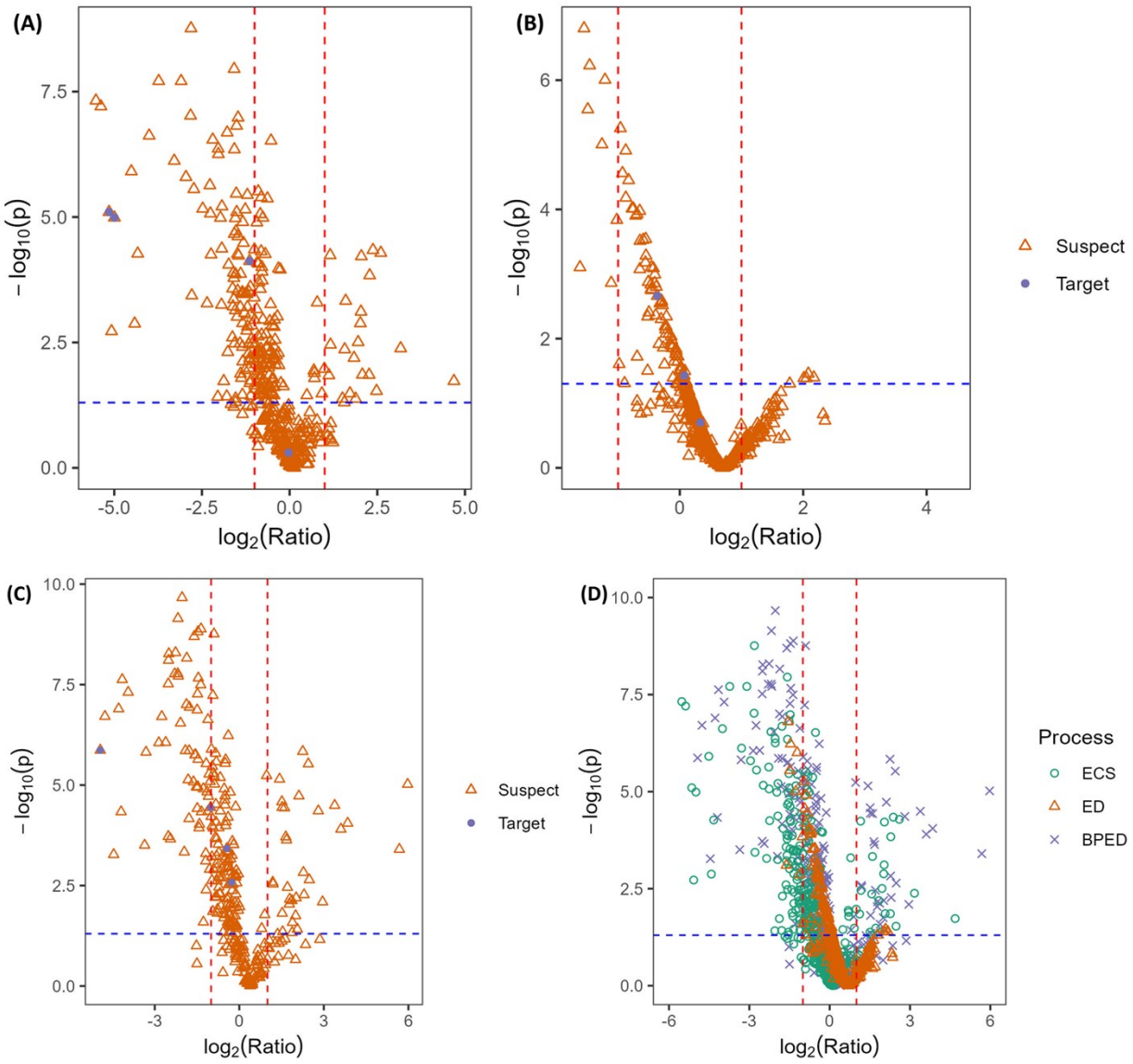

Figure S2-6. Volcano plots for removal ratio for ECS (A), ED (B), and BPED (C) as calculated for each of the target pharmaceuticals and all features detected during suspect screening. Volcano plots for removal ratio overlaid for all processes (D) based on all features detected during suspect screening.

Table S2-5. p-values for comparison between ratios calculated for processes based on all suspect data and feature intensity for targets determined via suspect screening. Statistically significant differences (p-values < 0.05) are highlighted in yellow. Pairwise Wilcox tests were used to compare data because the datasets were generally not normally distributed and did not have similar variances.

	Target Data		Suspect Data	
	Enrichment Ratio	Removal Ratio	Enrichment Ratio	Removal Ratio
ECS vs. ED	-	0.0024	7.87E-07	1.67E-168
ECS vs. BPED	0.0016	0.1359	0.1050	5.28E-18
ED vs. BPED	-	0.0024	1.58E-07	1.84E-57

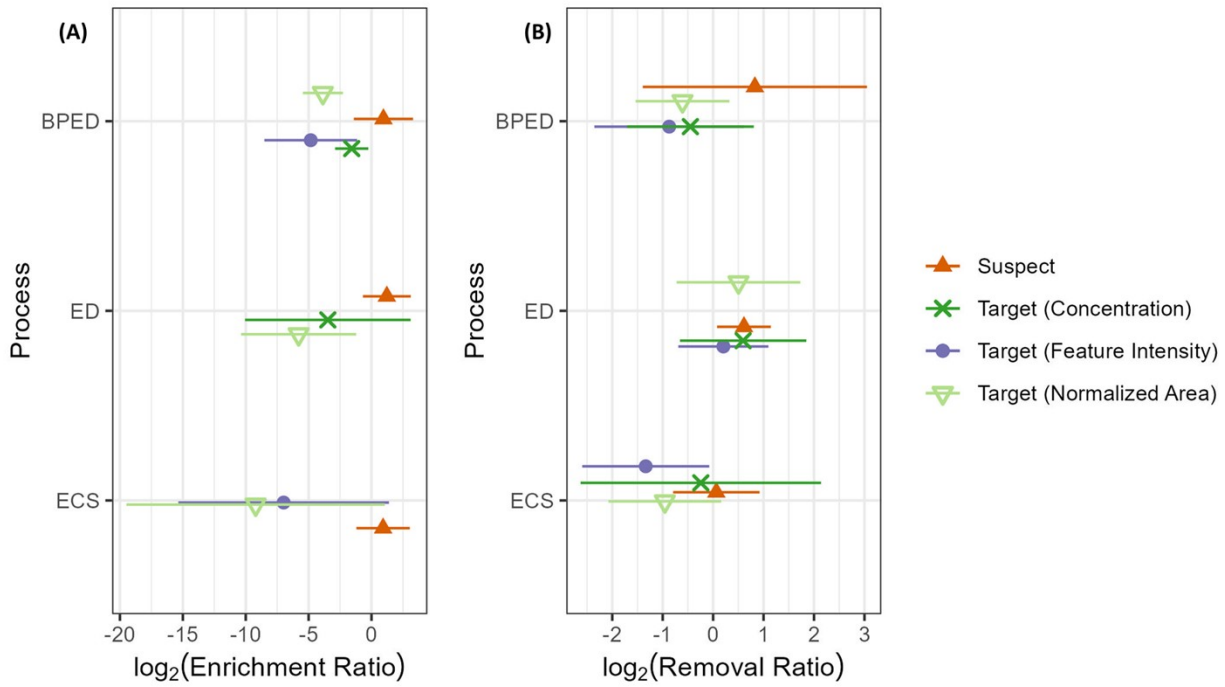

Figure S2-7. Average enrichment (A) and removal (B) ratios calculated for all features detected during suspect screening (orange), for features identified as target compounds during suspect screening (purple) and for target compounds quantified separately via target analysis (two shades of green). For target compounds quantified via target analysis, ER and RR were calculated in two ways: (1) using concentrations determined by target analysis and (2) using the peak area for the target compound normalized to the peak area for the respective internal standard. For ECS, no ER based on target concentrations is shown because the concentrations were determined to be below method LOQ/LOD. No average ER for targets is shown for ED because none of the features detected in the product chamber were identified as target compounds during suspect screening. Results of statistical analysis for comparisons of ratios calculated using different methods are shown in Table S2-7.

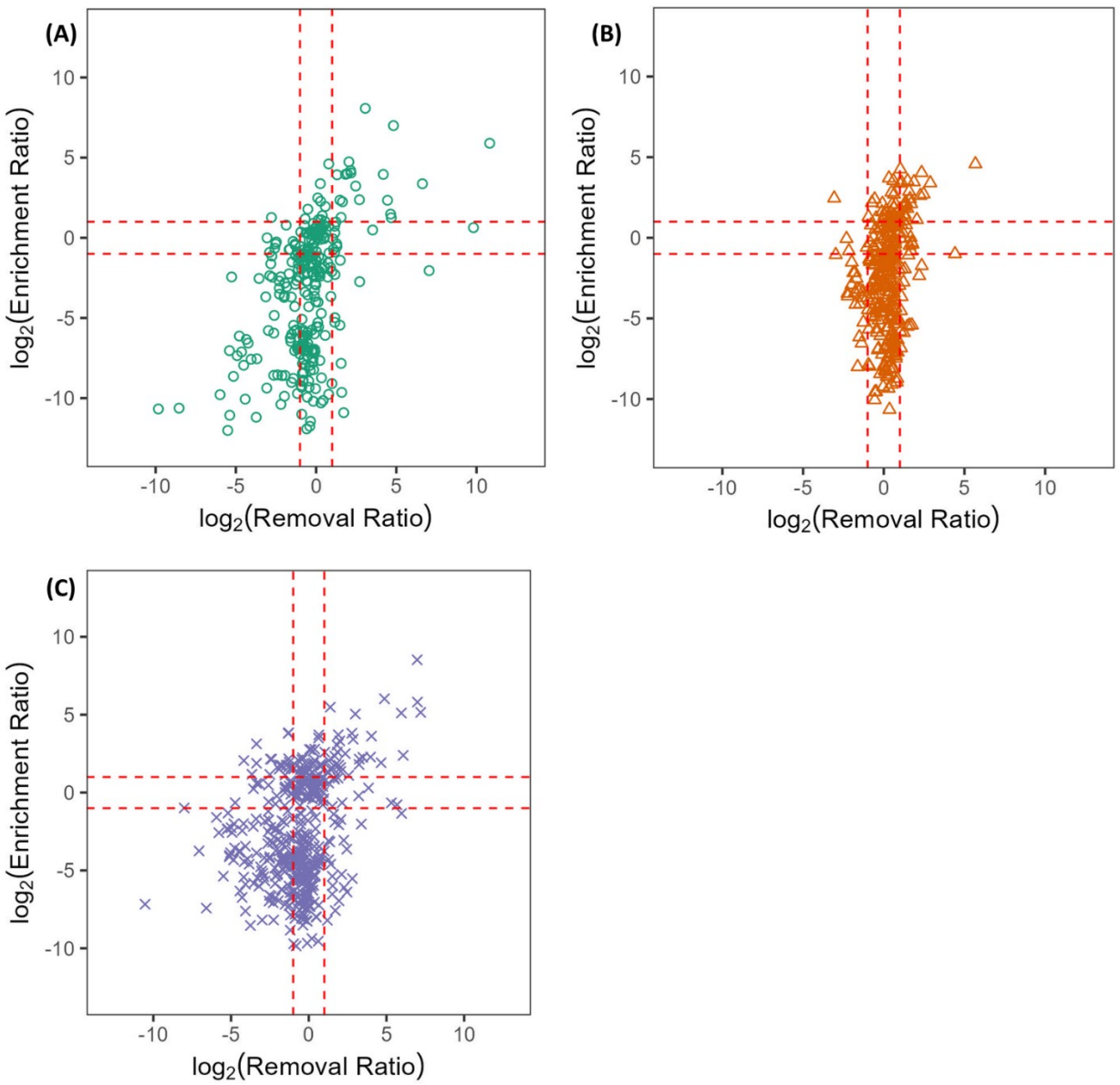

Figure S2-8. Enrichment ratio vs. removal ratio for ECS (A), ED (B), and BPED (C) for all features detected during suspect screening.

Table S2-6. p-values for comparison between ratios calculated from target and suspect screening data for each process. Statistically significant differences (p-values < 0.05) are highlighted in yellow. Pairwise Wilcox tests were used to compare data because the datasets were generally not normally distributed and did not have similar variances.

	ECS	ED	BPED
Enrichment Ratio	0.0002	-	2.94E-07
Removal Ratio	0.0004	0.0460	0.0038

Table S2-7. p-values for comparison between ratios calculated for target data for each process using different calculation methods. Statistically significant differences (p-values < 0.05) are highlighted in yellow. Pairwise Wilcox tests were used to compare data because the datasets were generally not normally distributed and did not have similar variances.

	ECS	ED	BPED
Enrichment Ratio			
Suspect screening intensity vs. normalized area	0.3355	-	0.0007
Suspect screening intensity vs. concentration	-	-	0.6805
Normalized area vs. concentration	-	0.0113	0.0062
Removal Ratio			
Suspect screening intensity vs. normalized area	0.1618	0.0262	0.6652
Suspect screening intensity vs. concentration	0.0012	0.0225	0.3491
Normalized area vs. concentration	0.0905	0.9214	0.6552

2.3 Product Purity

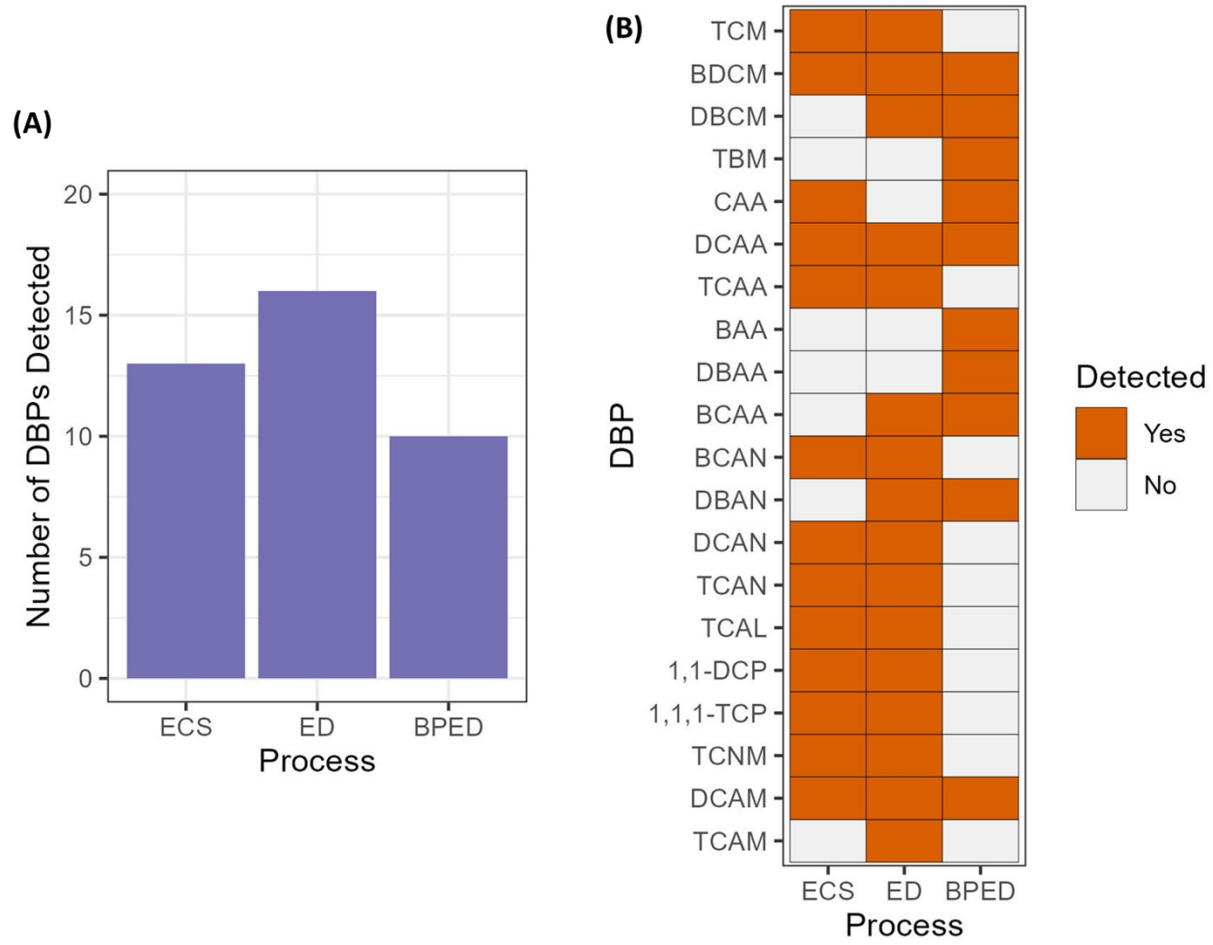

Figure S2-9. Disinfection byproducts detected in anode chambers. (A) Number of DBPs detected for each process. (B) Identity of DBPs detected.

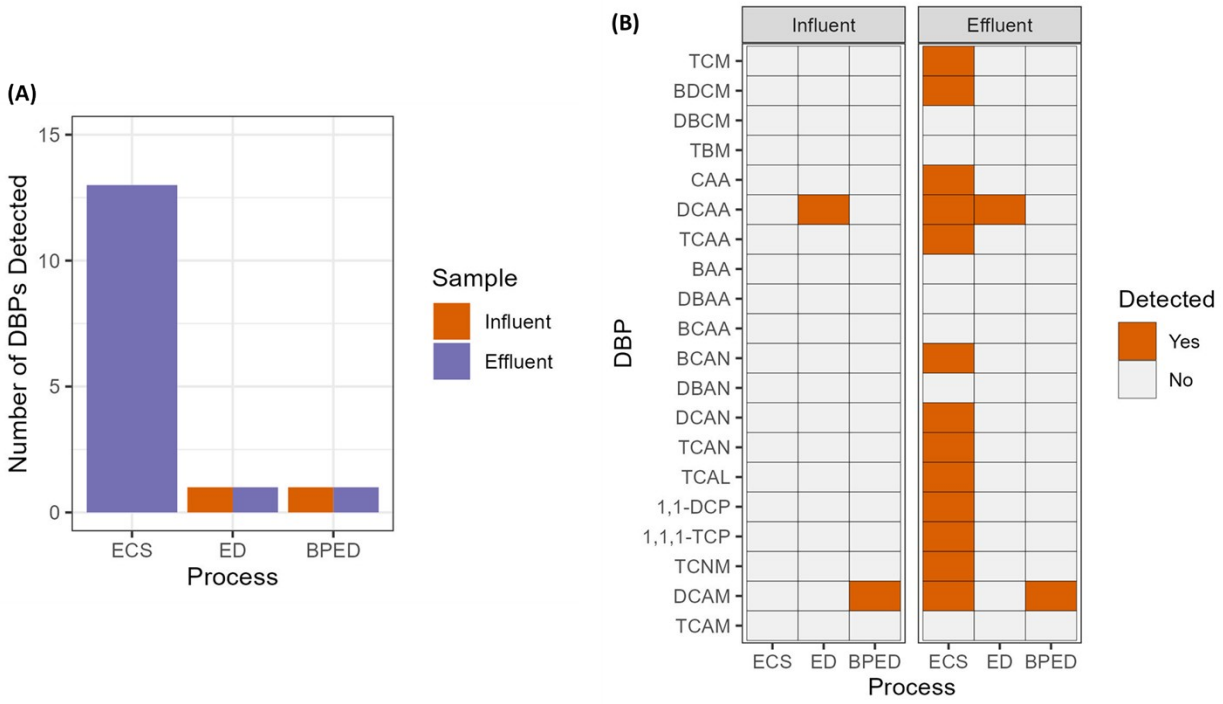

Figure S2-10. Disinfection byproducts detected in influent and treated urine. (A) Number of DBPs detected for each process. (B) Identity of DBPs detected.

Despite little DBP migration to products in all processes, significant DBP formation occurred in the anode chambers (Figure S2-9). All classes of DBPs were detected in the anode chamber for ED, and all except HNMs and HALs were detected in the anode chamber of BPED. In ED, chloride ions readily transferred from the diluate chamber to the anode chamber via electro-migration across the AEM (Figure 1B) and could then be oxidized at the anode. The observed DBP concentrations were greater than in ECS despite operating ED for only 4 hours (vs. 12 hours for ECS). Therefore, a greater proportion of the current passed through the system was likely consumed by chloride oxidation in ED than in ECS possibly because there were fewer other species present in the anolyte (0.1 M Na_2SO_4 vs. urine) that could interact with the electrode. With extended operation and continued recirculation of the anolyte, DBP formation in the anode chamber of ED would likely change in rate and types of compounds formed as the anolyte continues to accumulate chloride ions and organic species due to transmembrane migration of organics and buildup of DBPs in the anolyte. This accumulation of contaminants could result in diffusion of DBPs and other transformation products into the diluate chamber, affecting the quality of treated urine.

For BPED, mainly HAAs and THMs, and to a lesser extent HANs, formed in the anode. Therefore, the BPM separating the anode and diluate chambers appeared to be only partially effective in preventing ion and organic crossover from the diluate chamber to the anode chamber or the BPM released DBP precursors. Neutral organic molecules, such as organic acids at low pH conditions existing in urine during BPED, can accumulate in the low-pH cation exchange layer of the BPM by diffusion.[132,133] Neutral molecules can continue diffusing through the anion exchange layer, and deprotonation could also occur due to the high pH in this part of the BPM, enhancing transport of

negatively charged organics toward the anode. Amino acids are known precursors of HAAs[134] and found in urine,[135] which could explain HAA formation in BPED. DBP formation in the anode Chambers of ED and BPED illustrated the importance of considering systems-scale management of DBPs, rather than focusing only on product and effluent urine characteristics.

Speciation of DBPs in the anolyte (urine for ECS and 0.1 M Na_2SO_4 for ED and BPED) depended on chlorine concentrations, TAN concentrations, and pH. In ECS, TCM was the dominant THM, and the dominant HAAs were DCAA, followed by CAA and TCAA. DCAN was the dominant HAN, but TCAN was also observed. DCAM dominated HAMs, and for HKs, 1,1-DCP dominated over 1,1,1-TCP. Across groups, the less or intermediately chlorinated species dominated, and brominated DBPs were not detected in ECS-treated urine. For ED, as for ECS, TCM was the dominant THM and DCAN was the dominant HAN. However, for HAAs, HAMs, and HKs, the more chlorinated species accounted for greater fractions than in ECS. DCAA remained dominant but TCAA became a larger fraction of total HAAs over time. DCAM and TCAM accounted for similar fractions of total HAMs over time, and 1,1-DCP and 1,1,1-TCP accounted for similar fractions of HKs over time. The fact that more chlorinated species dominated in ED compared to ECS despite shorter operation of ED could be a result of a greater ratio of chloride ions (1,660 ± 370 mg/L in ED vs. 1,410 ± 26 mg/L in ECS at final time) to precursor organic compounds (812 mg/L COD in ED vs. 2,790 ± 52 mg/L COD in ECS at final time) in the ED anolyte than in urine, effectively equivalent to a greater free chlorine dose.[136,137] In ECS, $HOCl/OCl^-$ generated by chloride oxidation could react with NH_3/NH_4^+ to form monochloramine while these reactions are unlikely in ED due to the absence of TAN in the anode chamber. Reactions of organics with chlorine and chloramines favor formation of different DBPs; for example, oxidation with monochloramines can lead to greater 1,1-DCP formation than oxidation with free chlorine, and formation of trichlorinated species, such as 1,1,1-TCP, is less likely with monochloramines than free chlorine.[138] Conducting experiments with synthetic urine containing model DBP precursors could provide additional insights into the mechanisms at play.

In BPED, brominated DBPs played a significant role in the anode unlike in ECS and ED. TBM was the dominant THM, with BDCM and DBCM also detected. BAA and DBAA were the dominant HAAs, and DBAN was the dominant HAN. The greater occurrence of brominated DBPs in BPED than in ECS and ED increased concerns because brominated species are often more toxic than chlorinated analogues.[139] Bromide concentrations in urine and all reactor chambers were below detection (< 1 mg/L). The BPM was the only unique component to the reactor for BPED, suggesting that the formation of brominated DBPs could be related to the BPM, which showed some blistering and delamination after use (Figure S2-11). According to the manufacturer, the BPM (Fumasep FBM) consisted of sulfonated cross-linked poly-ether-ether-ketone (PEEK) as the cation exchange layer, a polysulfone with bicyclic amines as the anion exchange layer, and a polyacrylic acid/polyvinyl pyridine salt complex in the junction.[140] Therefore, its degradation would not have been expected to be a bromine source unless bromine-containing compounds were used during membrane synthesis and impurities remained. Despite visual evidence, degradation did not appear to allow significant mixing between Chambers 1 and 2 based on chloride, sulfate, and phosphate ion concentrations (Figure S2-12, Figure S2-13, Figure S2-14). The BPM was loaded with Na^+ and Cl^- in the cation and anion exchange layers, respectively,[141] and stored in

NaCl solution. Even though the BPM was rinsed and immersed in water for at least 12 hours before experiments, Na^+ and Cl^- ions likely remained inside the membrane, contributing to the measurable chloride concentration and chlorinated DBPs in Chamber 1 (Figure S2-12, Figure S2-9). Further investigation, including membrane characterization (e.g., scanning electron microscopy with energy dispersive x-ray spectroscopy, Fourier Transform Infrared Spectroscopy), is needed to understand membrane degradation and explain the unique formation of brominated DBPs in BPED.

DBPs pose a greater risk to effluent urine quality in ECS than ED and BPED (Figure S2-10). Although BPED and ECS were operated longer than ED (12 hours vs. 4 hours) and achieved greater TAN removal/recovery, comparing DBP occurrence at the final timepoints for each process is worthwhile because the final times represented the maximum DBP formation and TAN treatment given the study's experimental conditions. At least one species in each class of quantified DBPs, including regulated DBPs like HAAS and DCAN, was detected in urine treated by ECS. In contrast, for ED, only HAAs and HAMs were detected in the urine, and for BPED, only HAAs, HAMs, HKs, and THMs were detected in urine. In ECS, urine was directly exposed to the anode, while in ED and BPED, urine was separated from the anode by an anion exchange membrane (AEM) and a bipolar membrane (BPM), respectively. Therefore, chloride could be readily oxidized to chlorine at the anode, leading to the formation of hypochlorite. The active chlorine species could easily react with organic compounds in urine because the chamber was well-mixed. Initial and final chloride concentrations were similar (1,840 ± 69 initial vs. 1,410 ± 26 mg/L final, p-value = 0.0477), indicating only a small proportion of chloride was oxidized (Figure S2-12A). Given that separation of anodes from urine by a membrane in ED and BPED mitigated DBP formation in urine, such a reactor architecture would be beneficial in ECS.

Other approaches for DBP mitigation can prevent their formation or remove DBPs after formation. To prevent formation, DBP precursors could be removed from urine before electrochemical treatment (e.g., using ion exchange for chloride ions). Membranes to separate electrodes from urine could be combined with using alternative redox couples (e.g., iron-based with graphite electrodes[142]) instead of water splitting to both reduce DBP formation and energy consumption. Controlling operational parameters (e.g., applied current density, residence time in chambers, duration of treatment) could also reduce DBP formation, as could improved electrode designs.[67] Another strategy for preventing DBP formation is introducing influent urine to the cathode chamber instead of the anode chamber for ECS.[143] This configuration would prevent urine from being exposed to an oxidizing environment but could lead to other challenges, such as fouling of the gas permeable membrane and product contamination with small, volatile compounds present in the influent. If strategies for preventing DBP formation are ineffective or not practical, post-treatment with activated carbon can remove halogenated organics, while ion exchange or membrane filtration could remove inorganic DBPs (e.g., chlorate, perchlorate, bromate).[25,67] Electrochemical nutrient recovery technologies could also be coupled with electrochemical dehalogenation or reduction technologies to remove DBPs.[67]

Figure S2-11. Photo of bipolar membrane after use during BPED experiment. Two example areas showing blistering and delamination are circled in red.

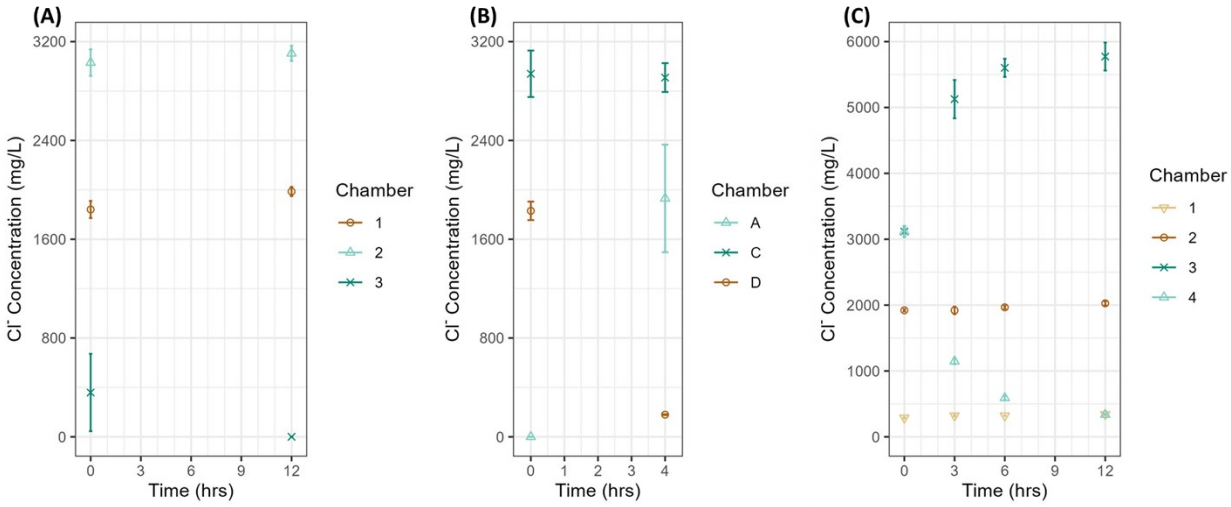

Figure S2-12. Chloride concentrations in all chambers for ECS (A), ED (B), and BPED (C). The concentrations shown account for volume reduction due to sample collection throughout experiments.

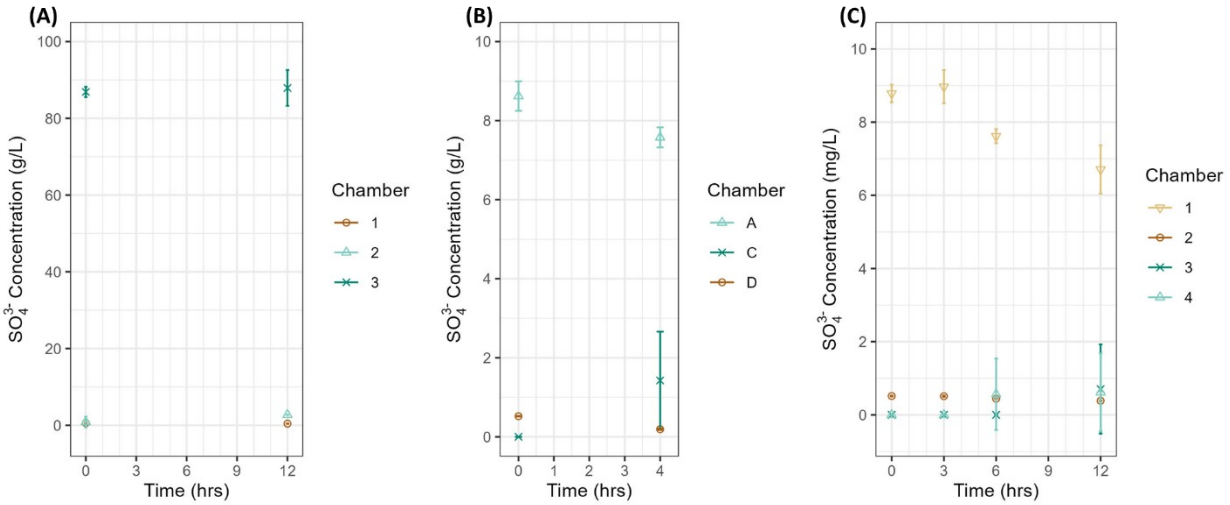

Figure S2-13. Sulfate concentrations in all chambers for ECS (A), ED (B), and BPED (C). The concentrations shown account for volume reduction due to sample collection throughout experiments.

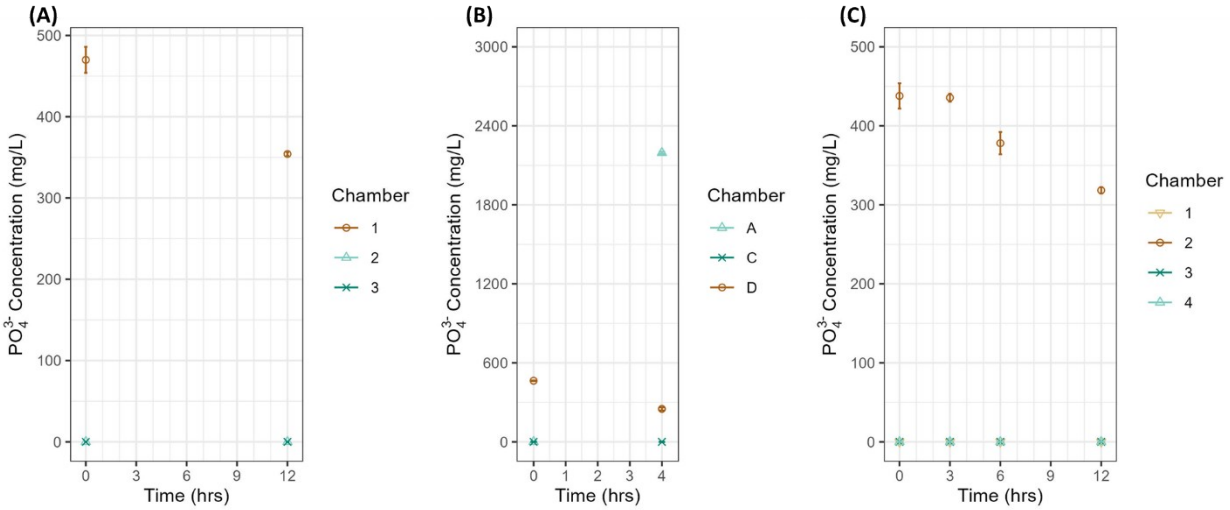

Figure S2-14. Phosphate concentrations in all chambers for ECS (A), ED (B), and BPED (C). The concentrations shown account for volume reduction due to sample collection throughout experiments.

2.4 Identification of Priority Compounds

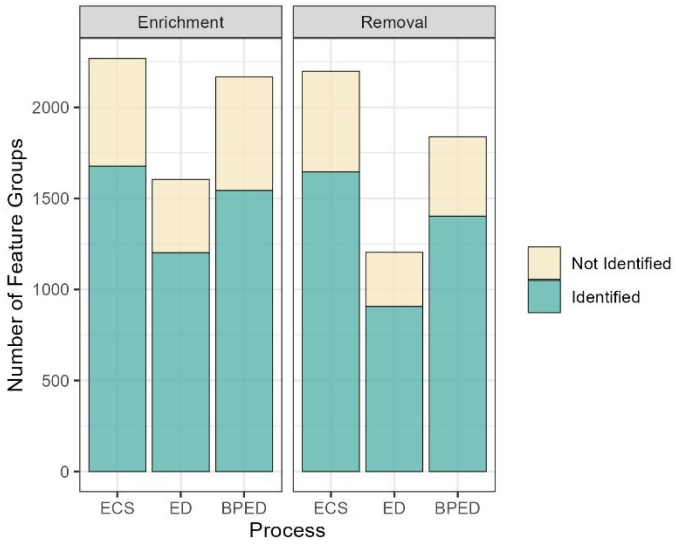

Figure S2-15. Fraction of all detected feature groups identified during suspect screening.

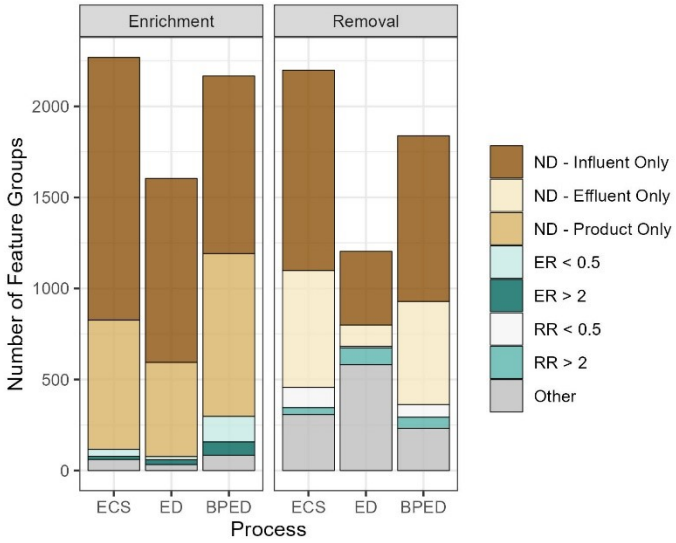

Figure S2-16. Fraction of priority compounds (enrichment ratio less than 0.5 or greater than 2, removal ratio less than 0.5 or greater than 2, and p-value less than 0.05) and fraction of non-detects (either influent only or effluent only). Feature groups labeled as "Other" were detected in both paired samples (i.e., influent and effluent or influent and product) but exhibited ER or RR values between 0.5 and 2 and/or had p-values greater than 0.05. Feature groups were discarded from analysis if they were detected in more than zero but less than 7 of 9 or 5 of 6 replicate samples. The discarded feature groups based on ER accounted for 83% (10,730 of 12,998), 91% (16,679 of 18,283), and 87% (14,627 of 16,794) of feature groups for ECS, ED, and BPED, respectively. The discarded feature groups based on RR accounted for 83% (10,799 of 12,998), 93% (17,079 of 18,283), and 89% (14,956 of 16,794) of feature groups for ECS, ED, and BPED, respectively.

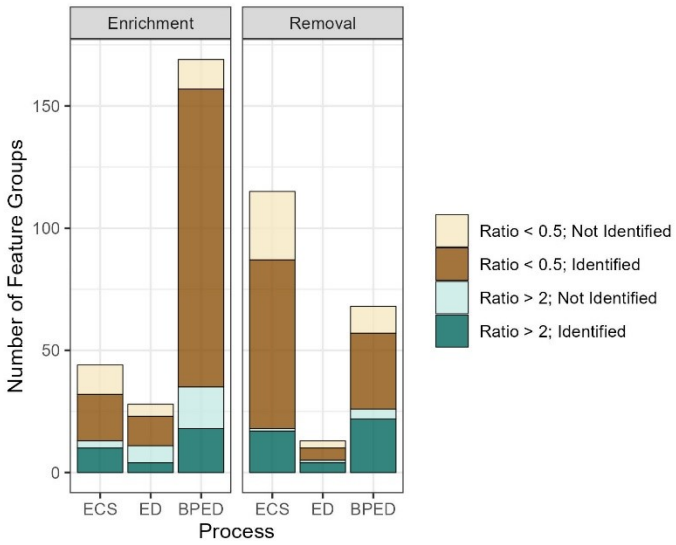

Figure S2-17. Fraction of priority feature groups identified during suspect screening.

Table S2-8. Priority compounds identified through suspect screening.

Table S2-8 is included as an Excel spreadsheet: Kogler_et_al_priorityCompoundIDs_TableS2-7.xlsx.

Table S2-9. Properties of identified compounds categorized as priority compounds based on ER for multiple processes. Properties were taken from Pubchem unless otherwise indicated.

Category	Compound	MW (g/mol)	pKa	K_H (atm-m^3/mol)	log K_{ow}	Structure
BPED & ED, ER > 2	Linoleic acid	280.4	4.77	$2.0x10^{-7}$	7.05	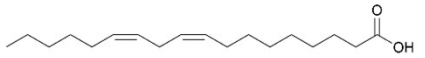
BPED & ED, ER > 2	Ricinoleic acid	298.5	4.74	-	6.19	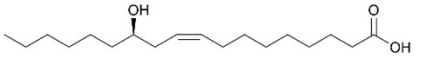
BPED & ED, ER > 2	Methyl ricinoleate	312.5	-	$1.47x10^{-7}$	6.48	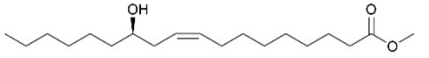
BPED & ED, ER < 0.5	Carbamazepine	236.27	~1, 13.9[116]	$1.1x10^{-10}$	2.45	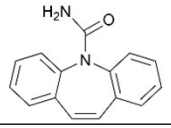
BPED & ED, ER < 0.5	Bakuchiol	256.4	-	-	-	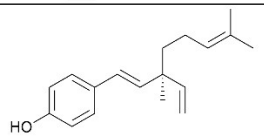
ECS & BPED, ER > 2	Ne-Boc-L-lysine	110.2	2.53 ~9-10[101,102]	-	-	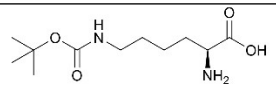
ECS & BPED, ER < 0.5	(2E,6Z)-N-ethylnona-2,6-dienamide	181.27	-	-	-	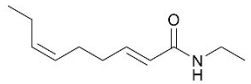
ECS & BPED, ER < 0.5	Benzylideneacetone	146.19	-	-	-	
ECS & BPED, ER < 0.5	beta-Damascenone	190.28	-	-	-	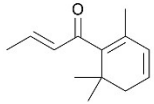
ECS, ER > 2 & BPED, ER < 0.5	Pinonic acid	184.23	4.82	-	-	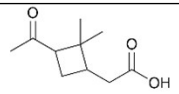
ECS & ED, ER > 2	1,4-dimethyl-2,3,4,5,6,7-hexahydro-1h-1,6-methano-4-benzazonin-10-ol	231.33	-	-	-	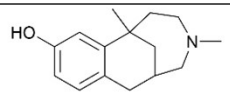
ECS & ED, ER < 0.5	Bicyclo(2.2.2)octane	110.2	-	-	-	

Several priority compounds had RR < 0.5, indicating high extent of removal from urine, for ECS and BPED: hexadecyl 4-chloro-3-[2-(5,5-dimethyl-2,4-dioxo-1,3-oxazolidin-3-yl)-4,4-dimethyl-3-oxopentamido]benzoate; linalool; lidocaine; 3-pyridin-3-ylpropyl (2S)-1-(3,3-dimethyl-2-oxopentanoyl)pyrrolidine-2-carboxylate; and levonorgestrel (Table S2-10). These compounds contain electron-rich groups (e.g., amines, aromatic rings, alkenes, alkynes, heterocycles), making them susceptible to reaction with electrophilic chlorine species that can form in Chamber 1 of ECS. Such degradation could have occurred in BPED due to potential loss of BPM integrity (see Section S2.3). Removal by electromigration is also possible for lidocaine due to protonation and a resulting positive charge at pH's below about 7.9. Two priority features with RR > 2 for ECS and BPED were identified: 1,3-bis(2,2-dimethyl-1,3-dioxolan-4-ylmethyl)carbodiimide and 1-ethylpiperidine. The high RR indicates that these compounds are degradation products and/or that they are not degraded or transported out of the urine. 1-Ethylpiperidine is an intermediate in pharmaceutical synthesis, suggesting that it could be a degradation product of pharmaceuticals.

Table S2-10. Properties of identified compounds categorized as priority compounds based on RR for BPED and ECS. Properties were taken from Pubchem unless otherwise indicated.

Category	Compound	MW (g/mol)	pKa	K_H (atm-m^3/mol)	log K_{ow}	Structure
RR < 0.5	Hexadecyl 4-chloro-3-[2-(5,5-dimethyl-2,4-dioxo-1,3-oxazolidin-3-yl)-4,4-dimethyl-3-oxopentamido]benzoate	649.3	-	-	-	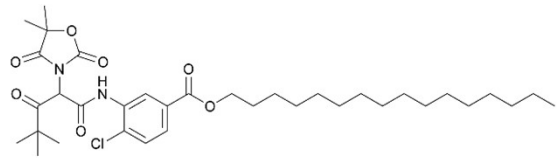
RR < 0.5	Linalool	154.25	-	2.15×10^{-5}	2.97	
RR < 0.5	Lidocaine	234.34	7.86	1.3×10^{-10}	2.44	
RR < 0.5	3-pyridin-3-ylpropyl (2S)-1-(3,3-dimethyl-2-oxopentanoyl)pyrrolidine-2-carboxylate	360.4	-	-	-	
RR < 0.5	Levonorgestrel	312.4	-1.5, 17.91	7.7×10^{-10}	3.48	
RR > 2	1,3-Bis(2,2-dimethyl-1,3-dioxolan-4-ylmethyl)carbodiimide	270.32	-	-	-	
RR > 2	1-Ethylpiperidine	113.2	10.45	-	-	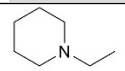

Table S2-11. Uses of identified priority compounds, as indicated on PubChem.

Category	Compound	Use
Priority compound based on ER	Linoleic acid	Component in topical medications and cosmetics, component of human diet
	Ricinoleic acid	Cosmetic ingredient, contraceptive gel
	Methyl ricinoleate	Cosmetic ingredient
	Carbamazepine	Anticonvulsant drug, analgesic drug
	Bakuchiol	Antimicrobial cosmetic
	Ne-Boc-L-lysine	Related to preparations of treatments for neoplasms, communicable diseases, diabetes, and other diseases
	(2E,6Z)-N-ethylnona-2,6-dienamide	Flavoring agent
	Benzylideneacetone	Flavoring agent, fragrance
	beta-Damascenone	Flavoring agent, fragrance
	Pinonic acid	Related to preparation of drugs for toxemia, cyanosis, typhoid fever, and other conditions
	1,4-dimethyl-2,3,4,5,6,7-hexahydro-1h-1,6-methano-4-benzazonin-10-ol	Related to preparation of drugs for pain, neoplasms, and other conditions
	Bicyclo(2.2.2)octane	Related to preparation of drugs for thrombosis, neoplasms, dementia, and other conditions
Priority compounds based on RR	Hexadecyl 4-chloro-3-[2-(5,5-dimethyl-2,4-dioxo-1,3-oxazolidin-3-yl)-4,4-dimethyl-3-oxopentamido]benzoate	Photosensitizer
	Linalool	Flavoring agent, adjuvant, insecticide
	Lidocaine	Anesthetic, anti-arrhythmia drug
	3-pyridin-3-ylpropyl (2S)-1-(3,3-dimethyl-2-oxopentanoyl)pyrrolidine-2-carboxylate	Parkinson disease drug (terminated)
	Levonorgestrel	Contraceptive drug, hormone therapy
	1,3-Bis(2,2-dimethyl-1,3-dioxolan-4-ylmethyl)carbodiimide	Related to preparation of treatments for neoplasms, thrombosis, spontaneous platelet aggregation, and other diseases
	1-Ethylpiperidine	Intermediate in chemical manufacturing

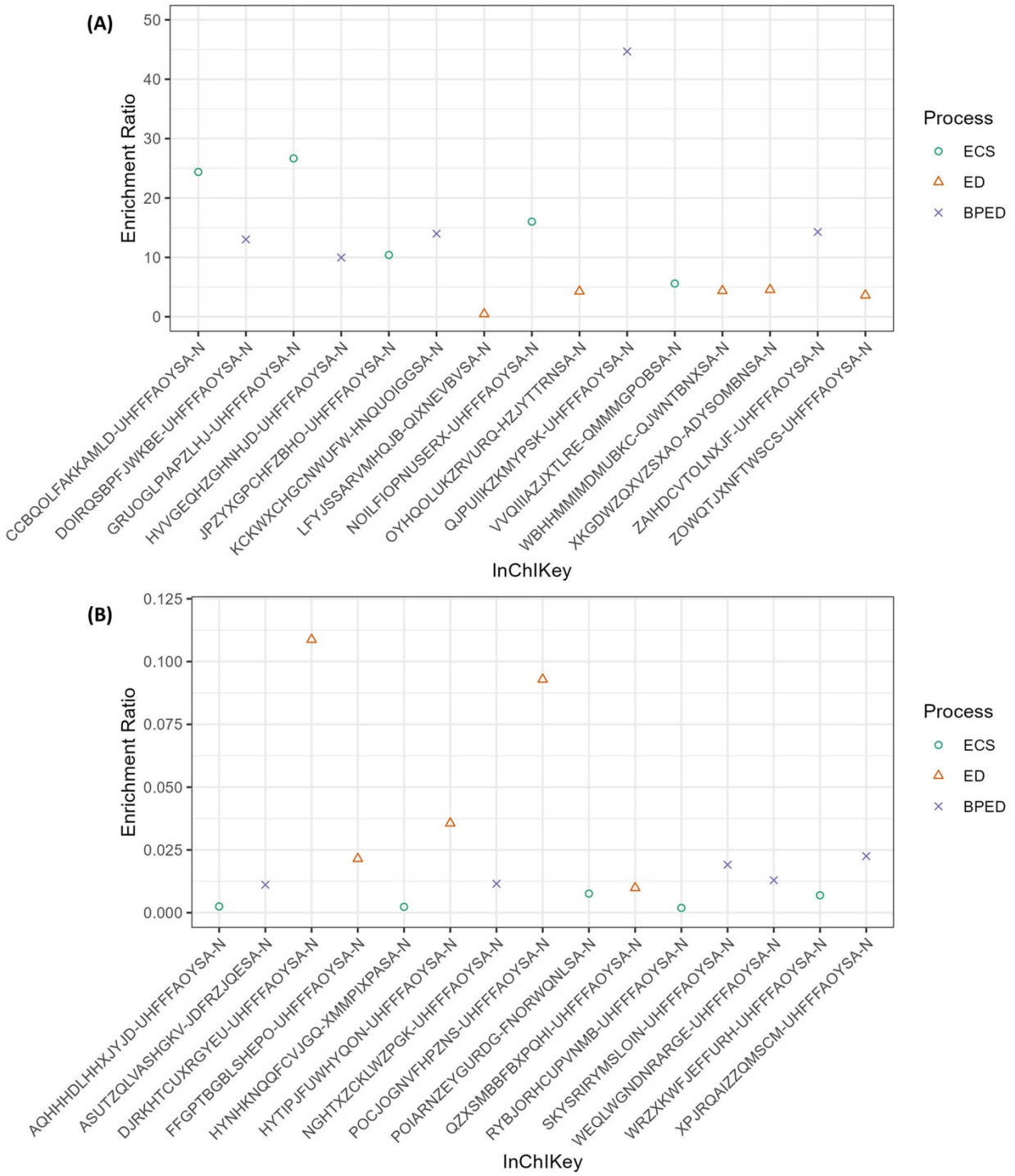

Figure S2-18. Extreme enrichment and removal ratios for priority features that were identified: highest 5 ERs (A), lowest 5 ERs (B), highest 5 RRs (C), and lowest 5 RRs (D) for each process.

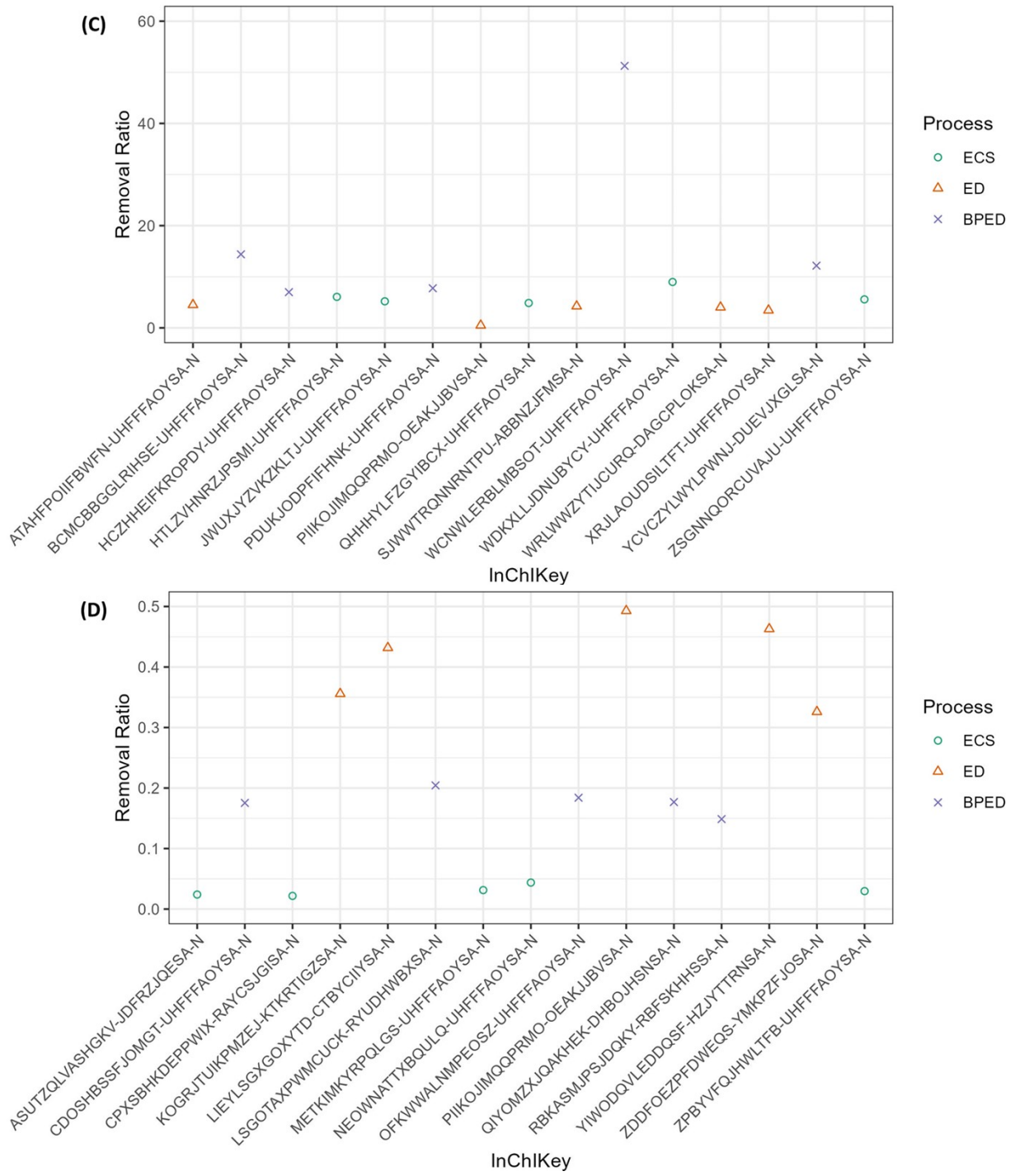

Figure S2-18. Extreme enrichment and removal ratios for priority features that were identified: highest 5 ERs (A), lowest 5 ERs (B), highest 5 RRs (C), and lowest 5 RRs (D) for each process. (continued)

2.5 Mechanistic Understanding of Compound Fate

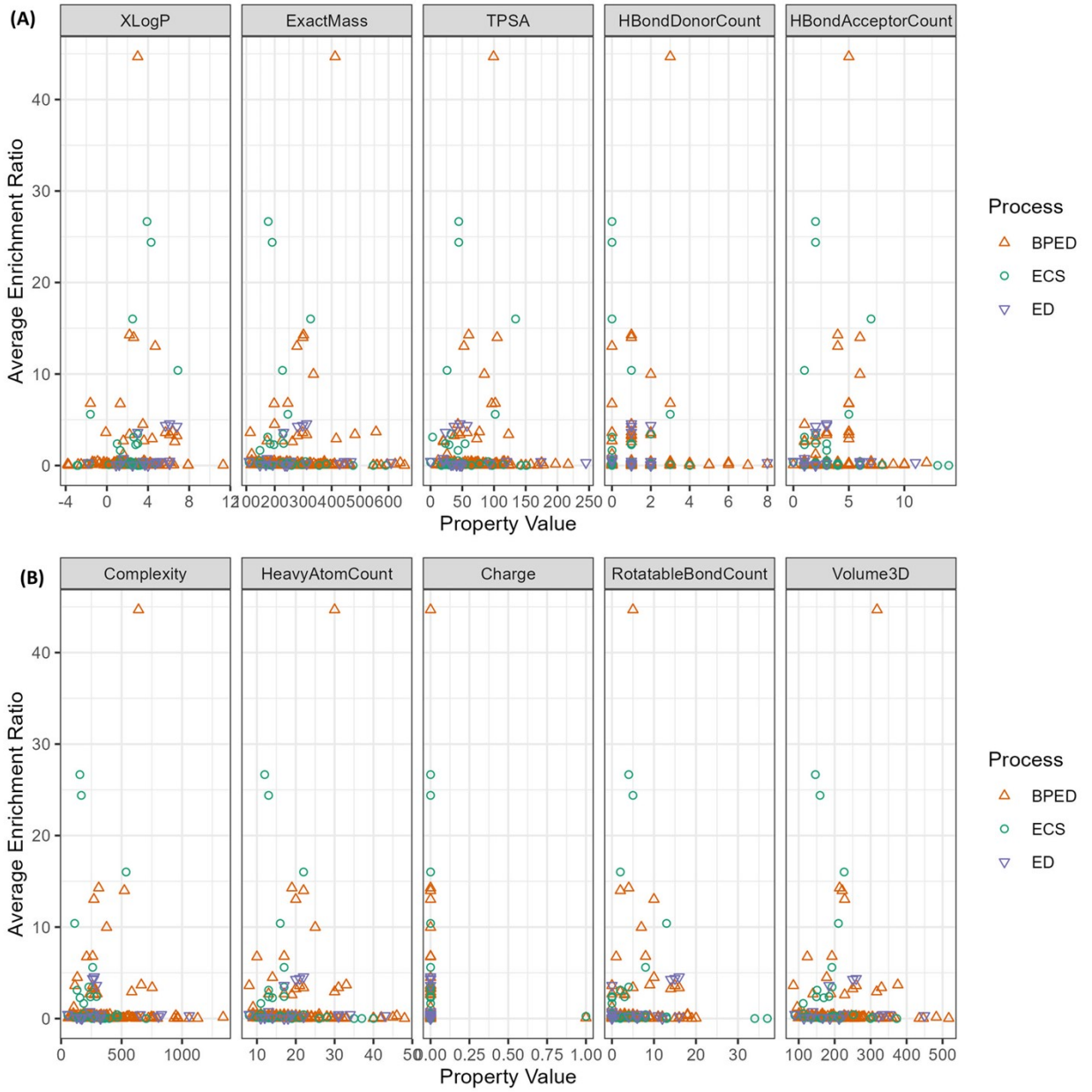

Figure S2-19. Relationships between compound properties and enrichment ratio for priority compounds. Figure 4 shows these relationships for the properties shown in panel A for ECS only. Spearman correlation and linear regression results are summarized in Table S2-12 and Table S2-13.

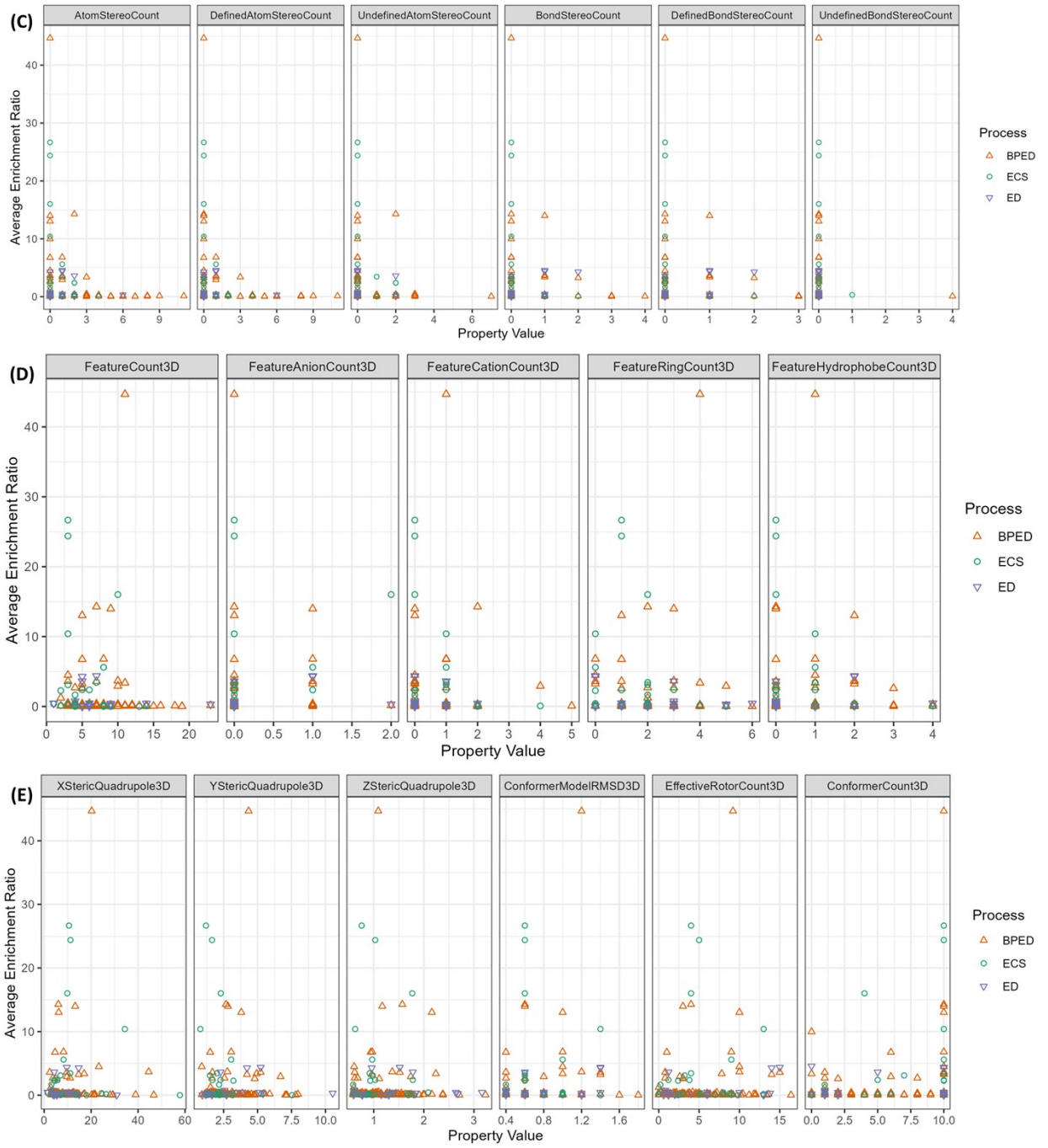

Figure S2-19. Relationships between compound properties and enrichment ratio for priority compounds. Figure 4 shows these relationships for the properties shown in panel A for ECS only. Spearman correlation and linear regression results are summarized in Table S2-12 and Table S2-13. (continued)

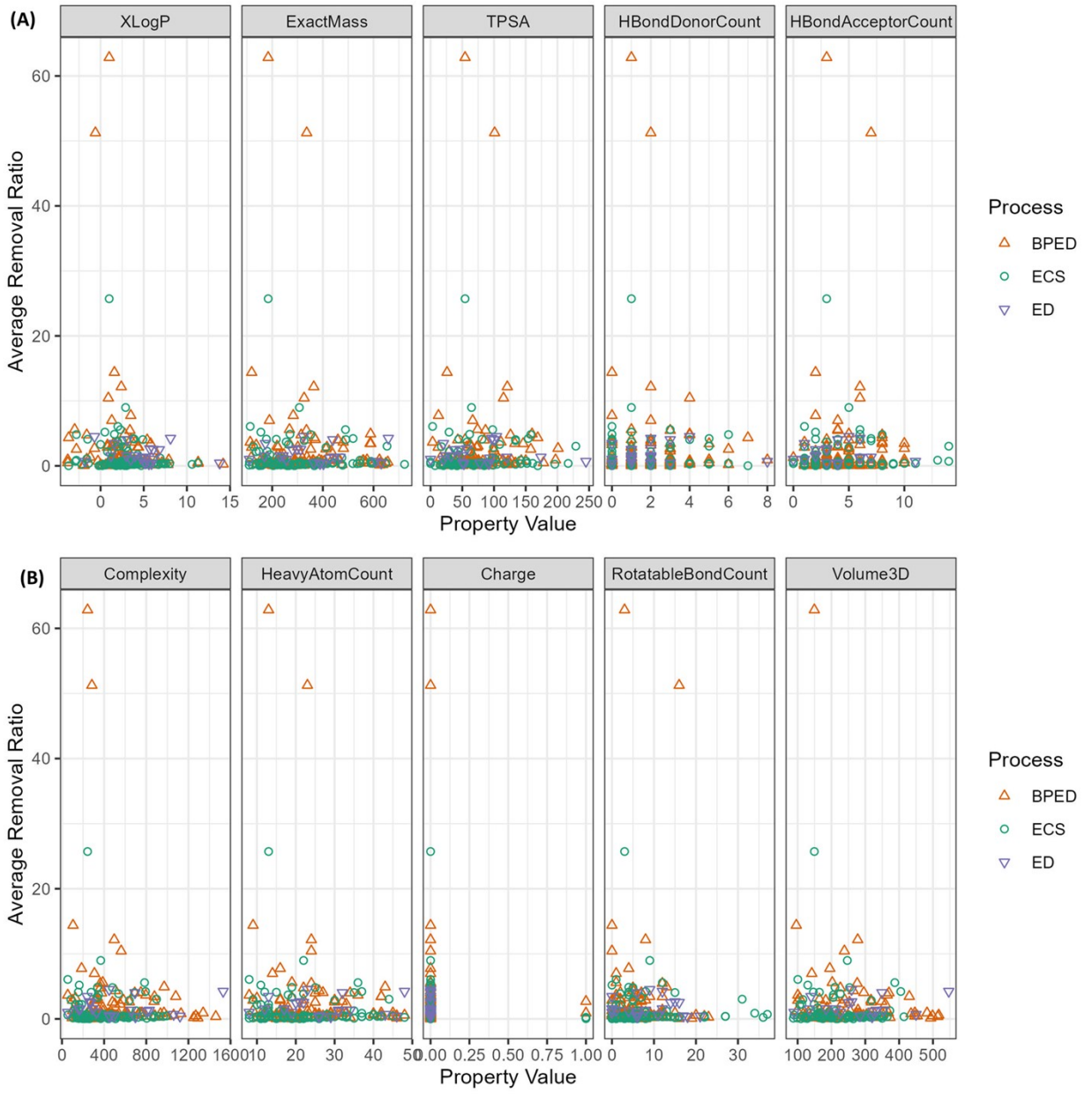

Figure S2-20. Relationships between compound properties and removal ratio for priority compounds. Figure 4 shows these relationships for the properties shown in panel A for ECS only. Spearman correlation and linear regression results are summarized in Table S2-12 and Table S2-13.

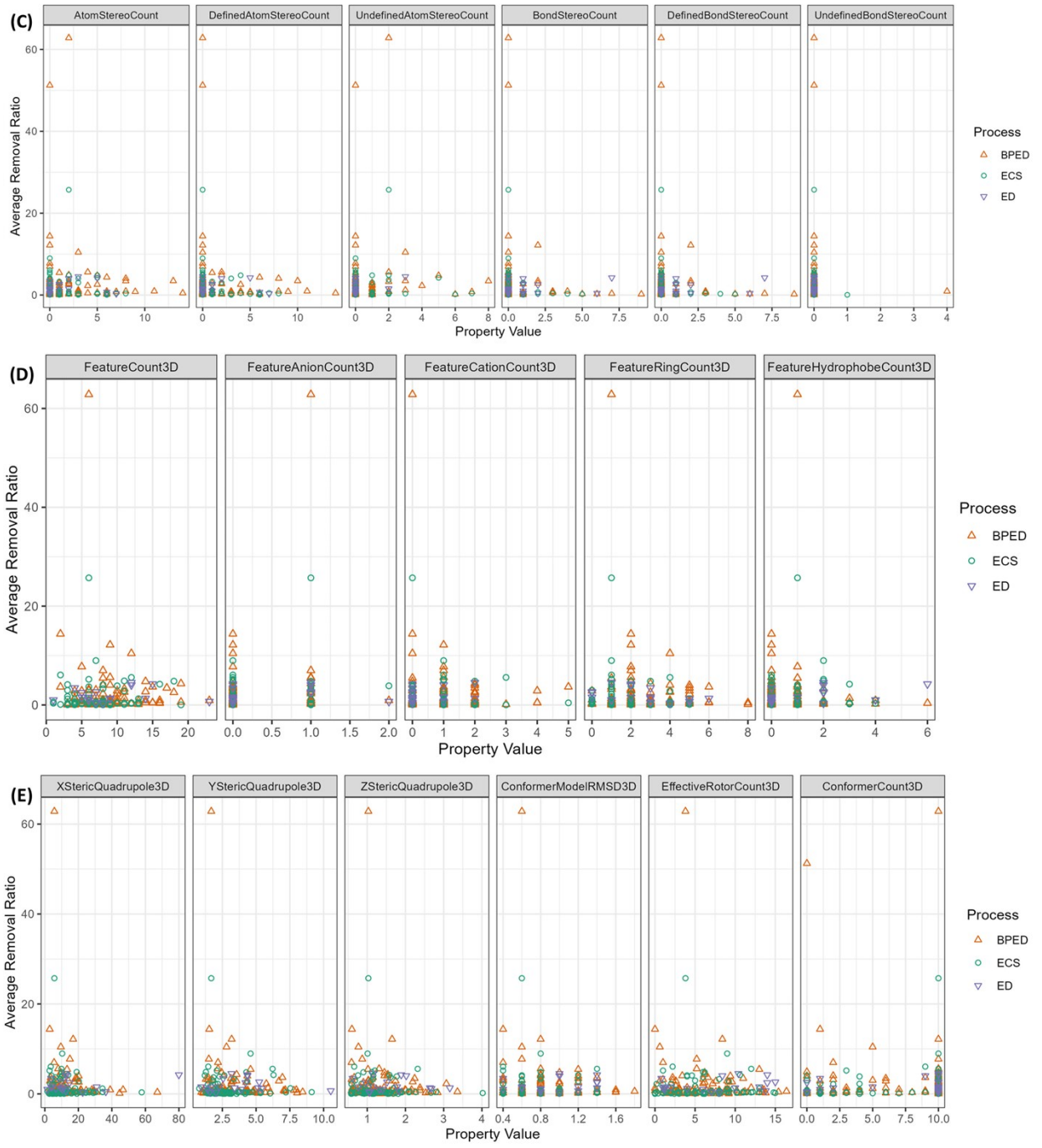

Figure S2-20. Relationships between compound properties and removal ratio for priority compounds. Figure 4 shows these relationships for the properties shown in panel A for ECS only. Spearman correlation and linear regression results are summarized in Table S2-12 and Table S2-13. (continued)

Table S2-12. Spearman correlation results for relationships between compound properties and fates for priority compounds. Boxes have a yellow background if correlations were statistically significant.

Enrichment Ratio						
	ECS		ED		BPED	
	p-value	rho	p-value	rho	p-value	rho
XLogP	0.1986	0.237	0.0477	0.486	0.4198	-0.069
ExactMass	0.1322	-0.276	0.4248	0.207	0.0068	-0.226
TPSA	0.5743	-0.105	0.5698	-0.148	0.5308	-0.053
Complexity	0.1225	-0.283	0.5570	0.153	0.0031	-0.246
Charge	0.9132	-0.020	-	-	0.6017	-0.044
HBondDonorCount	0.0255	-0.401	0.2231	-0.312	0.5232	-0.054
HBondAcceptorCount	0.2737	-0.203	0.8139	0.062	0.0694	-0.153
RotatableBondCount	0.0982	-0.302	0.2724	0.282	0.1398	-0.125
HeavyAtomCount	0.0939	-0.306	0.3833	0.226	0.0040	-0.240
AtomStereoCount	0.9557	-0.010	0.3159	0.259	0.1832	-0.112
DefinedAtomStereoCount	0.3784	-0.164	0.1870	0.336	0.2284	-0.102
UndefinedAtomStereoCount	0.3877	0.161	-	-	0.7338	-0.029
BondStereoCount	0.1384	-0.272	0.0189	0.562	0.9407	-0.006
DefinedBondStereoCount	0.0948	-0.305	0.0189	0.562	0.9422	0.006
UndefinedBondStereoCount	1.0000	0	-	-	0.6017	-0.044
Volume3D	0.3212	-0.191	0.5151	0.182	0.0103	-0.224
XStericQuadrupole3D	0.6021	-0.101	0.7131	-0.104	0.1545	-0.126
YStericQuadrupole3D	0.3787	-0.170	0.1261	0.414	0.0895	-0.150
ZStericQuadrupole3D	0.8840	-0.028	0.3268	0.271	0.0267	-0.194
FeatureCount3D	0.0943	-0.317	0.7519	-0.089	0.0467	-0.175
FeatureAnionCount3D	0.0408	0.382	0.1172	0.422	0.3590	0.081
FeatureCationCount3D	0.3231	-0.190	0.4983	-0.190	0.2036	-0.112
FeatureRingCount3D	0.2982	-0.200	0.6095	-0.144	0.0103	-0.224
FeatureHydrophobeCount3D	0.0910	-0.320	0.3161	0.278	0.4921	0.061
ConformerModelRMSD3D	0.2070	-0.241	0.4342	0.218	0.1852	-0.117
EffectiveRotorCount3D	0.3689	-0.173	0.4489	0.212	0.2097	-0.111
ConformerCount3D	0.7585	0.058	0.6577	-0.116	0.6371	-0.040

Table S2-12. Spearman correlation results for relationships between compound properties and fates for priority compounds. Boxes have a yellow background if correlations were statistically significant. (continued)

Removal Ratio						
	ECS		ED		BPED	
	p-value	rho	p-value	rho	p-value	rho
XLogP	0.3990	-0.084	0.3719	-0.205	0.1641	-0.128
ExactMass	0.9943	0.001	0.4022	-0.192	0.2094	0.115
TPSA	0.0990	0.163	0.9599	0.012	0.0862	0.157
Complexity	0.6382	-0.047	0.2424	-0.266	0.1302	0.138
Charge	0.0268	-0.217	-	-	0.3312	0.089
HBondDonorCount	0.6256	0.048	0.5543	0.137	0.1273	0.139
HBondAcceptorCount	0.1175	0.154	0.6956	-0.091	0.1250	0.140
RotatableBondCount	0.2241	0.120	0.5586	-0.135	0.4445	-0.070
HeavyAtomCount	0.9101	-0.011	0.4344	-0.180	0.2303	0.110
AtomStereoCount	0.4728	-0.071	0.2337	0.272	0.0186	0.214
DefinedAtomStereoCount	0.5620	-0.058	0.6983	0.090	0.2510	0.105
UndefinedAtomStereoCount	0.6309	0.048	0.1429	0.331	0.0327	0.194
BondStereoCount	0.3473	-0.093	0.9707	-0.009	0.6891	-0.037
DefinedBondStereoCount	0.6012	-0.052	0.9707	-0.009	0.6140	-0.046
UndefinedBondStereoCount	0.1219	-0.153	-	-	0.6903	0.037
Volume3D	0.5735	-0.060	0.9435	-0.020	0.3848	0.084
XStericQuadrupole3D	0.9352	0.009	0.8611	0.047	0.9583	0.005
YStericQuadrupole3D	0.6179	-0.053	0.4846	0.181	0.2991	0.100
ZStericQuadrupole3D	0.6639	-0.046	0.9330	-0.022	0.4386	-0.075
FeatureCount3D	0.6651	0.046	0.8474	0.050	0.0212	0.221
FeatureAnionCount3D	0.2045	0.135	0.2069	0.322	0.0111	0.242
FeatureCationCount3D	0.5964	-0.057	0.3836	0.226	0.2029	0.123
FeatureRingCount3D	0.0775	-0.187	0.0682	-0.453	0.0562	0.183
FeatureHydrophobeCount3D	0.1848	0.141	0.1104	0.401	0.1290	-0.146
ConformerModelRMSD3D	0.5909	0.057	0.3306	0.251	0.7876	0.026
EffectiveRotorCount3D	0.2502	0.122	0.2790	0.279	0.6043	-0.050
ConformerCount3D	0.1262	0.151	0.3418	0.218	0.1634	-0.128

Table S2-13. Slopes, intercepts (Int), and R^2 for relationships between compound properties and fates for priority compounds. Boxes have a yellow background if correlations were statistically significant based on Spearman correlation (Table S2-12).

Enrichment Ratio									
	ECS			ED			BPED		
	Slope	**Int**	**R^2**	**Slope**	**Int**	**R^2**	**Slope**	**Int**	**R^2**
XLogP	0.99	1.2	0.0972	0.33	-0.029	0.1882	0.13	0.83	0.0048
ExactMass	-0.0087	5.5	0.0213	-0.00011	1.2	0.0001	0.0029	0.33	0.0062
TPSA	0.0078	2.9	0.0021	-0.0052	1.5	0.0354	0.0079	0.64	0.0053
Complexity	-0.0050	4.6	0.0109	-0.0010	1.6	0.0283	0.0011	0.78	0.0030
Charge	-3.1	3.4	0.0067	-	-	-	-1.1	1.2	0.0005
HBondDonorCount	-1.6	4.9	0.0684	-0.14	1.4	0.0192	-0.011	1.2	0.0000
HBondAcceptorCount	-0.24	4.1	0.0132	-0.075	1.4	0.0145	0.14	0.63	0.0050
RotatableBondCount	-0.080	3.8	0.0102	0.13	0.39	0.2162	0.029	1.0	0.0009
HeavyAtomCount	-0.15	6.0	0.0319	-0.0037	1.3	0.0004	0.035	0.45	0.0045
AtomStereoCount	-1.5	4.3	0.0479	0.059	1.2	0.0026	-0.20	1.4	0.0094
DefinedAtomStereoCount	-1.4	3.8	0.0312	-0.015	1.2	0.0002	-0.17	1.3	0.0062
UndefinedAtomStereoCount	-1.0	3.5	0.0090	0.37	1.1	0.0203	-0.25	1.3	0.0027
BondStereoCount	-2.6	3.7	0.0286	1.9	0.54	0.4211	-0.058	1.2	0.0001
DefinedBondStereoCount	-2.3	3.6	0.0213	1.9	0.54	0.4211	0.013	1.2	0.0000
UndefinedBondStereoCount	-3.1	3.4	0.0064	-	-	-	-0.28	1.2	0.0005
Volume3D	-0.011	5.5	0.0095	0.00079	0.86	0.0025	0.0052	0.062	0.0087
XStericQuadrupole3D	0.015	3.3	0.0006	-0.0050	1.1	0.0005	0.053	0.60	0.0080
YStericQuadrupole3D	-1.2	6.3	0.0542	0.092	0.72	0.0201	0.28	0.37	0.0091
ZStericQuadrupole3D	-0.86	4.4	0.0027	-0.067	1.1	0.0011	0.35	0.76	0.0014
FeatureCount3D	-0.34	5.4	0.0234	-0.049	1.4	0.0252	0.063	0.71	0.0026
FeatureAnionCount3D	4.8	2.8	0.0895	1.0	0.77	0.1482	0.087	1.1	0.0001
FeatureCationCount3D	-1.6	4.5	0.0423	-0.39	1.2	0.0247	0.13	1.1	0.0006
FeatureRingCount3D	-0.94	4.9	0.0273	-0.30	1.7	0.1281	0.21	0.72	0.0032
FeatureHydrophobeCount3D	-1.6	4.5	0.0455	0.38	0.76	0.0839	0.23	1.0	0.0024
ConformerModelRMSD3D	-1.4	4.5	0.0028	1.8	-0.48	0.1953	2.9	-0.91	0.0277
EffectiveRotorCount3D	-0.010	3.6	0.0000	0.12	0.35	0.1660	0.15	0.40	0.0148
ConformerCount3D	0.31	1.0	0.0292	0.0031	1.2	0.0001	0.089	0.56	0.0063

Table S2-13. Slopes, intercepts (Int), and R^2 for relationships between compound properties and fates for priority compounds. Boxes have a yellow background if correlations were statistically significant based on Spearman correlation (Table S2-12). (continued)

Removal Ratio									
	ECS			ED			BPED		
	Slope	Int	R^2	Slope	Int	R^2	Slope	Int	R^2
XLogP	-0.17	1.8	0.0223	-0.097	2.2	0.0550	-0.41	3.6	0.0234
ExactMass	-0.0020	2.0	0.0096	-0.00039	1.9	0.0019	-0.0045	4.0	0.0070
TPSA	0.0032	1.1	0.0029	-0.0013	1.9	0.0031	0.0057	2.0	0.0009
Complexity	-0.00084	1.7	0.0045	0.00020	1.7	0.0031	-0.0026	3.7	0.0105
Charge	-1.2	1.3	0.0048	-	-	-	-0.68	2.5	0.0001
HBondDonorCount	0.048	1.2	0.0006	0.039	1.7	0.0026	-0.027	2.5	0.0000
HBondAcceptorCount	0.011	1.3	0.0001	-0.027	1.9	0.0025	0.16	1.7	0.0023
RotatableBondCount	-0.023	1.5	0.0038	-0.016	1.9	0.0064	0.063	2.1	0.0016
HeavyAtomCount	-0.032	2.0	0.0116	-0.0024	1.8	0.0004	-0.069	4.1	0.0089
AtomStereoCount	-0.057	1.4	0.0019	0.093	1.6	0.0221	-0.044	2.5	0.0003
DefinedAtomStereoCount	-0.16	1.5	0.0137	0.013	1.8	0.0004	-0.19	2.7	0.0041
UndefinedAtomStereoCount	0.32	1.2	0.0166	0.50	1.6	0.1023	0.49	2.2	0.0078
BondStereoCount	-0.31	1.4	0.0069	0.12	1.6	0.0275	-0.33	2.6	0.0038
DefinedBondStereoCount	-0.29	1.4	0.0061	0.12	1.6	0.0275	-0.32	2.6	0.0034
UndefinedBondStereoCount	-1.3	1.3	0.0019	-	-	-	-0.39	2.5	0.0004
Volume3D	-0.0040	2.3	0.0114	0.0020	1.4	0.0289	-0.0074	3.9	0.0136
XStericQuadrupole3D	-0.042	1.9	0.0161	0.019	1.6	0.0705	-0.065	2.9	0.0096
YStericQuadrupole3D	-0.053	1.5	0.0007	0.011	1.9	0.0003	-0.34	3.2	0.0094
ZStericQuadrupole3D	-0.47	2.0	0.0072	-0.20	2.3	0.0109	-0.98	3.4	0.0080
FeatureCount3D	0.036	1.1	0.0016	0.035	1.7	0.0185	-0.052	2.6	0.0011
FeatureAnionCount3D	2.0	1.0	0.0728	0.56	1.8	0.0626	2.6	1.5	0.0341
FeatureCationCount3D	-0.21	1.5	0.0037	0.46	1.7	0.0598	-0.36	2.4	0.0032
FeatureRingCount3D	-0.34	2.1	0.0228	-0.28	2.6	0.1465	-0.28	2.8	0.0052
FeatureHydrophobeCount3D	0.15	1.3	0.0027	0.38	1.5	0.2314	-0.26	2.3	0.0018
ConformerModelRMSD3D	-0.88	2.1	0.0080	0.87	1.1	0.0512	-2.2	3.9	0.0111
EffectiveRotorCount3D	-0.038	1.6	0.0021	0.068	1.4	0.0702	-0.16	3.1	0.0097
ConformerCount3D	0.096	0.67	0.0194	0.067	1.3	0.0506	-0.17	3.7	0.0078

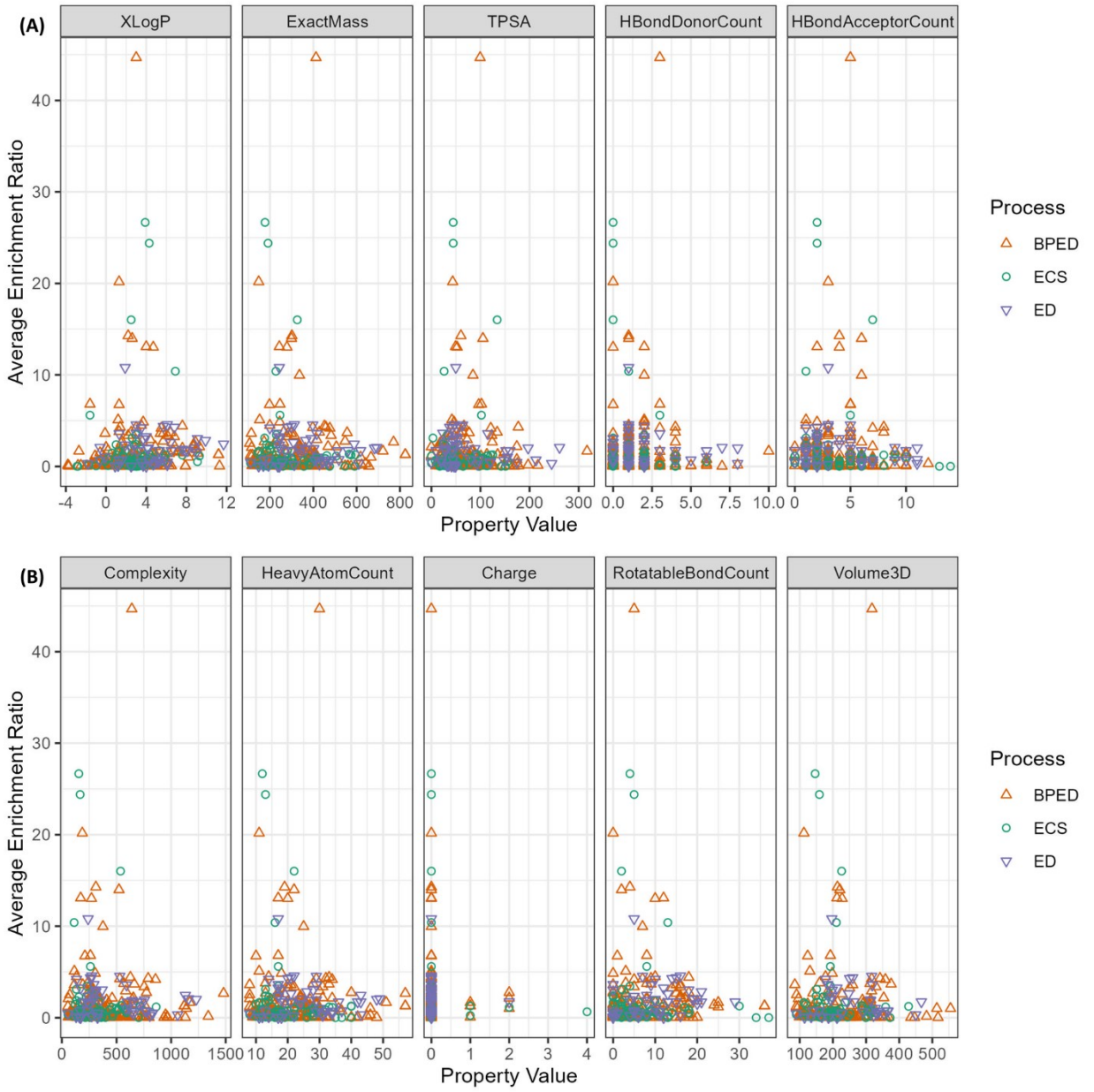

Figure S2-21. Relationships between compound properties and enrichment ratio for all identified compounds. Spearman correlation and linear regression results are summarized in Table S2-14 and Table S2-15.

Figure S2-21. Relationships between compound properties and enrichment ratio for all identified compounds. Spearman correlation and linear regression results are summarized in Table S2-14 and Table S2-15. (continued)

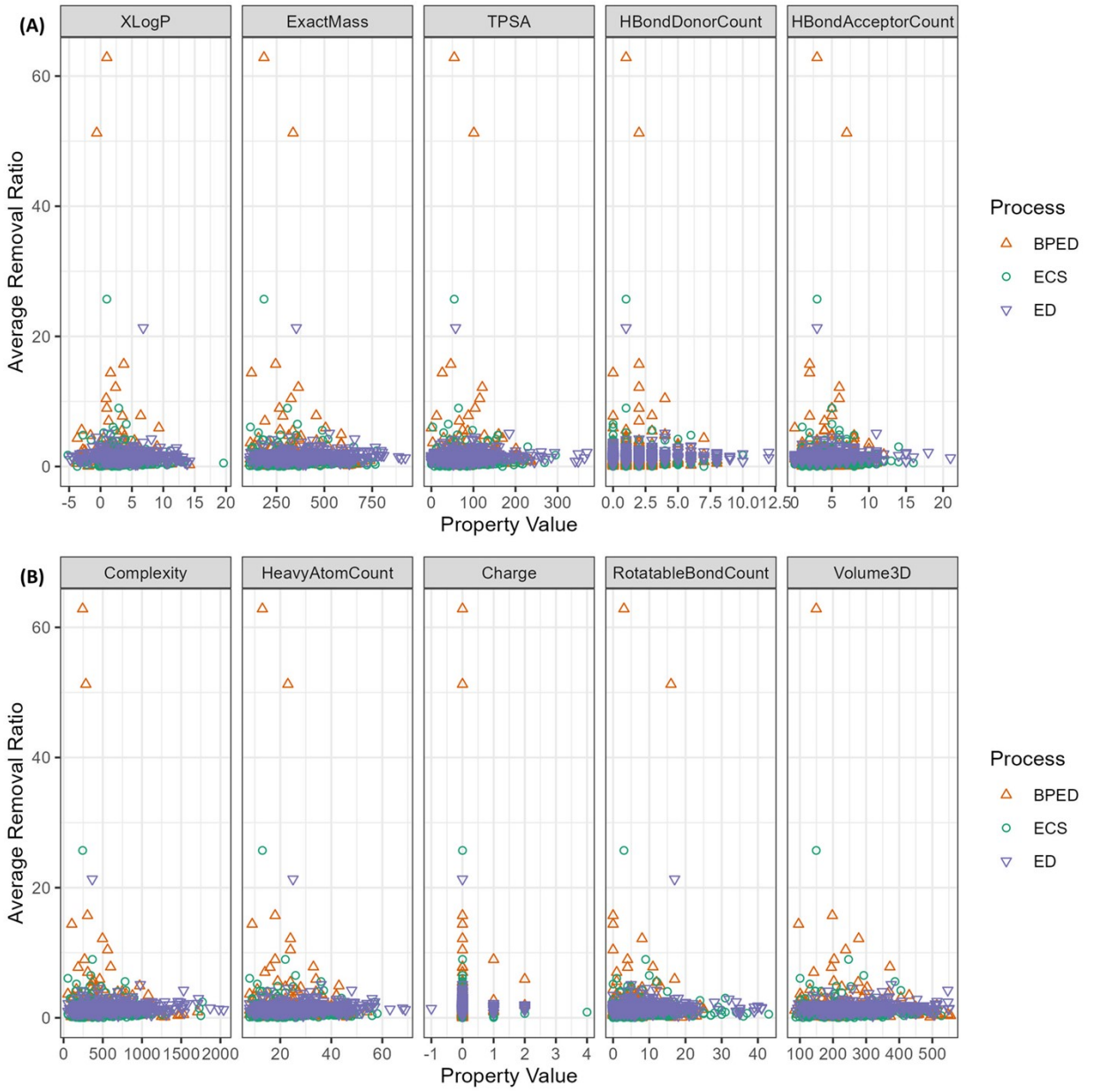

Figure S2-22. Relationships between compound properties and removal ratio for all identified compounds. Spearman correlation and linear regression results are summarized in Table S2-14 and Table S2-15.

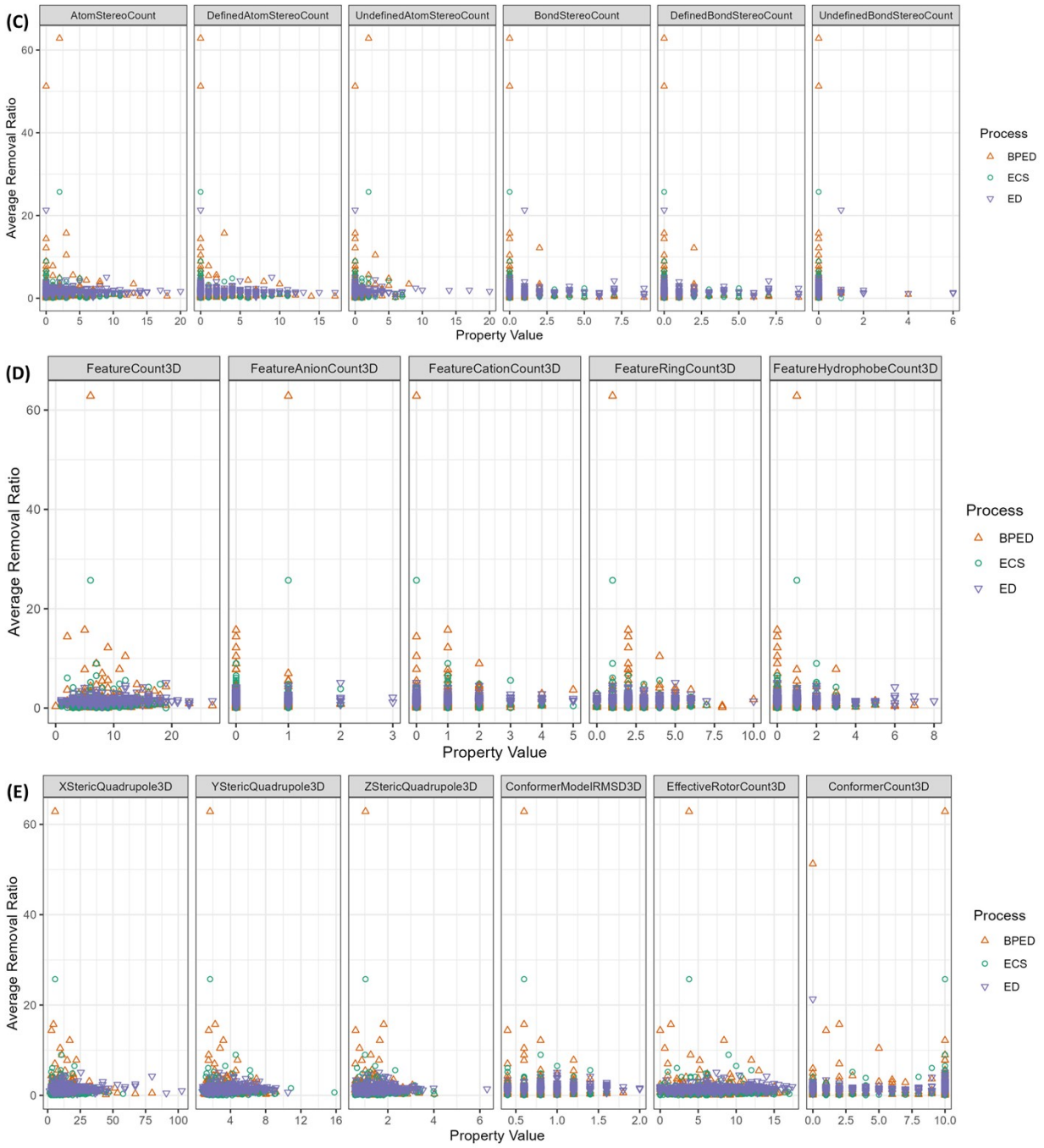

Figure S2-22. Relationships between compound properties and removal ratio for all identified compounds. Spearman correlation and linear regression results are summarized in Table S2-14 and Table S2-15. (continued)

Table S2-14. Spearman correlation results for relationships between compound properties and fates for all identified compounds. Boxes have a yellow background if correlations were statistically significant.

Enrichment Ratio						
	ECS		ED		BPED	
	p-value	rho	p-value	rho	p-value	rho
XLogP	0.0592	0.232	0.1609	0.208	0.0101	0.175
ExactMass	0.6864	-0.050	0.8570	0.027	0.6292	0.033
TPSA	0.8622	0.022	0.7031	-0.057	0.6741	-0.029
Complexity	0.9060	-0.015	0.8398	-0.030	0.2920	-0.072
Charge	0.7724	0.036	0.9422	0.011	0.0737	0.122
HBondDonorCount	0.3098	-0.126	0.3481	-0.140	0.3894	-0.059
HBondAcceptorCount	0.6668	-0.054	0.7478	-0.048	0.1965	-0.088
RotatableBondCount	0.1082	-0.198	0.0318	0.314	0.0607	0.128
HeavyAtomCount	0.5025	-0.083	0.9019	0.018	0.8994	0.009
AtomStereoCount	0.5739	-0.070	0.5243	0.095	0.0429	-0.138
DefinedAtomStereoCount	0.1423	-0.181	0.7782	0.042	0.6421	-0.032
UndefinedAtomStereoCount	0.2079	0.156	0.5790	0.083	0.0161	-0.163
BondStereoCount	0.4510	-0.094	0.0908	0.249	0.1336	0.102
DefinedBondStereoCount	0.5968	-0.066	0.0908	0.249	0.1659	0.094
UndefinedBondStereoCount	0.4733	-0.089	-	-	0.5395	0.042
Volume3D	0.5690	-0.074	0.9935	0.001	0.2686	-0.082
XStericQuadrupole3D	0.9606	-0.006	0.1793	0.229	0.3539	-0.069
YStericQuadrupole3D	0.7105	-0.048	0.8903	0.024	0.4192	-0.060
ZStericQuadrupole3D	0.9855	0.002	0.5410	-0.105	0.4940	-0.051
FeatureCount3D	0.5263	-0.083	0.2425	-0.200	0.1506	-0.107
FeatureAnionCount3D	0.0786	0.227	0.2664	0.190	0.1520	0.106
FeatureCationCount3D	0.3989	-0.110	0.6167	-0.086	0.3990	-0.063
FeatureRingCount3D	0.6941	0.051	0.0792	-0.296	0.0378	-0.154
FeatureHydrophobeCount3D	0.3542	-0.121	0.0273	0.368	0.5302	0.047
ConformerModelRMSD3D	0.2024	-0.166	0.0693	0.306	0.6466	0.034
EffectiveRotorCount3D	0.2333	-0.155	0.0296	0.363	0.9381	-0.006
ConformerCount3D	0.8963	0.016	0.6920	-0.059	0.0101	-0.174

Table S2-14. Spearman correlation results for relationships between compound properties and fates for all identified compounds. Boxes have a yellow background if correlations were statistically significant. (continued)

Removal Ratio						
	ECS		ED		BPED	
	p-value	rho	p-value	rho	p-value	rho
XLogP	0.1786	-0.076	0.0672	-0.079	0.2379	-0.072
ExactMass	0.0893	0.096	0.0007	0.144	0.4265	0.048
TPSA	0.0002	0.211	0.0031	0.127	0.2221	0.074
Complexity	0.2182	0.070	0.0039	0.124	0.6793	0.025
Charge	0.4905	-0.039	0.1581	0.061	0.0050	0.170
HBondDonorCount	0.0177	0.134	0.0008	0.144	0.1296	0.092
HBondAcceptorCount	0.0011	0.183	0.0036	0.125	0.5917	0.033
RotatableBondCount	0.2613	0.064	0.0017	0.135	0.6849	0.025
HeavyAtomCount	0.1797	0.076	0.0003	0.155	0.4693	0.044
AtomStereoCount	0.5660	-0.033	0.0007	0.145	0.5406	0.037
DefinedAtomStereoCount	0.7828	-0.016	0.0469	0.085	0.9424	-0.004
UndefinedAtomStereoCount	0.6820	-0.023	0.0146	0.105	0.2950	0.064
BondStereoCount	0.7841	-0.016	0.7039	0.016	0.4024	-0.051
DefinedBondStereoCount	0.9809	-0.001	0.9469	0.003	0.2114	-0.076
UndefinedBondStereoCount	0.0947	-0.095	0.4319	0.034	0.2305	0.073
Volume3D	0.2491	0.072	0.0003	0.170	0.7699	0.019
XStericQuadrupole3D	0.4131	0.051	0.0691	0.086	0.6960	-0.025
YStericQuadrupole3D	0.6151	0.032	0.0001	0.178	0.6435	0.030
ZStericQuadrupole3D	0.3378	0.060	0.1127	0.075	0.9425	0.005
FeatureCount3D	0.0197	0.146	0.0069	0.127	0.0645	0.119
FeatureAnionCount3D	0.2549	0.071	0.7479	-0.015	0.0243	0.145
FeatureCationCount3D	0.5988	0.033	0.0004	0.165	0.0421	0.131
FeatureRingCount3D	0.7172	-0.023	0.9809	0.001	0.3920	0.055
FeatureHydrophobeCount3D	0.4883	0.044	0.8150	-0.011	0.2267	-0.078
ConformerModelRMSD3D	0.3659	0.057	0.00001	0.208	0.9436	0.005
EffectiveRotorCount3D	0.2404	0.074	0.00002	0.202	0.7756	-0.018
ConformerCount3D	0.0538	0.109	0.3426	0.041	0.1942	-0.079

Table S2-15. Slopes, intercepts (Int), and R^2 for relationships between compound properties and fates for all identified compounds. Boxes have a yellow background if correlations were statistically significant based on Spearman correlation (Table S2-14).

Enrichment Ratio									
	ECS			ED			BPED		
	Slope	**Int**	**R^2**	**Slope**	**Int**	**R^2**	**Slope**	**Int**	**R^2**
XLogP	0.26	1.2	0.0167	0.057	1.7	0.0078	0.10	1.2	0.0053
ExactMass	-0.0058	3.7	0.0234	-0.0011	2.3	0.0073	0.0014	1.1	0.0023
TPSA	0.00042	2.0	1.23E-05	-0.0053	2.3	0.0309	0.0037	1.2	0.0018
Complexity	-0.0034	3.1	0.0157	-0.0010	2.4	0.0279	0.0005	1.3	0.0011
Charge	-0.45	2.0	0.0028	-0.10	1.9	0.0002	0.091	1.5	3.94E-05
HBondDonorCount	-0.75	2.9	0.0390	-0.13	2.2	0.0194	-0.026	1.5	0.0001
HBondAcceptorCount	-0.16	2.6	0.0092	-0.09	2.3	0.0236	0.059	1.3	0.0011
RotatableBondCount	-0.060	2.4	0.0084	0.045	1.5	0.0268	0.019	1.4	0.0009
HeavyAtomCount	-0.10	4.1	0.0306	-0.018	2.4	0.0090	0.017	1.1	0.0016
AtomStereoCount	-0.45	2.4	0.0192	-0.016	1.9	0.0007	-0.21	1.7	0.0116
DefinedAtomStereoCount	-0.38	2.2	0.0138	-0.074	2.0	0.0061	-0.17	1.6	0.0065
UndefinedAtomStereoCount	-0.50	2.1	0.0032	0.017	1.9	0.0006	-0.32	1.6	0.0051
BondStereoCount	-1.4	2.2	0.0135	0.54	1.8	0.0236	0.037	1.5	4.89E-05
DefinedBondStereoCount	-1.3	2.2	0.0114	0.54	1.8	0.0236	0.10	1.4	0.0003
UndefinedBondStereoCount	-1.7	2.0	0.0019	-	-	-	-0.34	1.5	0.0007
Volume3D	-0.010	4.3	0.0209	-0.0022	2.4	0.0087	0.0026	0.89	0.0030
XStericQuadrupole3D	0.0018	2.1	1.31E-05	0.0090	1.7	0.0026	0.049	0.92	0.0084
YStericQuadrupole3D	-0.61	3.7	0.0361	-0.092	2.1	0.0095	0.14	1.0	0.0030
ZStericQuadrupole3D	-1.1	3.4	0.0092	-0.68	2.8	0.0521	0.012	1.4	2.32E-06
FeatureCount3D	-0.24	3.7	0.0246	-0.11	2.7	0.0598	0.033	1.2	0.0008
FeatureAnionCount3D	2.6	1.7	0.0422	0.15	1.8	0.0015	0.15	1.4	0.0003
FeatureCationCount3D	-0.99	2.8	0.0311	-0.32	2.0	0.0187	-0.025	1.5	2.31E-05
FeatureRingCount3D	-0.49	3.0	0.0170	-0.35	2.7	0.1026	0.083	1.3	0.0007
FeatureHydrophobeCount3D	-0.94	2.8	0.0287	0.30	1.6	0.0260	0.10	1.4	0.0006
ConformerModelRMSD3D	-1.5	3.3	0.0060	1.1	0.84	0.0305	1.9	0.012	0.0167
EffectiveRotorCount3D	-0.078	2.6	0.0034	0.094	1.1	0.0491	0.10	0.93	0.0084
ConformerCount3D	0.10	1.2	0.0062	0.032	1.7	0.0060	0.019	1.4	0.0004

Table S2-15. Slopes, intercepts (Int), and R^2 for relationships between compound properties and fates for all identified compounds. Boxes have a yellow background if correlations were statistically significant based on Spearman correlation (Table S2-14). (continued)

Removal Ratio									
	ECS			ED			BPED		
	Slope	Int	R^2	Slope	Int	R^2	Slope	Int	R^2
XLogP	-0.057	1.3	0.0091	-0.0039	1.5	0.0002	-0.20	2.5	0.0114
ExactMass	-0.0010	1.5	0.0076	0.00037	1.4	0.0031	-0.0032	3.0	0.0071
TPSA	0.00077	1.0	0.0005	0.00082	1.4	0.0020	0.0010	1.8	7.22E-05
Complexity	-0.00038	1.3	0.0038	0.00017	1.4	0.0031	-0.0017	2.7	0.0095
Charge	-0.15	1.1	0.0007	0.029	1.5	0.0001	1.1	1.8	0.0022
HBondDonorCount	-0.00083	1.1	7.23E-07	0.024	1.5	0.0021	-0.0052	1.9	2.98E-06
HBondAcceptorCount	0.0029	1.1	2.14E-05	0.016	1.4	0.0020	0.0018	1.8	6.79E-07
RotatableBondCount	-0.012	1.2	0.0025	0.0079	1.4	0.0038	-0.0014	1.9	2.16E-06
HeavyAtomCount	-0.016	1.5	0.0086	0.0057	1.3	0.0038	-0.048	3.0	0.0083
AtomStereoCount	-0.035	1.2	0.0033	0.0084	1.5	0.0007	-0.054	2.0	0.0009
DefinedAtomStereoCount	-0.053	1.2	0.0076	0.0033	1.5	0.0001	-0.11	2.0	0.0038
UndefinedAtomStereoCount	0.14	1.0	0.0067	0.021	1.5	0.0013	0.34	1.7	0.0055
BondStereoCount	-0.072	1.1	0.0016	0.031	1.5	0.0019	-0.22	1.9	0.0029
DefinedBondStereoCount	-0.068	1.1	0.0015	0.018	1.5	0.0006	-0.21	1.9	0.0026
UndefinedBondStereoCount	-1.0	1.1	0.0011	0.15	1.5	0.0044	-0.28	1.9	0.0002
Volume3D	-0.0022	1.7	0.0112	0.00091	1.2	0.0230	-0.0049	3.0	0.0126
XStericQuadrupole3D	-0.022	1.4	0.0110	0.0048	1.4	0.0096	-0.040	2.3	0.0089
YStericQuadrupole3D	-0.038	1.2	0.0014	0.041	1.3	0.0159	-0.22	2.4	0.0074
ZStericQuadrupole3D	-0.18	1.4	0.0038	0.044	1.4	0.0025	-0.51	2.4	0.0044
FeatureCount3D	-0.0034	1.1	0.0000	0.017	1.3	0.0160	-0.046	2.1	0.0018
FeatureAnionCount3D	0.49	1.0	0.0134	0.083	1.5	0.0044	1.2	1.4	0.0130
FeatureCationCount3D	-0.035	1.1	0.0004	0.068	1.4	0.0139	-0.12	1.8	0.0007
FeatureRingCount3D	-0.12	1.4	0.0117	-0.0015	1.5	1.74E-05	-0.18	2.2	0.0046
FeatureHydrophobeCount3D	0.024	1.1	0.0002	0.012	1.5	0.0008	-0.14	1.8	0.0013
ConformerModelRMSD3D	-0.54	1.6	0.0072	0.32	1.2	0.0301	-1.6	3.0	0.0101
EffectiveRotorCount3D	-0.029	1.3	0.0037	0.025	1.3	0.0305	-0.11	2.4	0.0097
ConformerCount3D	0.033	0.86	0.0065	-0.0063	1.6	0.0007	-0.089	2.5	0.0046

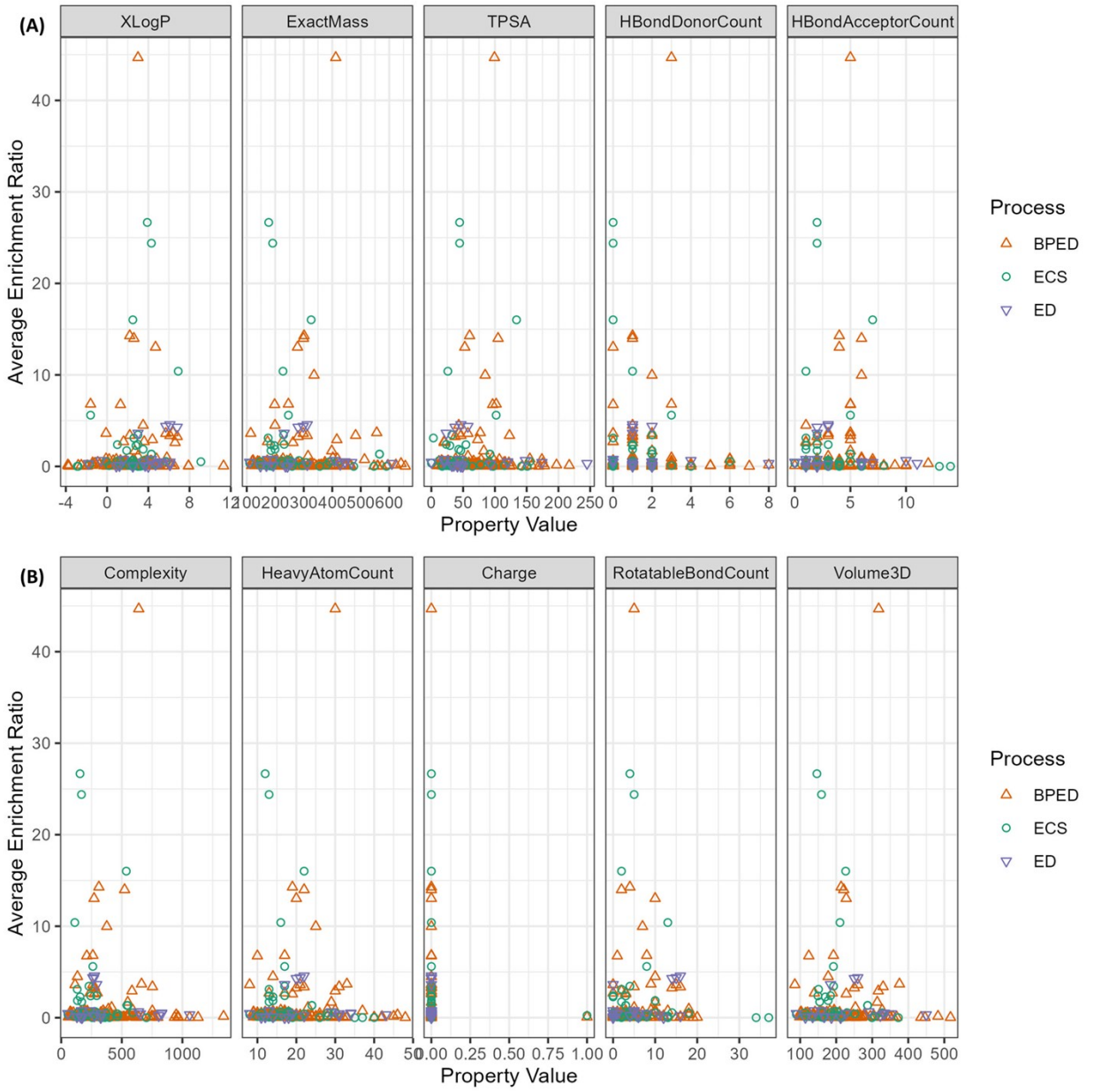

Figure S2-23. Relationships between compound properties and enrichment ratio for identified compounds that showed significant ($p < 0.05$) changes in feature intensity from influent to effluent or product. Spearman correlation and linear regression results are summarized in Table S2-16 and Table S2-17.

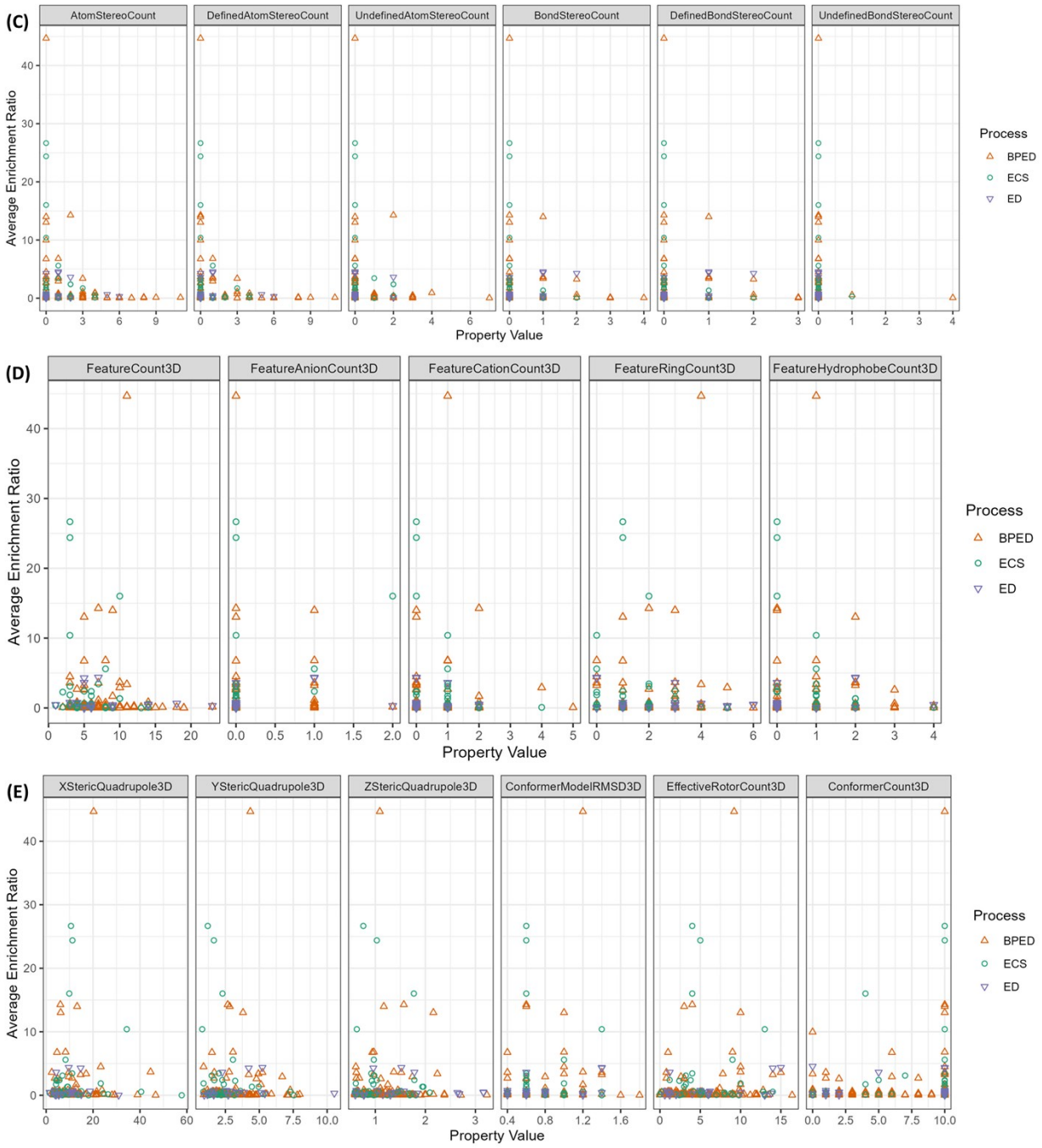

Figure S2-23. Relationships between compound properties and enrichment ratio for identified compounds that showed significant ($p < 0.05$) changes in feature intensity from influent to effluent or product. Spearman correlation and linear regression results are summarized in Table S2-16 and Table S2-17. (continued)

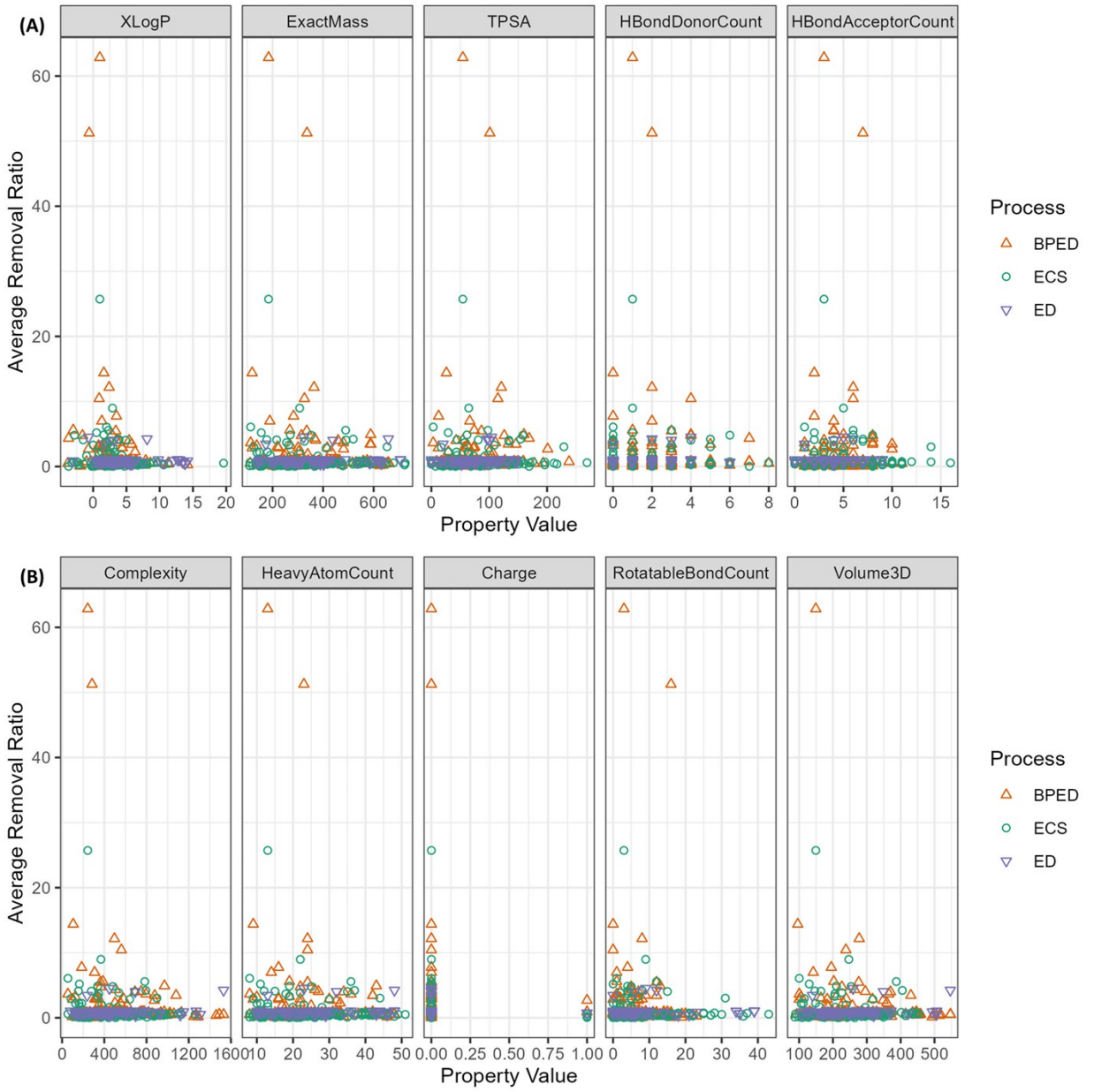

Figure S2-24. Relationships between compound properties and removal ratio for identified compounds that showed significant ($p < 0.05$) changes in feature intensity from influent to effluent or product. Spearman correlation and linear regression results are summarized in Table S2-16 and Table S2-17.

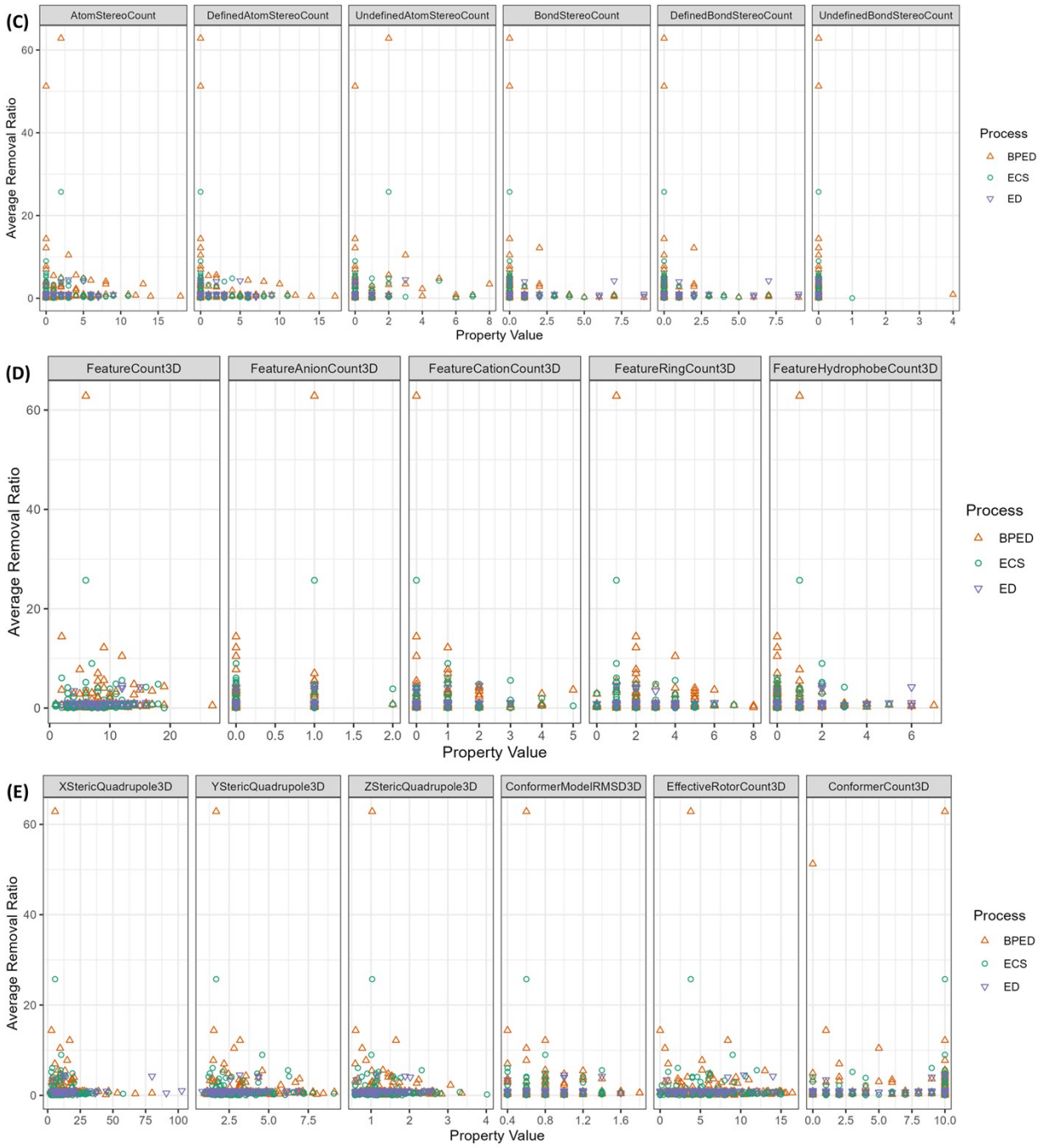

Figure S2-24. Relationships between compound properties and removal ratio for identified compounds that showed significant ($p < 0.05$) changes in feature intensity from influent to effluent or product. Spearman correlation and linear regression results are summarized in Table S2-16 and Table S2-17. (continued)

Table S2-16. Spearman correlation results for relationships between compound properties and fates for identified compounds that showed significant ($p < 0.05$) changes in feature intensity from influent to effluent or product. Boxes have a yellow background if correlations were statistically significant.

Enrichment Ratio						
	ECS		ED		BPED	
	p-value	rho	p-value	rho	p-value	rho
XLogP	0.1095	0.254	0.0831	0.397	0.7764	-0.023
ExactMass	0.3399	-0.153	0.5670	0.136	0.0167	-0.190
TPSA	0.7024	-0.062	0.7646	-0.071	0.6822	-0.033
Complexity	0.1924	-0.208	0.6980	0.093	0.0057	-0.219
Charge	0.6182	-0.080	-	-	0.5195	-0.052
HBondDonorCount	0.2266	-0.193	0.2862	-0.251	0.5122	-0.053
HBondAcceptorCount	0.2197	-0.196	0.7074	0.090	0.1235	-0.123
RotatableBondCount	0.1324	-0.239	0.3089	0.240	0.5493	-0.048
HeavyAtomCount	0.1574	-0.225	0.5136	0.155	0.0077	-0.211
AtomStereoCount	0.7979	-0.041	0.3473	0.222	0.2340	-0.095
DefinedAtomStereoCount	0.3199	-0.159	0.2523	0.269	0.3745	-0.071
UndefinedAtomStereoCount	0.4030	0.134	-	-	0.5092	-0.053
BondStereoCount	0.2539	-0.182	0.0400	0.463	0.9734	0.003
DefinedBondStereoCount	0.3050	-0.164	0.0400	0.463	0.9883	-0.001
UndefinedBondStereoCount	0.6781	-0.067	-	-	0.8101	0.019
Volume3D	0.4587	-0.124	0.6536	0.114	0.0145	-0.203
XStericQuadrupole3D	0.8387	-0.034	0.9675	0.010	0.2709	-0.092
YStericQuadrupole3D	0.5225	-0.107	0.1704	0.338	0.1075	-0.135
ZStericQuadrupole3D	0.8387	0.034	0.4552	0.188	0.0728	-0.150
FeatureCount3D	0.2294	-0.200	0.6893	-0.101	0.0279	-0.183
FeatureAnionCount3D	0.0219	0.371	0.1507	0.353	0.3236	0.083
FeatureCationCount3D	0.6133	-0.085	0.4664	-0.183	0.3222	-0.083
FeatureRingCount3D	0.3497	-0.156	0.6402	-0.118	0.0038	-0.240
FeatureHydrophobeCount3D	0.3981	-0.141	0.5297	0.159	0.3567	0.077
ConformerModelRMSD3D	0.2751	-0.182	0.5104	0.166	0.4168	-0.068
EffectiveRotorCount3D	0.4718	-0.120	0.4642	0.184	0.5195	-0.054
ConformerCount3D	0.3862	0.139	0.8518	-0.045	0.7424	-0.026

Table S2-16. Spearman correlation results for relationships between compound properties and fates for identified compounds that showed significant ($p < 0.05$) changes in feature intensity from influent to effluent or product. Boxes have a yellow background if correlations were statistically significant. (continued)

Removal Ratio						
	ECS		ED		BPED	
	p-value	rho	p-value	rho	p-value	rho
XLogP	0.0704	-0.138	0.9082	0.013	0.4565	-0.056
ExactMass	0.2477	0.088	0.1627	0.156	0.1979	0.096
TPSA	0.0194	0.178	0.1578	0.157	0.3898	0.064
Complexity	0.3269	0.075	0.0953	0.185	0.1599	0.104
Charge	0.0902	-0.129	0.3704	-0.100	0.1198	0.115
HBondDonorCount	0.3246	0.075	0.3683	0.101	0.7460	0.024
HBondAcceptorCount	0.0124	0.190	0.0668	0.203	0.2569	0.084
RotatableBondCount	0.4653	0.056	0.4567	0.083	0.3058	-0.076
HeavyAtomCount	0.2927	0.080	0.0645	0.205	0.2130	0.092
AtomStereoCount	0.7367	-0.026	0.3746	0.099	0.0390	0.153
DefinedAtomStereoCount	0.6352	-0.036	0.5361	0.069	0.4564	0.055
UndefinedAtomStereoCount	0.4977	0.052	0.9892	0.002	0.0634	0.137
BondStereoCount	0.5980	-0.040	0.7546	-0.035	0.8201	-0.017
DefinedBondStereoCount	0.8374	-0.016	0.7546	-0.035	0.6720	-0.032
UndefinedBondStereoCount	0.1050	-0.124	-	-	0.3453	0.070
Volume3D	0.5869	0.046	0.0267	0.265	0.2416	0.091
XStericQuadrupole3D	0.6618	0.037	0.4343	0.095	0.6928	0.031
YStericQuadrupole3D	0.7715	0.024	0.0187	0.280	0.5465	0.047
ZStericQuadrupole3D	0.7969	0.022	0.0602	0.226	0.8865	-0.011
FeatureCount3D	0.0983	0.138	0.0176	0.283	0.1477	0.112
FeatureAnionCount3D	0.2296	0.101	0.4036	0.101	0.0713	0.139
FeatureCationCount3D	0.6938	0.033	0.0043	0.337	0.3948	0.066
FeatureRingCount3D	0.8224	-0.019	0.1293	0.183	0.0626	0.144
FeatureHydrophobeCount3D	0.5273	0.053	0.1978	0.156	0.0736	-0.138
ConformerModelRMSD3D	0.8631	0.014	0.0857	0.207	0.9080	0.009
EffectiveRotorCount3D	0.4695	0.061	0.1139	0.191	0.5174	-0.050
ConformerCount3D	0.2306	0.092	0.1962	0.144	0.3462	-0.070

Table S2-17. Slopes, intercepts (Int), and R^2 for relationships between compound properties and fates for identified compounds that showed significant ($p < 0.05$) changes in feature intensity from influent to effluent or product. Boxes have a yellow background if correlations were statistically significant based on Spearman correlation (Table S2-16).

Enrichment Ratio									
	ECS			ED			BPED		
	Slope	Int	R^2	Slope	Int	R^2	Slope	Int	R^2
XLogP	0.52	1.4	0.0397	0.27	0.13	0.1594	0.12	0.80	0.0045
ExactMass	-0.0078	4.8	0.0259	-0.00046	1.3	0.0014	0.0029	0.30	0.0066
TPSA	0.0043	2.4	0.0008	-0.0054	1.5	0.0436	0.0071	0.65	0.0049
Complexity	-0.0045	3.9	0.0129	-0.0010	1.5	0.0352	0.0011	0.72	0.0036
Charge	-2.5	2.7	0.0042	-	-	-	-1.1	1.1	0.0004
HBondDonorCount	-1.1	3.9	0.0515	-0.13	1.3	0.0200	-0.0047	1.1	3.07E-06
HBondAcceptorCount	-0.20	3.4	0.0093	-0.079	1.4	0.0222	0.14	0.59	0.0052
RotatableBondCount	-0.082	3.2	0.0115	0.13	0.35	0.2258	0.027	0.98	0.0009
HeavyAtomCount	-0.15	5.5	0.0359	-0.0086	1.3	0.0025	0.035	0.41	0.0050
AtomStereoCount	-0.90	3.3	0.0271	0.018	1.1	0.0003	-0.18	1.3	0.0085
DefinedAtomStereoCount	-0.83	3.1	0.0207	-0.037	1.1	0.0015	-0.16	1.3	0.0057
UndefinedAtomStereoCount	-0.61	2.8	0.0032	0.41	1.0	0.0249	-0.21	1.2	0.0023
BondStereoCount	-2.0	3.0	0.0213	1.8	0.56	0.4298	-0.057	1.1	8.42E-05
DefinedBondStereoCount	-1.9	3.0	0.0168	1.8	0.56	0.4298	0.015	1.1	4.45E-06
UndefinedBondStereoCount	-2.4	2.7	0.0040	-	-	-	-0.28	1.1	0.0005
Volume3D	-0.014	5.6	0.0190	0.00035	0.89	0.0005	0.005	0.02	0.0095
XStericQuadrupole3D	0.0039	2.8	0.0001	-0.010	1.1	0.0021	0.051	0.58	0.0080
YStericQuadrupole3D	-0.86	5.1	0.0472	0.095	0.66	0.0222	0.27	0.37	0.0092
ZStericQuadrupole3D	-0.90	3.9	0.0041	-0.11	1.1	0.0040	0.36	0.70	0.0015
FeatureCount3D	-0.30	4.7	0.0247	-0.045	1.3	0.0296	0.067	0.64	0.0031
FeatureAnionCount3D	5.1	2.3	0.1011	1.1	0.74	0.1566	0.087	1.1	7.11E-05
FeatureCationCount3D	-1.7	4.1	0.0512	-0.32	1.1	0.0241	0.13	1.0	0.0007
FeatureRingCount3D	-0.74	4.0	0.0205	-0.25	1.6	0.1214	0.21	0.68	0.0037
FeatureHydrophobeCount3D	-1.6	4.1	0.0529	0.39	0.74	0.0932	0.20	0.98	0.0021
ConformerModelRMSD3D	-1.8	4.2	0.0060	1.8	-0.49	0.2009	2.6	-0.79	0.0261
EffectiveRotorCount3D	-0.072	3.3	0.0020	0.12	0.32	0.1710	0.14	0.40	0.0139
ConformerCount3D	0.20	1.2	0.0139	0.00050	1.1	1.91E-06	0.083	0.55	0.0060

Table S2-17. Slopes, intercepts (Int), and R^2 for relationships between compound properties and fates for identified compounds that showed significant ($p < 0.05$) changes in feature intensity from influent to effluent or product. Boxes have a yellow background if correlations were statistically significant based on Spearman correlation (Table S2-16). (continued)

Removal Ratio									
	ECS			ED			BPED		
	Slope	Int	R^2	Slope	Int	R^2	Slope	Int	R^2
XLogP	-0.10	1.4	0.0154	-0.017	1.1	0.0085	-0.40	3.0	0.0258
ExactMass	-0.0018	1.7	0.0129	0.00041	0.82	0.0071	-0.0039	3.1	0.0071
TPSA	0.0013	0.96	0.0007	0.0020	0.83	0.0090	0.0057	1.4	0.0014
Complexity	-0.00076	1.4	0.0075	0.00053	0.71	0.0410	-0.0020	2.8	0.0092
Charge	-0.74	1.1	0.0030	-0.250	0.98	0.0028	-0.021	1.8	1.29E-07
HBondDonorCount	0.0089	1.0	3.94E-05	0.069	0.86	0.0159	0.028	1.8	4.94E-05
HBondAcceptorCount	-0.0033	1.1	1.79E-05	0.018	0.90	0.0025	0.11	1.4	0.0014
RotatableBondCount	-0.019	1.2	0.0042	-0.0013	0.99	0.0003	0.025	1.7	0.0004
HeavyAtomCount	-0.027	1.7	0.0145	0.0077	0.78	0.0122	-0.059	3.3	0.0086
AtomStereoCount	-0.043	1.1	0.0028	0.046	0.92	0.0174	-0.048	1.9	0.0006
DefinedAtomStereoCount	-0.084	1.2	0.0103	0.021	0.95	0.0035	-0.14	2.0	0.0040
UndefinedAtomStereoCount	0.25	0.94	0.0143	0.52	0.91	0.1100	0.45	1.6	0.0081
BondStereoCount	-0.15	1.1	0.0042	0.052	0.94	0.0171	-0.20	1.9	0.0024
DefinedBondStereoCount	-0.15	1.1	0.0038	0.052	0.94	0.0171	-0.20	1.9	0.0023
UndefinedBondStereoCount	-1.0	1.1	0.0011	0.15	1.5	0.0044	-0.23	1.8	0.0001
Volume3D	-0.0034	1.9	0.0151	0.0019	0.52	0.0536	-0.0061	3.2	0.0140
XStericQuadrupole3D	-0.032	1.5	0.0155	0.0071	0.90	0.0267	-0.046	2.2	0.0092
YStericQuadrupole3D	-0.074	1.3	0.0021	0.10	0.72	0.0332	-0.26	2.4	0.0079
ZStericQuadrupole3D	-0.36	1.6	0.0070	0.16	0.80	0.0112	-0.77	2.6	0.0067
FeatureCount3D	0.0017	1.1	6.60E-06	0.064	0.49	0.0717	-0.04	1.9	0.0010
FeatureAnionCount3D	0.98	0.91	0.0326	0.29	0.94	0.0264	2.2	1.2	0.0303
FeatureCationCount3D	-0.096	1.2	0.0015	0.15	0.93	0.0241	-0.18	1.7	0.0014
FeatureRingCount3D	-0.22	1.6	0.0197	-0.062	1.2	0.0079	-0.22	2.2	0.0046
FeatureHydrophobeCount3D	0.10	1.0	0.0018	0.13	0.88	0.0658	-0.18	1.7	0.0019
ConformerModelRMSD3D	-0.75	1.7	0.0086	0.65	0.51	0.0455	-1.7	3.0	0.0097
EffectiveRotorCount3D	-0.035	1.3	0.0031	0.048	0.75	0.0527	-0.12	2.4	0.0094
ConformerCount3D	0.064	0.63	0.0146	0.019	0.85	0.0115	-0.13	2.8	0.0062

References

1 D. J. Sobota, J. E. Compton, M. L. McCrackin and S. Singh, Cost of reactive nitrogen release from human activities to the environment in the United States, *Environ. Res. Lett.*, 2015, **10**, 025006.

2 EPA, 2007.

3 P. L. McCarty, J. Bae and J. Kim, Domestic Wastewater Treatment as a Net Energy Producer–Can This be Achieved?, *Environ. Sci. Technol.*, 2011, **45**, 7100–7106.

4 I. Chorkendorff and J. W. Niemantsverdriet, *Concepts of Modern Catalysis and Kinetics*, Wiley, 1st edn., 2003.

5 J. W. Erisman, M. A. Sutton, J. Galloway, Z. Klimont and W. Winiwarter, How a century of ammonia synthesis changed the world, *Nature Geosci*, 2008, **1**, 636–639.

6 V. Kyriakou, I. Garagounis, A. Vourros, E. Vasileiou and M. Stoukides, An Electrochemical Haber-Bosch Process, *Joule*, 2020, **4**, 142–158.

7 H. Jönsson, A. Baky, U. Jeppsson, D. Hellström and E. Kärrman, Composition of urine, faeces, greywater and biowaste, 2005, 49.

8 T. A. Larsen, A. C. Alder, R. I. L. Eggen, M. Maurer and J. Lienert, Source Separation: Will We See a Paradigm Shift in Wastewater Handling?, *Environ. Sci. Technol.*, 2009, **43**, 6121–6125.

9 J. Lienert, M. Haller, A. Berner, M. Stauffacher and T. A. Larsen, How farmers in Switzerland perceive fertilizers from recycled anthropogenic nutrients (urine), *Water Science and Technology*, 2003, **48**, 47–56.

10 C. Pahl-Wostl, A. Schönborn, N. Willi, J. Muncke and T. A. Larsen, Investigating consumer attitudes towards the new technology of urine separation, *Water Sci Technol*, 2003, **48**, 57–65.

11 T. A. Larsen, H. Gruendl and C. Binz, The potential contribution of urine source separation to the SDG agenda – a review of the progress so far and future development options, *Environ. Sci.: Water Res. Technol.*, 2021, **7**, 1161–1176.

12 A. Segrè Cohen, N. G. Love, K. K. Nace and J. Árvai, Consumers' Acceptance of Agricultural Fertilizers Derived from Diverted and Recycled Human Urine, *Environ. Sci. Technol.*, 2020, **54**, 5297–5305.

13 T. Schreiber, S. Opperman, R. Hardin, J. Cavicchi, A. Pallmeyer, K. Nace and N. Love, Nested risks and responsibilities: Perspectives on fertilizer from human urine in two U.S. regions, *Journal of Agriculture, Food Systems, and Community Development*, 2021, **10**, 1-22-1–22.

14 J. Lienert and T. A. Larsen, High Acceptance of Urine Source Separation in Seven European Countries: A Review, *Environ. Sci. Technol.*, 2010, **44**, 556–566.

15 P. Simha, M. A. Barton, L. F. Perez-Mercado, J. R. McConville, C. Lalander, M. E. Magri, S. Dutta, H. Kabir, A. Selvakumar, X. Zhou, T. Martin, T. Kizos, R. Kataki, Y. Gerchman, R. Herscu-Kluska, D. Alrousan, E. G. Goh, D. Elenciuc, A. Głowacka, L. Korculanin, R. V. Tzeng, S. S. Ray, C. Niwagaba, C. Prouty, J. R. Mihelcic and B. Vinnerås, Willingness among food consumers to recycle human urine as crop fertiliser: Evidence from a multinational survey, *Science of The Total Environment*, 2021, **765**, 144438.

16 P. Kuntke, M. Rodríguez Arredondo, L. Widyakristi, A. ter Heijne, T. H. J. A. Sleutels, H. V. M. Hamelers and C. J. N. Buisman, Hydrogen Gas Recycling for Energy Efficient Ammonia Recovery in Electrochemical Systems, *Environ. Sci. Technol.*, 2017, **51**, 3110–3116.

17 P. Zamora, T. Georgieva, A. Ter Heijne, T. H. J. A. Sleutels, A. W. Jeremiasse, M. Saakes, C. J. N. Buisman and P. Kuntke, Ammonia recovery from urine in a scaled-up Microbial Electrolysis Cell, *Journal of Power Sources*, 2017, **356**, 491–499.

18 P. Kuntke, K. M. Śmiech, H. Bruning, G. Zeeman, M. Saakes, T. H. J. A. Sleutels, H. V. M. Hamelers and C. J. N. Buisman, Ammonium recovery and energy production from urine by a microbial fuel cell, *Water Research*, 2012, **46**, 2627–2636.

19 W. A. Tarpeh, J. M. Barazesh, T. Y. Cath and K. L. Nelson, Electrochemical Stripping to Recover Nitrogen from Source-Separated Urine, *Environ. Sci. Technol.*, 2018, **52**, 1453–1460.

20 D. Appling, M. Habteselassie, D. Radcliffe and J. Bradshaw, Preliminary Study on the Effect of Wastewater Storage in Septic Tank on E. coli Concentration in Summer, *Water*, 2013, **5**, 1141–1151.
21 H. Dong, L. Wei and W. A. Tarpeh, Electro-assisted regeneration of pH-sensitive ion exchangers for sustainable phosphate removal and recovery, *Water Research*, 2020, **184**, 116167.
22 Codiga Resource Recovery Center, CR2C Treatment Monitoring Dashboard, http://cr2c-monitoring.appspot.com/, (accessed 8 March 2021).
23 T. A. Larsen, M. E. Riechmann and K. M. Udert, State of the art of urine treatment technologies: A critical review., *Water Research X*, 2021, **13**, 100114.
24 B. P. Chaplin, The Prospect of Electrochemical Technologies Advancing Worldwide Water Treatment, *Acc. Chem. Res.*, 2019, **52**, 596–604.
25 J. Radjenovic and D. L. Sedlak, Challenges and Opportunities for Electrochemical Processes as Next-Generation Technologies for the Treatment of Contaminated Water, *Environ. Sci. Technol.*, 2015, **49**, 11292–11302.
26 J. Lienert, T. Bürki and B. I. Escher, Reducing micropollutants with source control: substance flow analysis of 212 pharmaceuticals in faeces and urine, *Water Science and Technology*, 2007, **56**, 87–96.
27 T. Heberer, Occurrence, fate, and removal of pharmaceutical residues in the aquatic environment: a review of recent research data, *Toxicology Letters*, 2002, **131**, 5–17.
28 O. González, B. Bayarri, J. Aceña, S. Pérez and D. Barceló, Treatment Technologies for Wastewater Reuse: Fate of Contaminants of Emerging Concern, *Handbook of Environmental Chemistry*, 2016, **45**, 5–37.
29 D. W. Kolpin, E. T. Furlong, M. T. Meyer, E. M. Thurman, S. D. Zaugg, L. B. Barber and H. T. Buxton, Pharmaceuticals, Hormones, and Other Organic Wastewater Contaminants in U.S. Streams, 1999−2000: A National Reconnaissance, *Environ. Sci. Technol.*, 2002, **36**, 1202–1211.
30 T. R. Romeyn, W. Harijanto, S. Sandoval, S. Delagah and M. Sharbatmaleki, Contaminants of emerging concern in reverse osmosis brine concentrate from indirect/direct water reuse applications, *Water Science and Technology*, 2016, **73**, 236–250.
31 S. H. Joo and B. Tansel, Novel technologies for reverse osmosis concentrate treatment: A review, *Journal of Environmental Management*, 2015, **150**, 322–335.
32 I. Köpping, C. S. McArdell, E. Borowska, M. A. Böhler and K. M. Udert, Removal of pharmaceuticals from nitrified urine by adsorption on granular activated carbon, *Water Research X*, 2020, **9**, 100057.
33 W. Pronk, H. Palmquist, M. Biebow and M. Boller, Nanofiltration for the separation of pharmaceuticals from nutrients in source-separated urine, *Water Research*, 2006, **40**, 1405–1412.
34 J. A. Clark, Y. Yang, N. C. Ramos and H. W. Hillhouse, Selective oxidation of pharmaceuticals and suppression of perchlorate formation during electrolysis of fresh human urine, *Water Research*, 2021, **198**, 117106.
35 N. Demissie, P. Simha, F. Y. Lai, L. Ahrens, D. Mussabek, A. Desta and B. Vinnerås, Degradation of 75 organic micropollutants in fresh human urine and water by UV advanced oxidation process, *Water Research*, 2023, **242**, 120221.
36 A. Recherche, F. Tettenborn, J. Behrendt and R. Otterpohl, *Resource recovery and removal of pharmaceutical residues Treatment of separate collected urine*, Institute of Wastewater Management and Water Protection Hamburg University of Technology, 2007.
37 W. A. Tarpeh, I. Wald, M. Wiprächtiger and K. L. Nelson, Effects of operating and design parameters on ion exchange columns for nutrient recovery from urine, *Environ. Sci.: Water Res. Technol.*, 2018, **4**, 828–838.
38 B. Schürmann, W. Everding, D. Montag and J. Pinnekamp, Fate of pharmaceuticals and bacteria in stored urine during precipitation and drying of struvite, *Water Science and Technology*, 2012, **65**, 1774–1780.
39 B. I. Escher, W. Pronk, M. J.-F. Suter and M. Maurer, Monitoring the Removal Efficiency of Pharmaceuticals and Hormones in Different Treatment Processes of Source-Separated Urine with Bioassays, *Environ. Sci. Technol.*, 2006, **40**, 5095–5101.

40 Z. Pan, C. Song, L. Li, H. Wang, Y. Pan, C. Wang, J. Li, T. Wang and X. Feng, Membrane technology coupled with electrochemical advanced oxidation processes for organic wastewater treatment: Recent advances and future prospects, *Chemical Engineering Journal*, 2019, **376**, 120909.
41 E. Mordačíková, M. Vojs, K. Grabicová, M. Marton, P. Michniak, V. Řeháček, A. Bořík, R. Grabic, J. Bruncko, T. Mackuľak and A. Vojs Staňová, Influence of boron doped diamond electrodes properties on the elimination of selected pharmaceuticals from wastewater, *Journal of Electroanalytical Chemistry*, 2020, **862**, 114007.
42 C. Heim, M. Rajab, G. Greco, S. Grosse, J. E. Drewes, T. Letzel and B. Helmreich, Fate of Diclofenac and Its Transformation and Inorganic By-Products in Different Water Matrices during Electrochemical Advanced Oxidation Process Using a Boron-Doped Diamond Electrode, *Water*, 2020, **12**, 1686.
43 J. T. Jasper, O. S. Shafaat and M. R. Hoffmann, Electrochemical Transformation of Trace Organic Contaminants in Latrine Wastewater, *Environ. Sci. Technol.*, 2016, **50**, 10198–10208.
44 S. Garcia-Segura, J. Keller, E. Brillas and J. Radjenovic, Removal of organic contaminants from secondary effluent by anodic oxidation with a boron-doped diamond anode as tertiary treatment, *Journal of Hazardous Materials*, 2015, **283**, 551–557.
45 A. Farhat, J. Keller, S. Tait and J. Radjenovic, Removal of Persistent Organic Contaminants by Electrochemically Activated Sulfate, *Environ. Sci. Technol.*, 2015, **49**, 14326–14333.
46 Y. Chen, S. Li and J. Hu, Photoelectrocatalytic degradation of organics and formation of disinfection byproducts in reverse osmosis concentrate, *Water Research*, 2020, **168**, 115105.
47 H. Lu, W. Zou, P. Chai, J. Wang and L. Bazinet, Feasibility of antibiotic and sulfate ions separation from wastewater using electrodialysis with ultrafiltration membrane, *Journal of Cleaner Production*, 2016, **112**, 3097–3105.
48 A. R. Ferreira, N. Couto, P. Guedes, J. Pinto, E. P. Mateus and A. B. Ribeiro, Electrodialytic 2-compartment cells for emerging organic contaminants removal from effluent, *Journal of Hazardous Materials*, 2018, **358**, 467–474.
49 Z. Li, R. Dai, B. Yang, M. Chen, X. Wang and Z. Wang, An electrochemical membrane biofilm reactor for removing sulfonamides from wastewater and suppressing antibiotic resistance development: Performance and mechanisms, *Journal of Hazardous Materials*, 2021, **404**, 124198.
50 P. Guedes, E. P. Mateus, J. Almeida, A. R. Ferreira, N. Couto and A. B. Ribeiro, Electrodialytic treatment of sewage sludge: Current intensity influence on phosphorus recovery and organic contaminants removal, *Chemical Engineering Journal*, 2016, **306**, 1058–1066.
51 L. J. Banasiak and A. I. Schäfer, Sorption of steroidal hormones by electrodialysis membranes, *Journal of Membrane Science*, 2010, **365**, 198–205.
52 K. Arola, A. Ward, M. Mänttäri, M. Kallioinen and D. Batstone, Transport of pharmaceuticals during electrodialysis treatment of wastewater, *Water Research*, 2019, **161**, 496–504.
53 K. Noguera-Oviedo and D. S. Aga, Lessons learned from more than two decades of research on emerging contaminants in the environment, *Journal of Hazardous Materials*, 2016, **316**, 242–251.
54 K. E. Manz, A. Feerick, J. M. Braun, Y.-L. Feng, A. Hall, J. Koelmel, C. Manzano, S. R. Newton, K. D. Pennell, B. J. Place, K. J. Godri Pollitt, C. Prasse and J. A. Young, Non-targeted analysis (NTA) and suspect screening analysis (SSA): a review of examining the chemical exposome, *J Expo Sci Environ Epidemiol*, 2023, **33**, 524–536.
55 D. E. Helbling, J. Hollender, H.-P. E. Kohler, H. Singer and K. Fenner, High-Throughput Identification of Microbial Transformation Products of Organic Micropollutants, *Environ. Sci. Technol.*, 2010, **44**, 6621–6627.
56 M. Krauss, H. Singer and J. Hollender, LC–high resolution MS in environmental analysis: from target screening to the identification of unknowns, *Anal Bioanal Chem*, 2010, **397**, 943–951.
57 A. Agüera, P. Plaza-Bolaños and F. G. A. Fernández, in *Current Developments in Biotechnology and Bioengineering*, eds S. Varjani, A. Pandey, R. D. Tyagi, H. H. Ngo and C. Larroche, Elsevier, 2020, pp. 503–525.
58 T. Bader, W. Schulz, T. Lucke, W. Seitz and R. Winzenbacher, in *ACS Symposium Series*, eds J. E. Drewes and T. Letzel, American Chemical Society, Washington, DC, 2016, vol. 1242, pp. 49–70.

59 A. Lai, R. R. Singh, L. Kovalova, O. Jaeggi, T. Kondic and E. L. Schymanski, *Retrospective Non-target Analysis to Support Regulatory Water Monitoring: From Masses of Interest to Recommendations via in silico workflows*, In Review, 2020.
60 W. Brack, J. Hollender, M. L. de Alda, C. Müller, T. Schulze, E. Schymanski, J. Slobodnik and M. Krauss, High-resolution mass spectrometry to complement monitoring and track emerging chemicals and pollution trends in European water resources, *Environ Sci Eur*, 2019, **31**, 62.
61 A. López, P. Dualde, V. Yusà and C. Coscollà, Retrospective analysis of pesticide metabolites in urine using liquid chromatography coupled to high-resolution mass spectrometry, *Talanta*, 2016, **160**, 547–555.
62 B. González-Gaya, N. Lopez-Herguedas, D. Bilbao, L. Mijangos, A. M. Iker, N. Etxebarria, M. Irazola, A. Prieto, M. Olivares and O. Zuloaga, Suspect and non-target screening: the last frontier in environmental analysis, *Analytical Methods*, 2021, **13**, 1876–1904.
63 S. Murgolo, S. Franz, H. Arab, M. Bestetti, E. Falletta and G. Mascolo, Degradation of emerging organic pollutants in wastewater effluents by electrochemical photocatalysis on nanostructured TiO2 meshes, *Water Research*, 2019, **164**, 114920.
64 M. Rajab, G. Greco, C. Heim, B. Helmreich and T. Letzel, Serial coupling of RP and zwitterionic hydrophilic interaction LC–MS: Suspects screening of diclofenac transformation products by oxidation with a boron-doped diamond electrode, *Journal of Separation Science*, 2013, **36**, 3011–3018.
65 Rich Earth Institute, Rich Earth Institute: Regulation, https://richearthinstitute.org/our-work/regulation/, (accessed 11 May 2022).
66 B. P. Chaplin, Critical review of electrochemical advanced oxidation processes for water treatment applications, *Environ. Sci.: Processes Impacts*, 2014, **16**, 1182–1203.
67 S. Garcia-Segura, A. B. Nienhauser, A. S. Fajardo, R. Bansal, C. L. Coonrod, J. D. Fortner, M. Marcos-Hernández, T. Rogers, D. Villagran, M. S. Wong and P. Westerhoff, Disparities between experimental and environmental conditions: Research steps toward making electrochemical water treatment a reality, *Current Opinion in Electrochemistry*, 2020, **22**, 9–16.
68 A. Kogler, M. Farmer, J. A. Simon, S. Tilmans, G. F. Wells and W. A. Tarpeh, Systematic Evaluation of Emerging Wastewater Nutrient Removal and Recovery Technologies to Inform Practice and Advance Resource Efficiency, *ACS EST Eng.*, 2021, **1**, 662–684.
69 S. D. Richardson, M. J. Plewa, E. D. Wagner, R. Schoeny and D. M. DeMarini, Occurrence, genotoxicity, and carcinogenicity of regulated and emerging disinfection by-products in drinking water: A review and roadmap for research, *Mutation Research/Reviews in Mutation Research*, 2007, **636**, 178–242.
70 E. D. Wagner, K.-M. Hsu, A. Lagunas, W. A. Mitch and M. J. Plewa, Comparative genotoxicity of nitrosamine drinking water disinfection byproducts in Salmonella and mammalian cells, *Mutat Res*, 2012, **741**, 109–115.
71 E. D. Wagner and M. J. Plewa, CHO cell cytotoxicity and genotoxicity analyses of disinfection by-products: An updated review, *Journal of Environmental Sciences*, 2017, **58**, 64–76.
72 M. Diana, M. Felipe-Sotelo and T. Bond, Disinfection byproducts potentially responsible for the association between chlorinated drinking water and bladder cancer: A review, *Water Research*, 2019, **162**, 492–504.
73 C. M. Villanueva, S. Cordier, L. Font-Ribera, L. A. Salas and P. Levallois, Overview of Disinfection By-products and Associated Health Effects, *Curr Envir Health Rpt*, 2015, **2**, 107–115.
74 S. D. Richardson and M. J. Plewa, To regulate or not to regulate? What to do with more toxic disinfection by-products?, *Journal of Environmental Chemical Engineering*, 2020, **8**, 103939.
75 X.-F. Li and W. A. Mitch, Drinking Water Disinfection Byproducts (DBPs) and Human Health Effects: Multidisciplinary Challenges and Opportunities, *Environ. Sci. Technol.*, 2018, **52**, 1681–1689.
76 Y. Chen, W. Chen, H. Huang, H. Zeng, L. Tan, Y. Pang, J. Ghani and S. Qi, Occurrence of N-nitrosamines and their precursors in the middle and lower reaches of Yangtze River water, *Environmental Research*, 2021, **195**, 110673.

77 Z. Li, G. Song, Y. Bi, W. Gao, A. He, Y. Lu, Y. Wang and G. Jiang, Occurrence and Distribution of Disinfection Byproducts in Domestic Wastewater Effluent, Tap Water, and Surface Water during the SARS-CoV-2 Pandemic in China, *Environ. Sci. Technol.*, 2021, **55**, 4103–4114.
78 X. Luan, X. Liu, C. Fang, W. Chu and Z. Xu, Ecotoxicological effects of disinfected wastewater effluents: a short review of in vivo toxicity bioassays on aquatic organisms, *Environ. Sci.: Water Res. Technol.*, 2020, **6**, 2275–2286.
79 R. Xiao, T. Ou, S. Ding, C. Fang, Z. Xu and W. Chu, Disinfection by-products as environmental contaminants of emerging concern: a review on their occurrence, fate and removal in the urban water cycle, *Critical Reviews in Environmental Science and Technology*, 2022, 1–28.
80 K. Watson, G. Shaw, F. D. L. Leusch and N. L. Knight, Chlorine disinfection by-products in wastewater effluent: Bioassay-based assessment of toxicological impact, *Water Research*, 2012, **46**, 6069–6083.
81 H. Cui, B. Chen, Y. Jiang, Y. Tao, X. Zhu and Z. Cai, Toxicity of 17 Disinfection By-products to Different Trophic Levels of Aquatic Organisms: Ecological Risks and Mechanisms, *Environ. Sci. Technol.*, 2021, **55**, 10534–10541.
82 J. Liu and X. Zhang, Comparative toxicity of new halophenolic DBPs in chlorinated saline wastewater effluents against a marine alga: Halophenolic DBPs are generally more toxic than haloaliphatic ones, *Water Research*, 2014, **65**, 64–72.
83 M. Yang and X. Zhang, Comparative Developmental Toxicity of New Aromatic Halogenated DBPs in a Chlorinated Saline Sewage Effluent to the Marine Polychaete *Platynereis dumerilii*, *Environ. Sci. Technol.*, 2013, **47**, 10868–10876.
84 A. Fumasoli, B. Etter, B. Sterkele, E. Morgenroth and K. M. Udert, Operating a pilot-scale nitrification/distillation plant for complete nutrient recovery from urine, *Water Sci Technol*, 2016, **73**, 215–222.
85 J. M. Barazesh, C. Prasse and D. L. Sedlak, Electrochemical Transformation of Trace Organic Contaminants in the Presence of Halide and Carbonate Ions, *Environ. Sci. Technol.*, 2016, **50**, 10143–10152.
86 M. Rodríguez Arredondo, P. Kuntke, A. ter Heijne, H. V. M. Hamelers and C. J. N. Buisman, Load ratio determines the ammonia recovery and energy input of an electrochemical system, *Water Research*, 2017, **111**, 330–337.
87 E. Lacasa, S. Cotillas, C. Saez, J. Lobato, P. Cañizares and M. A. Rodrigo, Environmental applications of electrochemical technology. What is needed to enable full-scale applications?, *Current Opinion in Electrochemistry*, 2019, **16**, 149–156.
88 M. Rodrigues, T. T. de Mattos, T. Sleutels, A. ter Heijne, H. V. M. Hamelers, C. J. N. Buisman and P. Kuntke, Minimal Bipolar Membrane Cell Configuration for Scaling Up Ammonium Recovery, *ACS Sustainable Chem. Eng.*, 2020, **8**, 17359–17367.
89 M. A. Blommaert, D. Aili, R. A. Tufa, Q. Li, W. A. Smith and D. A. Vermaas, Insights and Challenges for Applying Bipolar Membranes in Advanced Electrochemical Energy Systems, *ACS Energy Lett.*, 2021, **6**, 2539–2548.
90 W. A. Tarpeh, Y. Du, C. M. G. Carpenter, E. E. Rodriguez, D. E. Helbling, D. S. Aga, N. G. Love and K. R. Wigginton, A Unit Process Approach to Nontarget Screening of Organic Contaminants during Urine Treatment, *ACS EST Eng.*, 2023, **3**, 590–601.
91 R. Helmus, T. L. ter Laak, A. P. van Wezel, P. de Voogt and E. L. Schymanski, patRoon: open source software platform for environmental mass spectrometry based non-target screening, *J Cheminform*, 2021, **13**, 1.
92 R. Helmus, B. van de Velde, A. M. Brunner, T. L. ter Laak, A. P. van Wezel and E. L. Schymanski, patRoon 2.0: Improved non-target analysis workflows including automated transformation product screening, *Journal of Open Source Software*, 2022, **7**, 4029.
93 A. L. Pochodylo and D. E. Helbling, Emerging investigators series: prioritization of suspect hits in a sensitive suspect screening workflow for comprehensive micropollutant characterization in environmental samples, *Environ. Sci.: Water Res. Technol.*, 2017, **3**, 54–65.

94 E. Parry and T. M. Young, Comparing targeted and non-targeted high-resolution mass spectrometric approaches for assessing advanced oxidation reactor performance, *Water Research*, 2016, **104**, 72–81.
95 J. E. Schollée, E. L. Schymanski and J. Hollender, in *ACS Symposium Series*, eds J. E. Drewes and T. Letzel, American Chemical Society, Washington, DC, 2016, vol. 1241, pp. 45–65.
96 K. E. Furst, R. M. Coyte, M. Wood, A. Vengosh and W. A. Mitch, Disinfection Byproducts in Rajasthan, India: Are Trihalomethanes a Sufficient Indicator of Disinfection Byproduct Exposure in Low-Income Countries?, *Environ. Sci. Technol.*, 2019, **53**, 12007–12017.
97 Y.-H. Chuang, D. L. McCurry, H. Tung and W. A. Mitch, Formation Pathways and Trade-Offs between Haloacetamides and Haloacetaldehydes during Combined Chlorination and Chloramination of Lignin Phenols and Natural Waters, *Environ. Sci. Technol.*, 2015, **49**, 14432–14440.
98 M. Roman, L. H. Van Dijk, L. Gutierrez, M. Vanoppen, J. W. Post, B. A. Wols, E. R. Cornelissen and A. R. D. Verliefde, Key physicochemical characteristics governing organic micropollutant adsorption and transport in ion-exchange membranes during reverse electrodialysis, *Desalination*, 2019, **468**, 114084.
99 M. Roman, L. Gutierrez, L. H. Van Dijk, M. Vanoppen, J. W. Post, B. A. Wols, E. R. Cornelissen and A. R. D. Verliefde, Effect of pH on the transport and adsorption of organic micropollutants in ion-exchange membranes in electrodialysis-based desalination, *Separation and Purification Technology*, 2020, **252**, 117487.
100 J. D. García-Espinoza, P. Mijaylova-Nacheva and M. Avilés-Flores, Electrochemical carbamazepine degradation: Effect of the generated active chlorine, transformation pathways and toxicity, *Chemosphere*, 2018, **192**, 142–151.
101 Ne-Boc-L-Lysine, https://www.chembk.com/en/chem/Ne-Boc-L-Lysine, (accessed 27 November 2025).
102 Amino Acids, https://www.vanderbilt.edu/AnS/Chemistry/Rizzo/stuff/AA/AminoAcids.html, (accessed 27 November 2025).
103 C. Wald, The urine revolution: how recycling pee could help to save the world, *Nature*, 2022, **602**, 202–206.
104 N. Moore, S. Ebrahimi, Y. Zhu, C. Wang, R. Hofmann and S. Andrews, A comparison of sodium sulfite, ammonium chloride, and ascorbic acid for quenching chlorine prior to disinfection byproduct analysis, *Water Supply*, 2021, ws2021059.
105 M. J. Liu, B. S. Neo and W. A. Tarpeh, Building an operational framework for selective nitrogen recovery via electrochemical stripping, *Water Research*, 2020, **169**, 115226.
106 W. Pronk, M. Biebow and M. Boller, Electrodialysis for Recovering Salts from a Urine Solution Containing Micropollutants, *Environ. Sci. Technol.*, 2006, **40**, 2414–2420.
107 W. Pronk, S. Zuleeg, J. Lienert, B. Escher, M. Koller, A. Berner, G. Koch and M. Boller, Pilot experiments with electrodialysis and ozonation for the production of a fertiliser from urine, *Water Science and Technology*, 2007, **56**, 219–227.
108 L. Gurreri, A. Tamburini, A. Cipollina and G. Micale, Electrodialysis Applications in Wastewater Treatment for Environmental Protection and Resources Recovery: A Systematic Review on Progress and Perspectives, *Membranes*, 2020, **10**, 146.
109 J. De Paepe, R. E. F. Lindeboom, M. Vanoppen, K. De Paepe, D. Demey, W. Coessens, B. Lamaze, A. R. D. Verliefde, P. Clauwaert and S. E. Vlaeminck, Refinery and concentration of nutrients from urine with electrodialysis enabled by upstream precipitation and nitrification, *Water Research*, 2018, **144**, 76–86.
110 Y.-K. Wang, Y.-K. Geng, X.-R. Pan and G.-P. Sheng, In situ utilization of generated electricity for nutrient recovery in urine treatment using a selective electrodialysis membrane bioreactor, *Chemical Engineering Science*, 2017, **171**, 451–458.
111 F. Gao, L. Wang, J. Wang, H. Zhang and S. Lin, Nutrient recovery from treated wastewater by a hybrid electrochemical sequence integrating bipolar membrane electrodialysis and membrane capacitive deionization, *Environ. Sci.: Water Res. Technol.*, 2020, **6**, 383–391.

112 N. van Linden, G. L. Bandinu, D. A. Vermaas, H. Spanjers and J. B. van Lier, Bipolar membrane electrodialysis for energetically competitive ammonium removal and dissolved ammonia production, *Journal of Cleaner Production*, 2020, **259**, 120788.
113 X. Wang, Y. Wang, X. Zhang, H. Feng, C. Li and T. Xu, Phosphate Recovery from Excess Sludge by Conventional Electrodialysis (CED) and Electrodialysis with Bipolar Membranes (EDBM), *Ind. Eng. Chem. Res.*, 2013, **52**, 15896–15904.
114 W. Pronk, M. Biebow and M. Boller, Treatment of source-separated urine by a combination of bipolar electrodialysis and a gas transfer membrane, *Water Science and Technology*, 2006, **53**, 139–146.
115 European Molecular Biology Laboratory, Compound: Bezafibrate (CHEMBL264374), https://www.ebi.ac.uk/explore/compound/CHEMBL264374, (accessed 14 September 2025).
116 R. M. A. Viegas, M. L. Melo, L. C. Brandão Lima, R. R. P. Garcia, E. C. S. Filho, J. A. Osajima and O. Chiavone-Filho, Carbamazepine adsorption with a series of organoclays: removal and toxicity analyses, *Appl Water Sci*, 2024, **14**, 133.
117 National Center for Biotechnology Information, PubChem Compound Summary for CID 3033, Diclofenac, https://pubchem.ncbi.nlm.nih.gov/compound/3033, (accessed 14 September 2025).
118 K. Chetnik, L. Petrick and G. Pandey, MetaClean: a machine learning-based classifier for reduced false positive peak detection in untargeted LC–MS metabolomics data, *Metabolomics*, 2020, **16**, 117.
119 State Water Resources Control Board, 2019.
120 N. R. M. M. C. (Australia) Environment Protection and Heritage Council (Australia), *Australian guidelines for water recycling: managing health and environmental risks (phase 2): augmentation of drinking water supplies*, Natural Resource Management Ministerial Council : Environment Protection and Heritage Council, Canberra, 2008.
121 Disinfection By-Products | The Safe Water System | CDC, https://www.cdc.gov/safewater/chlorination-byproducts.html, (accessed 12 February 2021).
122 Z. Zhang, Y.-H. Chuang, A. Szczuka, K. P. Ishida, S. Roback, M. H. Plumlee and W. A. Mitch, Pilot-scale evaluation of oxidant speciation, 1,4-dioxane degradation and disinfection byproduct formation during UV/hydrogen peroxide, UV/free chlorine and UV/chloramines advanced oxidation process treatment for potable reuse, *Water Research*, 2019, **164**, 114939.
123 S. S. Lau, X. Wei, K. Bokenkamp, E. D. Wagner, M. J. Plewa and W. A. Mitch, Assessing Additivity of Cytotoxicity Associated with Disinfection Byproducts in Potable Reuse and Conventional Drinking Waters, *Environ. Sci. Technol.*, 2020, **54**, 5729–5736.
124 L. Font-Ribera, E. Marco, J. O. Grimalt, S. Pastor, R. Marcos, L. Abramsson-Zetterberg, M. Pedersen, T. Grummt, R. Junek, E. Barreiro, D. Heederik, J. Spithoven, R. Critelli, A. Naccarati, C. Schmalz, C. Zwiener, J. Liu, X. Zhang, W. Mitch, E. Gracia-Lavedan, L. Arjona, J. de Bont, L. Tarès, P. Vineis, M. Kogevinas and C. M. Villanueva, Exposure to disinfection by-products in swimming pools and biomarkers of genotoxicity and respiratory damage – The PISCINA2 Study, *Environment International*, 2019, **131**, 104988.
125 T. Zeng and W. A. Mitch, Impact of Nitrification on the Formation of *N* -Nitrosamines and Halogenated Disinfection Byproducts within Distribution System Storage Facilities, *Environ. Sci. Technol.*, 2016, **50**, 2964–2973.
126 T. Zeng, M. J. Plewa and W. A. Mitch, N-Nitrosamines and halogenated disinfection byproducts in U.S. Full Advanced Treatment trains for potable reuse, *Water Research*, 2016, **101**, 176–186.
127 L. Font-Ribera, M. Kogevinas, C. Schmalz, C. Zwiener, E. Marco, J. O. Grimalt, J. Liu, X. Zhang, W. Mitch, R. Critelli, A. Naccarati, D. Heederik, J. Spithoven, L. Arjona, J. de Bont, E. Gracia-Lavedan and C. M. Villanueva, Environmental and personal determinants of the uptake of disinfection by-products during swimming, *Environmental Research*, 2016, **149**, 206–215.
128 A. Küster, A. C. Alder, B. I. Escher, K. Duis, K. Fenner, J. Garric, T. H. Hutchinson, D. R. Lapen, A. Péry, J. Römbke, J. Snape, T. Ternes, E. Topp, A. Wehrhan and T. Knacker, Environmental risk assessment of human pharmaceuticals in the European Union: A case study with the β-blocker atenolol, *Integrated Environmental Assessment and Management*, 2010, **6**, 514–523.
129 Environmental Protection Agency, 2025.

130 Drug Discovery and Chemical Biology Biocenter Finland, DrugMapper, https://drugmapper.helsinki.fi/CompoundInfo?compound_id=2127933, (accessed 14 March 2026).
131 C. Tixier, H. P. Singer, S. Oellers and S. R. Müller, Occurrence and Fate of Carbamazepine, Clofibric Acid, Diclofenac, Ibuprofen, Ketoprofen, and Naproxen in Surface Waters, *Environ. Sci. Technol.*, 2003, **37**, 1061–1068.
132 R. Pärnamäe, S. Mareev, V. Nikonenko, S. Melnikov, N. Sheldeshov, V. Zabolotskii, H. V. M. Hamelers and M. Tedesco, Bipolar membranes: A review on principles, latest developments, and applications, *Journal of Membrane Science*, 2021, **617**, 118538.
133 R. Wódzki and J. Nowaczyk, Membrane transport of organics. III. Permeation of some carboxylic acids through bipolar polymer membrane, *Journal of Applied Polymer Science*, 2001, **80**, 2705–2717.
134 T. Bond, E. H. Goslan, S. A. Parsons and B. Jefferson, Treatment of disinfection by-product precursors, *Environmental Technology*, 2011, **32**, 1–25.
135 K. M. Udert, T. A. Larsen and W. Gujer, Fate of major compounds in source-separated urine, *Water Science and Technology*, 2006, **54**, 413–420.
136 A. D. Shah and W. A. Mitch, Halonitroalkanes, Halonitriles, Haloamides, and N-Nitrosamines: A Critical Review of Nitrogenous Disinfection Byproduct Formation Pathways, *Environ. Sci. Technol.*, 2012, **46**, 119–131.
137 A. C. Diehl, G. E. Speitel Jr., J. M. Symons, S. W. Krasner, C. J. Hwang and S. E. Barrett, DBP formation during chloramination, *Journal AWWA*, 2000, **92**, 76–90.
138 G. Hua and D. A. Reckhow, Comparison of disinfection byproduct formation from chlorine and alternative disinfectants, *Water Research*, 2007, **41**, 1667–1678.
139 Y.-H. Chuang, A. Szczuka and W. A. Mitch, Comparison of Toxicity-Weighted Disinfection Byproduct Concentrations in Potable Reuse Waters and Conventional Drinking Waters as a New Approach to Assessing the Quality of Advanced Treatment Train Waters, *Environ. Sci. Technol.*, 2019, **53**, 3729–3738.
140 Y. Chen, J. A. Wrubel, W. E. Klein, S. Kabir, W. A. Smith, K. C. Neyerlin and T. G. Deutsch, High-Performance Bipolar Membrane Development for Improved Water Dissociation, *ACS Appl Polym Mater*, 2020, **2**, 4559–4569.
141 Fuel Cell Store, .
142 G. Mohandass, W. Chen, S. Krishnan and T. Kim, Asymmetric and Symmetric Redox Flow Batteries for Energy-Efficient, High-Recovery Water Desalination, *Environ. Sci. Technol.*, 2022, **56**, 4477–4488.
143 A. Xie and S. C. Popat, Electrochemical ammonia stripping from non-nitrified animal rendering wastewater, *Chemical Engineering Journal Advances*, 2020, **3**, 100020.